TABLE OF CONTENTS

LIST OF TABLES

Page

LIST OF FIGURES

Page

LIST OF SYMBOLS

$\square^{p}$	Refers to satellite p
$\square_{k}$	Refers to receiver k
$\square_{L1}$	Refers to L1 frequency
$\square_{L2}$	Refers to L2 frequency
$\square_{IF}$	Refers to the iono-free measurement
$\hat{\square}$	Refers as fixed values in the LAMBDA method
$\breve{\square}$	Refers as 'true' values in the LAMBDA method
φ	Carrier phase observation [radians]
P	Pseudo-range measurement [m]
$\dot{P}$	Doppler-range measurement [m/s]
dt	Clock error bias [m].
$\dot{dt}$	Clock error drift [m/s]
ρ	'True' range between satellite and receiver [m]
$\dot{\rho}$	'True' Doppler range between satellite and receiver [m/s]
I	Ionospheric delay [m]
T	Tropospheric delay [m]
$\dot{I}$	Tropospheric delay drift [m/s]
$\dot{T}$	Ionospheric delay drift [m/s]
c	Speed of light in vacuum [m/s]
τ	Time of transmission through space
a	Ambiguity parameters in the LAMBDA method
b	Position vector in the LAMBDA method
$\ddot{x}$	Receiver acceleration
u_k	Receiver acceleration associated noise
f	Process function in the system
g	Observation function in the system

F	Process matrix in the Kalman filter
Q	Process covariance matrix in the Kalman filter
R	Measurements covariance matrix in the Kalman filter
X	State space vector in the Kalman filter
Y	Observation vector in the Kalman filter

LIST OF ACRONYMS

ADR	Accumulated Doppler Range
BIE	Best Integer Equivariant
BOC	Binary Offset Code
C/A	Coarse Acquisition
DD	Double Difference
DGPS	Differential GPS
DLL	Delay Lock Loop
DOT	Department Of Transport
EGNOS	European Geostationary Navigation Overlay Service
ESA	European Space Agency
EU	European Union
FAA	Federal Aviation Administration
FLL	Frequency Lock Loop
GAGAN	Global And Geo Augmentation System
GBAS	Ground Based Augmentation System
GLONASS	GLObal NAvigation System
GNSS	Global Navigation Satellite System
GPS	Global Positioning System
GUI	Graphic User Interface
IA	Integer Aperture
IB	Integer Bootstrapping
IGS	International GNSS Service
ILS	Instrument Landing System
ILS	Integer Least Squares
INS	Inertial Navigation System
IR	Integer Rounding

ITRF	International Terrestrial Reference Frame
LAAS	Local Area Augmentation System
LAMBDA	Least-squares AMBiguity Decorrelation Adjustments
LT	Lock Time
MBOC	Multiple Binary Offset Code
MSAS	Mult-functional Satellite Augmentation System
PCF	Probability of Correct Fix
PDOP	Position Dilution of Precision
PLL	Phase Lock Loop
PPP	Precise Point Positioning
PRN	Pseudo-Random Noise
PVT	Position Velocity Time
QZSS	Quasi-Zenith satellite System
RTK	Real Time Kinematics
SA	Selective Availability
SBAS	Satellite Based Augmentation System
SD	Single Difference
SV	Space Vehicle
TEC	Total Electron Content
WAAS	Wide Area Augmentation System

LISTE OF MEASURE UNITS

GEOMETRIC UNITS

Length

km	kilometer
m	meter
dm	decimeter
cm	centimeter
mm	millimeter

Angle

rad	radians
º	degree
’	minute arc
”	second arc

MECHANIC UNITS

Speed

m/s	meter per second
km/h	kilometer per hour
rad/s	radian per second

Acceleration

m/s^2	meter per second square
rad/s^2	radian per second square

Jerk

m/s^3	meter per second cube
rad/s^3	radian per second cube

TIME UNITS

h	hour
min	minute
s	second
ms	millisecond
µs	microsecond
ns	nanosecond
ps	picosecond

FREQUENCY UNITS

Hz	hertz
GHz	gigahertz
MHz	megahertz

THERMAL UNITS

°C	Celsius degree
K	Kelvin degree

ATMOSPHERIC UNITS

Pa	Pascal pressure

INTRODUCTION

The Global Positioning System (GPS) has transformed the world around us. Today, everyone is able to locate himself precisely on Earth. It has changed the human relation toward space and travels. But this system is also used for the planet itself. With GPS, surveyors and geophysics analyze data to determine the exact geodesy of the planet. It can also monitor small changes in sea level or tectonic movement. How is it possible to achieve such precision and interesting capabilities with this satellite system?

The precision of the GPS improved constantly. When the GPS was launched, the SA (Selective Availability) system intentionally induced noise in the GPS satellite clock, to degrade the position solution. The position solution for civilian was precise at around 100 meters. In May 2000, SA was turned off and the system suddenly becomes more precise, around 5 to 10 meters for civilian users. SA could be overcome because differential positioning technique appeared and this technique is able to remove SA by using differential corrections from a base station. This major technique brings new solution in high precision positioning, such as Real Time Kinematic (RTK).

The basis of RTK technique is to use differential correction from a base station to improve the solution precision. It also uses at the same time the carrier-phase of the signal instead of the common code-phase, for satellite to receiver range determination. In fact, the phase is up to one hundred times more precise than the code itself, allowing a corresponding precision in the solution. The main drawback of using the carrier-phase in RTK is the necessity of an ambiguity resolution technique. Indeed, the carrier phase keeps track of the satellite receiver distance changes at the beginning of each satellite locking, but does not know the initial ambiguity distance. This unknown is called the ambiguity and is an integer cycle in differential technique. The development of RTK has been possible using new integer ambiguity resolution ‘on the fly’. It started with the work of Hwang (Hwang 1991) and has been since then intensively developed for commercial receiver (Neumann, Manz et al. 1996) or real-time industrial system (Kim and Langley 2003).

But the technique still has problems to overcome in order to become a widespread used technique. First, ambiguity resolution and validation is still a major issue, both for solution precision, and also for solution integrity (Teunissen and Verhagen 2007). But the main problem facing the industry is the development of long baseline, when the distance between the base and the rover (i.e. the mobile using the GPS receiver) increased to 100 km and more (Kim and Langley 2000). At this point, the main errors decorrelate and are not completely removed in differential technique, as it is in short baseline (less than 20 km) and in medium baseline (from 20 to 80 km). Atmospheric delays, ephemeris error, degrade the ambiguity resolution success and the solution precision.

The purpose of this work is to overcome these limitations and bring the full RTK precision to real-time long baseline positioning. Our industrial partner, Gedex inc, based in Toronto, need real-time high precision positioning for an aircraft doing mineral survey across Canada with INS material. To achieve this goal, different works have been done in the GRN (Navigation Research Group) at LACIME. First, a state-of-the art real-time RTK algorithm has been developed, mainly working in static and dynamic short baseline scenario, using real-time data from Novatel receiver and the developed LACIME-NRG universal GNSS receiver. Then, the goal was to analyze the specific errors in long baseline, and to find innovative solutions for the new RTK software.

This thesis will start with the history of GPS satellite constellations and signals. It will bring an interesting perspective of the GPS development and the benefit of new coming constellations and new signal frequencies. History of precise positioning is presented as well as the actual and upcoming related technologies. In the second chapter, the observations from the GPS system, namely the pseudo-range, the carrier phase and the Doppler, which are needed to perform a position, are detailed intensively. The errors and parameters related to these signal measurements are analyzed and studies will be presented to correctly define them. The differential technique used in RTK which remove these errors in short baseline is presented with special care.

The chapters three presents the real-time Kalman filter theory developed for the RTK algorithm, from the basics to the state-of-the-art details of such applications. The Kalman filter is presented such a way that other new GNSS signals can be easily inserted in the developed solution to improved global future performance. Functional and stochastic model of the Kalman filter, an important point for reliable and robust estimation are presented in detail. The real-time aspect of this section is highlighted, presenting the different challenge for a robust solution in real-time, as satellite selection and robust ambiguity resolution.

The last two chapters are dedicated to data analysis and performance results. First, the chapter four presents short baseline scenario in static and dynamic mode. Short baseline static tests are used to validate the basics of the developed real-time RTK algorithm. The LACIME-NRG universal GNSS receiver is used and its performances are compared to the Novatel receiver using the algorithm, showing promising results for further research on new signals tracking and positioning technique. Other short baseline test are analyzed, both in static and dynamic mode. The solution precision is at the centimeter level.

In the chapter five, the long baseline problem is finally presented and developed. A real-time ionosphere errors modeling is presented in details, as well as geometric error corrections. Medium static baseline test are analyzed. These tests show faster ambiguity results than classic technique and centimeter precisions. Finally, the long baseline data coming from Gedex are processed with the developed RTK algorithm. The solution shows centimeter precision and has millimeter similarity to the commercial post process Novatel software called Waypoint. This is very promising for further applications and research in the field of high precision RTK positioning.

The conclusion will end this thesis and will summarize the works done during this master degree, the obtained results and the contributions of the Author. Finally, a list of recommendations for further works will be presented in details to orient future research on that field in the NRG laboratory.

CHAPITRE 1

HISTORY AND PERSPECTIVE OF GNSS FOR PRECISE POSITIONING

1.1 Overview of GNSS history

In this section, a brief overview of the Global Navigation Satellite Systems (GNSS) is presented and how it is related to the high precision positioning capabilities offered to the users, both actually and in the future. The GNSS are mainly composed nowadays of the U.S Global Positioning System (GPS) and the Russian GLObal NAvigation Satellite System (GLONASS), but the European Union (EU) has already 2 satellites in orbit with his GALILEO system and China has satellites in orbit with his COMPASS system (also known as Beidou-2) The number of signals available for the users is also increasing, allowing more and more possibilities with new signal processing techniques.

All these systems will provide worldwide positioning capabilities to users. Many others systems (commercial or not) can improve the overall accuracy. One of the most known systems is WAAS (Wide Area Augmentation System), which is a Satellite Base Augmented System (SBAS). But there exist others SBAS like EGNOS (European Geostationary Navigation Overlay Service) or StarFire (Sahmoudi, Landry et al. 2007), and many Ground Based Augmentation System (GBAS) such as Differential GPS (DGPS), which provide corrections and drastically improve the precision for all users, from military to Safety-of-Life operations. Finally, the Real Time Kinematics (RTK) is one of the most precise systems, allowing performance accuracy at the centimeter level.

New techniques have been developed in the past few years to achieve the precision of such systems using only one receiver. The PPP (Precise Point Positioning) system is one of them. It uses undifferenced measurements and, as for RTK, an ambiguity resolution technique. In the same way, network RTK allows users to only one GPS receiver using multiple base corrections.

1.2 Evolution of the GNSS and the satellite constellations

1.2.1 GPS Space Segment: from Block II to Block IIF

The GPS has started with NAVSTAR and the first satellite was launched in 1978 by the U.S Air Force. The GPS constellation is now composed from different generation of satellites: the II/IIA block, the IIR/IIR-M block and the IIF block which is actually in deployment.

The 9 satellites of Block II Satellite Vehicle (SV) were launched from February 1989 through October 1990. None of them is actually in use. The 19 Block IIAs satellites were launched from November 1990 through November 1997. Actually 6 of them are out of use. Despite a design life of 7.5 years, the first constellation of GPS satellite shows an incredible robustness. The satellite Pseudo-Random Noise (PRN) 01 launched on November 1992 was only decommissioned on March 2008, after 16 years of active service! The Block II was implemented with SA capabilities (GlobalSecurity 2007).

The next generation of satellite, the IIR and IIR-M Block, manufactured by Lockheed Martin, were designed to have 33% lower cost and more autonomous capacities. The IIR-M capabilities include developmental military-use-only M-code on the L1 and L2 signals and a civil code on the L2 signal (namely L2C). For block IIR, 12 satellites were successfully launched from July 1997 to November 2004. The first IIR-M Block satellite was launched on September 2005 and 6 are actually in orbit. This makes a total of 32 active GPS satellites in use for general users nowadays.

The GPS IIF satellites will have all of the capabilities of the previous blocks, but will feature an extended design life of 12 years, faster processors with more memory, and a third civil signal, L5. The first launch is planned for 2010. A total of 12 block IIF GPS satellites constellation is planned.

Table 1.1
Evolution and characteristics of the GPS Blocks

	Block II	**Block IIA**	**Block IIR**	**Block IIR-M**	**Block IIF**	**Block III**
First launch	1989	1990	1997	2005	2010	~2014
# of SV	9	19	13	6	12	/
# in Use	0	13	12	6	0	/
Planned	completed	completed	completed	9	12	8
Signals	L1 (C/A), L1/L2-P	L1 (C/A), L1/L2-P	L1 (C/A), L1/L2-P	+L1M/L2M, +L2C	+L5	+L5

1.2.2 Other satellite constellations

The Russian system named GLONASS, began service in 1983 and was already an operating system like GPS in 1995. The GLONASS constellation consisted of 24 satellites. The lifetime of the satellite constellation was short and the economical and political situation in Russia made the system declined and lost credibility. Today, this system is pursuing successfully and GLONASS commercial receivers, like Javad receivers, can propose higher precision than GPS-only. Twenty-one GLONASS satellites are operating nowadays. The system is intended to be further developed for worldwide users. In a same time, the Russian government allowed more and more resources to the Federal Space Agency for maintenance and development of the system (RussianSpaceAgency 2007).

The Galileo system is a project under development and is proposed to be a 30 satellites navigation system operating by 2013. It is conducted by the EU and the European Space Agency (ESA), to produce a completely autonomous satellite constellation. But the public-private partnership and political situation delayed and drastically changed the program. Today, the Galileo program is financed by the European Community and ESA acts as its procurement and design agent. The 2 Galileo satellites in orbit for now, namely GIOVE-A in December 2005 and GIOVE-B in April 2008, allows the EU to keep the allocated frequencies (Gibbons 2008).

China also has a navigation satellite system under development. The Beidu-2 or COMPASS system will be a constellation of 35 satellites, with 5 geostationary orbit satellites and 30 medium earth orbit satellites which will offer complete coverage of the globe (Gibbons 2008). Compass-M1 is the first experimental satellite launched by China for signal testing, validation and for the frequency filing on April 13th 2007.

One another new coming satellite system to be mentioned is the one by Japan, the Quasi-Zenith Satellite System (QZSS) that will supplement and be interoperable with GPS.

All these system developments show the economic and strategic importance of satellite navigation in nowadays commercial applications and economy. Taking GPS as a model and trying to improve it, the new satellite constellations will be a great benefit for users. There will be more satellite coverage, more interoperate signals, more robustness and this will improve accessibility and precision for the user's applications. On the other hand, nations who develop new constellations will become more independent towards GPS.

1.2.3 SBAS system, a novel constellation

SBAS is a general term referring to any satellite-based augmentation system that supports wide-area or regional augmentation through the use of additional satellite-broadcast messages. The purpose of the SBAS system is to provide corrections of various errors corrupting the GPS code and carrier measurements, such as the atmospheric delay, the satellite clock error, and to provide satellite ephemeris corrections. As a consequence of its importance, SBAS system can be considered as a new proper satellite constellation, improving the precision and accuracy of the already existing ones.

WAAS was the first SBAS to be developed for the North American continent by the FAA (Federal Aviation Administration) and the U.S DOT (Department of Transportation) in 1994. It currently consists of 2 geostationary satellites covering the US and 38 reference stations

located in the US, Alaska, Canada and Mexico. These reference stations monitor the GPS signals and provide corrections to the user. It computes the estimated ionosphere errors for every 5x5 degrees grid spaces. These corrections are then transmitted to the WAAS satellite which broadcast the correction to the users.

The main function of WAAS, besides increasing overall accuracy, is to bring better integrity performance. Integrity refers to the availability and the confidence of the computed position. For example, the FAA has defined the CAT (category) 1 standards for Instrument Landing System (ILS) (FAA 1990). It provides standards for en-route phase of flight to approach and landing with minimum visibility. WAAS associated with GPS meet this requirements since 2007 and allow 1.6m positioning accuracy 95% of the time (FAA 2008).

The European Geostationary Navigation Overlay Service (EGNOS) is also a SBAS on development by the European Space Agency. It consists of 3 geostationary satellite and different reference stations. The system started its initial operations in July 2005, and proposes a 3 meter positioning accuracy 95% of the time and enhanced integrity (Gauthier, P.Michel et al. 2001). The Multi-functional Satellite Augmentation System (MSAS) and the GPS and Geo Augmented Navigation system (GAGAN) are also SBAS system from Japan and India.

Two commercial SBAS systems have been developed in recent years: the Starfire and the Omnistar networks. These systems have worldwide satellite coverage to provide corrections to GPS receiver who bought the subscription. The accuracy proposed is sensibly the same for both networks and it is the best precision accuracy possible with a single receiver (Sahmoudi, Landry et al. 2007). The Starfire network have been developed by John Deere Navcom and proposes since 2004 a SF2 service with standard deviation precision below 10 cm (Starfire 2008). Omnistar developed by Fugro has 3 different services, VBS, HP, and XP, where XP offers also a 10 cm precision (Omnistar 2008).

1.3 Signals for high precision positioning

1.3.1 Actual GNSS signals

There are mainly 3 frequencies in use for GPS: L1 (1575.42 MHz), L2 (1227.64 MHz) and L5 (1176.45 MHz). These frequencies are used with different types of code, for different users and type of application (civil or military).

The Block II of satellites broadcast on the L1 and L2 band. A Coarse/Acquisition (C/A) code is broadcast on L1 and is accessible to all users. A precise code or P(Y) is broadcast on L1 and L2 and the navigation message was only accessible for military purpose. The precision of the position with the C/A code can reach 5 meters easily, but when the Selective Availability (SA) was on in the beginning of GPS, the user could only achieve a 100 meters precision on the position. With the removal of SA, the improvement in the ground segment and the benefits of SBAS, the precision is now at the meter level.

The new L2C code is available since January 2006 with the IIR-M satellite block. L2C was designed for civil use. It is transmitted with a higher effective power to improve the performance of GPS receivers in urban areas and indoors, as well as providing a dual-frequency measurement for improved atmospheric correction (Leveson 2006).

The Block IIR-M satellites will broadcast new message and code. The M (for 'Modernized') code is military code and will be broadcast on L1 and L2 band. It was designed to further improve the anti-jamming and secure access of the military GPS signals. Unlike the P(Y) code, the M-code is designed to be autonomous, meaning that a user can calculate their position by directly using the M-code signal.

GLONASS satellites transmit two types of signal: a standard precision (SP) signal and an high precision (HP) military signal. Both signals are centered on L1 (1602 MHz) and L2 (1246 MHz) but using Frequency Division Multiple Access (FDMA) techniques, so each satellite transmits on its own frequency. The HP signal is broadcast in quadrature with the SP

signal, and it shares the same carrier wave as the SP signal, but with a higher bandwidth. The precision of the SP GLONASS signals is about 50 meters, which makes it interesting only combine with GPS (Glonass 2008).

1.3.2 New GNSS Signals

With the rise of new constellations like GALILEO and the modernization of GLONASS, it was necessary to have international agreement to interoperate the different signals between them. Interoperating means to be easy to use by the user and to prevent common jamming. As a consequence, the GPS Block III will broadcast a L1C signal; compatible with the E1 signal of Galileo (1575.42 MHz). It will be broadcast at a higher power level, and include advanced design for enhanced performance.

GALILEO will mainly broadcast 6 signals in the E1 (1575.42 MHz), E5 (1191.795 MHz) and E6 (1278.75 MHz) frequency bands. It is a compromise for all the different kinds of application needed. The *open service* uses the signals at L1, E5a and E5b for high precision service. The *safety-of-life* services are based on the measurements obtained from the open signal and use the integrity data carried in special messages designated for this purposed within the open signals. The *commercial service* is realized with E6. The *Public Regulated Service* is realized by E1 and E6. These signals are encrypted, allowing the implementation of an access control scheme. The Galileo signals uses in general the Binary Offset Carrier (BOC) and the Multiplexed Binary Offset Carrier (MBOC) modulation (Avila-Rodriguez, Hein et al. 2008).

GPS broadcasts a L5 signal with the Block IIF and IIR satellites. It has a spreading code rate 10 times that the C/A code and also a code length ten times longer. These properties make it a more robust and reliable signal, which will also be used as a safety-of-life signal. All these new signals are based on the previous development of GPS and will be more robust and reliable, allowing more service and more precision for a wider variety of users. For more information on the promising L5 civil signal, one can refer to (ARINC 2005).

1.4 From DGPS to network RTK

Differential GPS could take its origin from astronomy interferometers and the use of multiple telescopes to compute a single image. Indeed, using two close-by receivers and differentiating the signals can remove important common errors. The U.S Coast Guard first used differential code pseudo-range GPS to remove the effect of Selective Availability (SA), which was the same for two close-by receivers. These system leads to radical improvement in accuracy and the development of DGPS.

The RTK system takes ideas from DGPS and uses differential corrections to have a solution free from common errors. The improvement with RTK technique is the specific use of the precise carrier phase and the computation of a relative position (i.e. relative to a reference station).

1.4.1 Differential Global Positioning System

DGPS is more refer here as local DGPS compared to wide area DGPS, like WAAS, MSAS or EGNOS. The DGPS principle is based on a reference station, whose position is known, that collects the GPS measurements and computes measurements corrections. These corrections come mainly from the satellites' ephemerides and clocks errors, and the atmospheric delays. They are then transmitted through radio frequency to users able to receive them (usually from 100 kHz to 1.5 GHz).

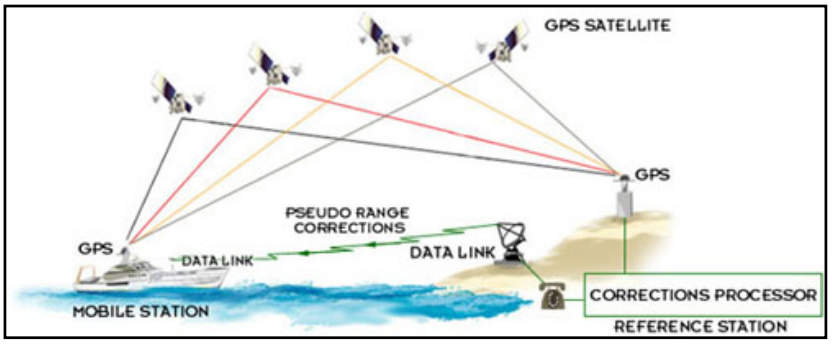

Figure 1.1 Principle of DGPS for marine coast guard.
from http://www.magellangps.com

The success of maritime DGPS service has led to development of the Nationwide Differential GPS (NDGPS) in the United States. With one hundred of reference stations across the country, the accuracy of a single receiver receiving corrections can reach sub-meter accuracy near the base station (Allen 1999). Many countries developed their own network to enhance the accuracy for users. The applications and the requirements for such system are increasing, from farmers to train transportation, or maritime safety. The Local Augmentation Area System (LAAS), an aircraft landing system, is also under development by the FAA to provide category III landing (zero-visibility and precision < 1m).

To provide DGPS radio corrections, the RTCM-104 standard can be used, and has been developed by the Radio Technical Commission for Maritime. It standardized corrections transmissions for observations (message RTCM1819), atmospheric delays (message RTCM15), position (message RTCM3), and others errors sources. For more details on RTCM standards, please refer to (RTCM 2001).

1.4.2 Development of RTK technology

The RTK technology appears in the early 1990's with the use of the carrier phase measurements instead of the C/A code. In fact, the carrier phase measurements is a 'gift' from the US army to the civil users since it was not originally intended to be of any use in the original project. It is impressive, because the carrier-phase is a much more precise observation. But in the same time, it has some inherent ambiguity which needs to be resolved. Long static observations sessions were necessary to obtain accurate precision and kinematic use was not possible in the beginning. An important step has been made by the development of the ambiguity resolution 'on-the-Fly' (i.e. on the move) and proper algorithms to resolve the ambiguities in a short term (Hwang 1991) or (Talbot 1991). This technique estimates at the same time the ambiguities and the baseline position in the Kalman filter state space vector.

The principle of RTK is to combine the carrier-phase measurements from the reference station and the user's receiver to obtain double difference observations where the sought position is the baseline between the two receivers. Only the carrier phase is used in the process due to its precision. Indeed, the precision of the carrier-phase when the ambiguities are resolved is phenomenal compared to the C/A code: 1-2 mm precision compared to 1 meter. This system has been very attractive for survey and geophysical purposes and is still widely used.

1.4.3 Future evolution of RTK

RTK is a relatively mature technology nowadays, although it is still very costly. The guaranteed precision is not always achievable in short terms and the kinematic precision in real-time requires static observations and validation steps. In addition, the long baseline issue, especially for ambiguity resolution, and the radio link are also crucial. The distance between the reference receiver and the user receiver cannot exceed a certain amount without degrading the accuracy. And the radio link between the base and the rover has to be robust enough to guarantee continuous and reliable data transfer to ensure high precision positioning.

Network RTK has also been an important development in the survey and geodetic community recently. Some countries developed their existing reference station network to broadcast nationwide RTK correction across country using different communication networks. If this RTK system can provide accurate positioning for baseline length of less than 40 km in 'small' countries like in Europe, the challenge is more important for vast countries like Australia, USA or Canada, where the cost of a reference station compared to the number of user is prohibitive (Zhang, Wu et al. 2007). Commercial RTK networks are also provided by industrials like Trimble, for example. The complexity of setting up such network system for real-time applications studies could be prohibitive for universities research.

Network RTK may be a solution for long baseline distance problems, but it is very expensive and has to be deployed efficiently. It is also more difficult to achieve the equivalent one baseline precision of RTK. The ambiguity resolution and their integrity is also still a current matter of research (Teunissen and Verhagen 2007) and new techniques are needed to improve reliability, execution time, and cost.

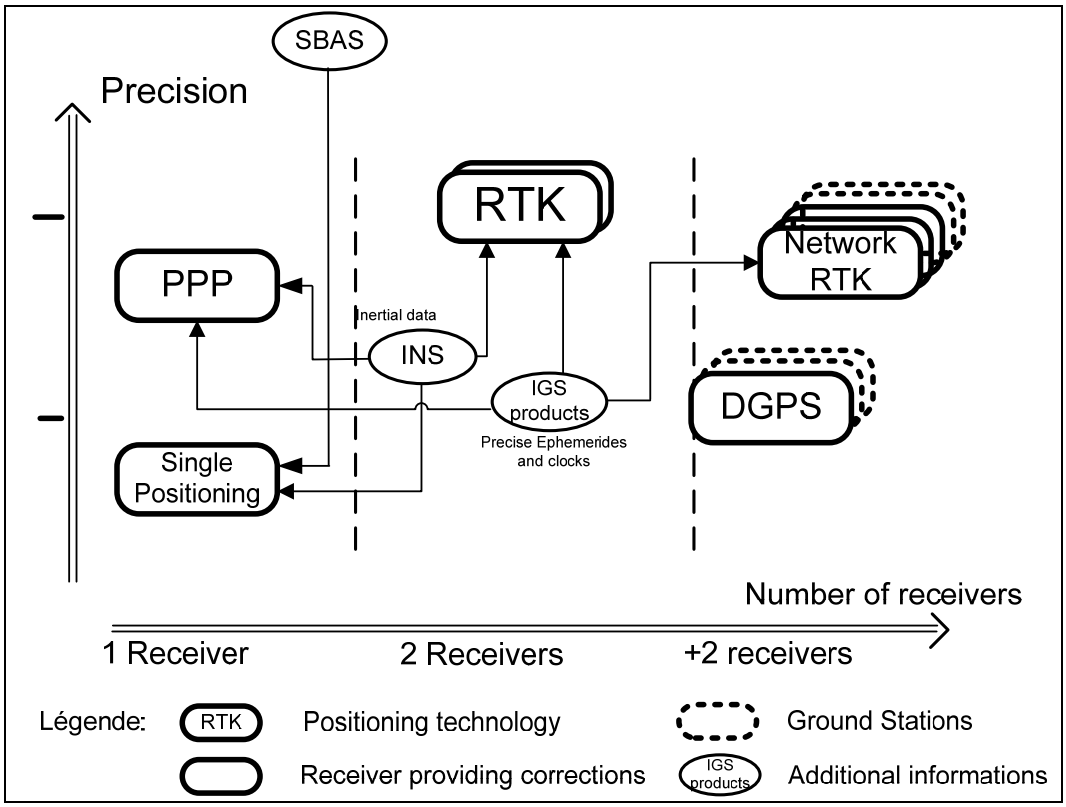

Figure 1.2 Summary of the different positioning technology in terms of precision and number of receivers.

On the other hand, Precise Point Positioning (PPP) technique is also promising for the future. It can provide centimeter precision to the users, since it also uses the carrier-phase measurement with ambiguity resolution. It uses IGS products for precise satellite orbits, as well as pseudo-range and carrier phase combination for ambiguity resolution. The main advantage is that the receiver is in stand-alone mode and does not need any additional base station or differential link. The main drawback is a long convergence time (~ hours) and a

lack of robustness. Many research are made in this domain, for undifferenced ambiguity resolution (Banville, Santerre et al. 2008), (Laurichesse and Berthias 2008) and low cost PPP receiver (Beran, Langley et al. 2007).

The RTK technology remains a dominant high precision positioning system in the industry and research. Its efficiency and precision brought new perspective for precise positioning and applications. Its main drawback, the non-common mode errors and the long baseline problem, can be overcome in many ways, as it will be developed in this thesis. With improved atmospheric errors modeling, robustness, fast ambiguity resolution, and a cheap baseline link, the RTK is a technology on the way for further innovative high precision applications. It is expected in the future that the use of new signals and constellations will improve the overall performance of ambiguity resolution, as well as integrity and stability.

CHAPITRE 2

OBSERVATIONS FROM THE GPS SIGNALS AND THEIR ASSOCIATED ERRORS FOR PRECISE POSITIONING

2.1 Backgrounds

Theoretically, to determine its 3D position, a GPS receiver use the 'true' distances to 3 satellites with known position and resolve the navigation equation. This is the ultimate goal to find the user's position. Unfortunately, these scenarios will never happen, because of the signal errors that induce incertitude in the receiver-satellite distance (e.g. clock bias), and because of the uncertainty in the satellite positions. The goal of this section is to describe all the errors that can corrupt the GPS signals and the position determination.

To obtain the distance between the satellites and the receiver, the user can use two main observations: pseudo-range and carrier-phase measurements.

The pseudo-range measurement uses the C/A code or P(Y) code to obtain the transit time of the GPS signal through the vacuum and atmosphere. By doing so, it provides the noisy distance between the satellites and the receiver. This observation is the easiest way to find the user's position and has been widely used in the beginning of GPS and also nowadays for low-cost single receiver, although its accuracy is very limited.

On the other hand, the carrier-phase measurement is much more precise and can provide position accuracy to the centimeter level in relative mode. This measurement comes from the discriminator of the PLL and the tracking of the phase of the GPS signal. Its main drawback is that an unknown number of integers are present in the measurement and need to be estimated to determine the true distance between the satellite and the receiver. This is known as phase ambiguity and will be the discussion of section 3.3.

2.2 Pseudo-range and carrier phase observations overview

2.2.1 Pseudo-range measurement

The pseudo-range represents the true distance ρ between the receiver k and the satellite p, and its associated errors Δρ. It is obtained using C/A code of the GPS signal.

To obtain the pseudo-range, the time of emission of the GPS signal is needed. To do so, the receiver counts the amount of chips and fraction of chips of the C/A code to align the code replica, generated at the receiver, with the signal emitted by the satellite. With the Z-count included in the current navigation message at the beginning of the subframe, the receiver can have the time of emission of the satellite. The chip's length of the C/A code is 1ms and is measured with the DLL.

Comparing the time of emission versus the time of reception, the receiver can calculate the transit time of the GPS signal (between 60 ms and 80 ms) and thus obtaining the pseudo-distance or pseudo-range.

$$P_k^p = c[t_k(t) - t^p(t-\tau)] \tag{2.1}$$

$$P_k^p = \rho_k^p + \Delta\rho \tag{2.2}$$

and

$$\rho_k^p = \tau c \tag{2.3}$$

Where:

t	is the reference GPS time,
τ	is the transit time,
$t_k(t)$	is the time of reception for receiver k,
$t^p(t-\tau)$	is the time of emission of satellite p,
P_k^p	is the pseudo-range [m],

ρ_k^p is the true geometric distance [m].

Unfortunately, the clock receiver has some inherent bias, as the satellite clock. This introduces large errors in the pseudo-range. The time of emission and reception can be related to the true GPS time as (Misra and Enge 2006):

$$t_k(t) = t + \delta t_u(t) \tag{2.4}$$

$$t^p(t-\tau) = (t-\tau) + \delta t^p(t-\tau) \tag{2.5}$$

There are also the errors due to the atmospheric delay (troposphere and ionosphere), the multipath, the hardware delay and the random error. All of these lead to the final expression of the pseudo-range (Leick 2003):

$$\begin{aligned} P_k^p(t) = \rho_k^p(t) - c[dt_k(t) - dt^p(t-\tau)] + I_{k,P}^p(t) + T_k^p(t) \\ + d_{k,P}(t) + d_{k,P}^p(t) + dM_P^p(t) + \varepsilon_P \end{aligned} \tag{2.6}$$

Where:

$P_k^p(t)$	is the pseudo-range of satellite p measured by the receiver k at time t,
$\rho_k^p(t)$	is the true-distance receiver-satellite,
dt_k, dt^p	are the receiver and the satellite clock bias respectively,
$I_{k,P}^p(t)$, $T_k^p(t)$	are the ionospheric and the tropospheric delays respectively,
$d_{k,P}(t)$, $d_P^p(t)$	are the receiver and satellite hardware code delays respectively,
$dM_{k,P}^p(t)$	is the multipath error,
ε_P	is the pseudo-range random noise.

Usually, the receiver clock error can be estimated using 4 satellites and an estimation process (least-square estimator or Kalman filter). The satellite clock error is computed using the parameters included in the navigation message (*see* Appendix A).

2.2.2 Carrier phase measurements

The carrier phase observable is the difference between the received satellite carrier phase and the phase of the internal receiver oscillator. The measurements are recorded at equally spaced time. As the distance between the satellite and the receiver changes in time, the carrier phase difference changes with the same proportions. The carrier phase observable represents the distance variations between the satellite and the receiver. If integrated over time, it can reflect the distance between the receiver and the satellite from the beginning of tracking.

The carrier phase measurements can be expressed in units of cycles and is sometimes referred as Accumulated Doppler Range (ADR). It is a much more precise measurement than the pseudo-range measurement. But it is obvious that there exists a certain amount of cycles, representing the initial distance, which is unknown at the beginning of the tracking. This unknown number of cycle is referred as phase ambiguity and needs to be estimated to obtain the full receiver-satellite range (Figure 2.1).

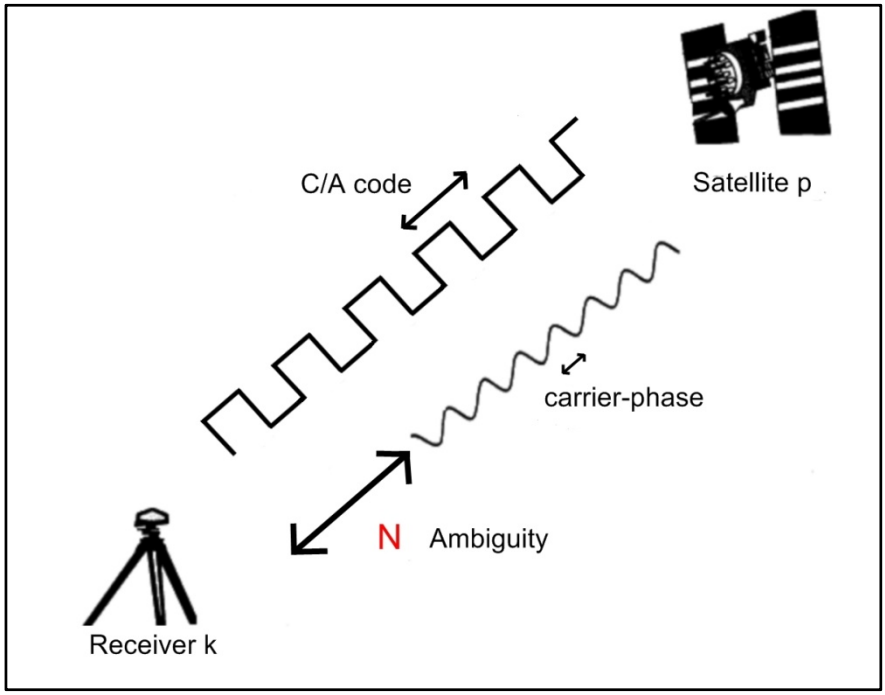

Figure 2.1 Representation of the carrier-phase measurement's ambiguity.

The ADR for receiver k and satellite p can be expressed as:

$$\varphi_k^p(t) = \varphi_k(t) - \varphi^P(t) + N_k^P \tag{2.7}$$

Where:

$\varphi_k^p(t)$	is the ADR of receiver k from satellite p [cycles],
$\varphi^P(t)$	is the received satellite phase,
$\varphi_k(t)$	is the phase of the receiver internal oscillator,
N_k^P	is the initial carrier phase ambiguity.

The initial ambiguity term N_k^P is added in equation (2.7) because there is no way that the receiver phase lock loop knows at which cycle its starts locking. The ADR will add measurements until it loses the lock which is the case where the ADR has to be reset.

The idea in the development of the carrier phase equation is the equivalence of the received phase and the emitted phase at the satellite, exactly τ second earlier (Leick 2003) :

$$\varphi^p(t) = \varphi_T^p(t-\tau) \tag{2.8}$$

And using the satellite frequency model, (2.8) is expanded as:

$$\varphi_T^p(t-\tau) = \varphi_T^p(t) - (f + a^p)\tau \tag{2.9}$$

Where:

$\varphi^P(t)$	is the received satellite phase [cycles],
$\varphi_T^p(t-\tau)$	is the phase emitted by the satellite [cycles],
$\varphi_T^p(t)$	is the satellite phase at the time of reception [cycles],
a^p	is the frequency offset of the satellite clock [Hz],
f	is the signal frequency [Hz],

τ is the time of transmission through space [s].

Using the equation (2.7), the clock error terms is added to the carrier measurements and the term $\varphi_k(t)-\varphi_T^p(t)$ is incorporated in the clock error terms of the satellite and the receiver. The final equation is:

$$\varphi_k^p(t) = -fdt_k + fdt^p + (f + a^p)\tau_k^p + N_k^P \tag{2.10}$$

Using (2.3) and the different terms expressed in (2.6), the final equation of the received phase, or ADR are obtained:

$$\begin{aligned}\varphi_k^p(t) = \frac{f}{c}[\rho_k^p(t) - I_{k,\varphi}^P(t) + T_k^P(t)] - fdt_k + fdt^p + N_k^P \\ + \frac{a^p}{c}\rho_k^p(t) + d_{k,\varphi}(t) + d_\varphi^P(t) + dM_{k,\varphi}^P(t) + \varepsilon_\varphi\end{aligned} \tag{2.11}$$

Where:

$\rho_k^p(t)$	is the true geometric range between the receiver and the satellite [m],
dt_k, dt^p	is the receiver and satellites clock errors respectively [s],
N_k^P	is the initial carrier phase ambiguity [cycles],
$I_{k,\varphi}^p(t)$,	is the ADR ionospheric delays [m],
$T_k^p(t)$	is the tropospheric delay [m],
a^p	is the frequency offset of the satellite clock [Hz],
$d_{k,\varphi}(t)$, $d_\varphi^p(t)$	are the receiver and satellite hardware phase delays respectively
$dM_{k,\varphi}^p(t)$	is the multipath errors [cycles],
ε_φ	is the phase random noise [cycles],
f	is the signal frequency [Hz].
c	is the speed of light [m/s]

As for the pseudo-range, the main errors of the ADR will be coming from the satellite and receiver clock bias and the atmospheric delays. The ambiguity is of main importance in this equation.

2.2.3 Doppler measurements

The motion of the satellite and/or the receiver induces changes in the observed frequency of the signal. It is referred as the Doppler shift and indicates the relative motion between the satellite and the receiver. This Doppler measurement is measured routinely in the phase lock loop (PLL) of the receiver during acquisition and tracking. This PLL provides frequency variations for the Doppler measurements as well as phase variations by the ADR measurements.

The Doppler measurement is equivalent to the carrier-phase rates over the time interval. As a consequence, it can simply be considered as the derivation in time of the carrier-phase measurement between the satellite and the receiver. It is usually use to compute the velocity of the rover, using satellite velocity (Misra and Enge 2006).

$$\dot{\varphi}(t) = \dot{\rho}_k^p(t) - c\,\dot{d}\,t_k + c\,\dot{d}\,t^p - \dot{I}_k^p(t) + \dot{T}_k^p(t) + d_{k,\varphi}^{\cdot}(t) + d_{\varphi}^{P\cdot}(t) + dM_{k,\varphi}^{P\cdot}(t) + \varepsilon_{\varphi}^{\cdot} \tag{2.12}$$

Where:

$\dot{\varphi}_k^p$	is the Doppler measurement [m/s],
$\dot{\rho}_k^p$	is the relative velocity between receiver k and satellite p [m/s],
$\dot{d}\,t_k, \dot{d}\,t^p$	is the receiver and satellites clock drift respectively [s/s],
$\dot{I}_{k,\varphi}^p(t)$,	is the ionospheric drift [m/s],
$\dot{T}_k^p(t)$	is the tropospheric drift [m/s].

The Doppler frequency does not offer more information in the system compared to the carrier phase. It can be used as additional observations to have an estimation of the velocity of the rover.

2.2.4 Summary of the GPS observations

This section is a summary of the three main observations a GPS receiver can provide to users in order to compute their position. The proposed RTK algorithm will use these three measures at the same time in the estimation process.

Table 2.1
Summary of the main GPS observations with associated errors

Pseudo-range measurement [m]:	
$$P_k^p(t) = \rho_k^p(t) - c[dt_k(t) - dt^p(t-\tau)] + I_{k,P}^p(t) + T_k^p(t) + d_{k,P}(t) + d_P^p(t) + dM_{k,P}^p(t) + \varepsilon_P$$	(2.13)
Carrier-phase measurement [cycle]:	
$$\varphi_k^p(t) = \frac{f}{c}[\rho_k^p(t) - I_{k,\varphi}^P(t) + T_k^P(t)] - fdt_k + fdt^p + N_k^P + \frac{a^p}{c}\rho_k^p(t) + d_{k,\varphi}(t) + d_\varphi^P(t) + dM_{k,\varphi}^P(t) + \varepsilon_\varphi$$	(2.14)
Doppler measurement [m/s]:	
$$\dot{\varphi}(t) = \dot{\rho}_k^p(t) - \dot{d}t_k + \dot{d}t^p - \dot{I}_k^p(t) + \dot{T}_k^p + \dot{d}_{k,\varphi}(t) + \dot{d}_\varphi^P(t) + \dot{dM}_{k,\varphi}^P(t) + \dot{\varepsilon}_\varphi$$	(2.15)

The table 2.2 summarizes the measurement errors presented in these observations and a brief analysis of the common-mode errors characteristic.

The pseudo-range and the carrier-phase measurements have in their equations the main parameter to estimate: the satellite-receiver range. These parameters, for all visible satellites, provide the receiver position. All the remaining terms will be errors, delays or additional parameters that have to be evaluated with the most precision to be effectively removed.

Two kinds of errors are presented: the common mode errors and the non-common mode errors. The common errors are the errors in the GPS signal that have nearly identical effects on all receivers operating in a limited area (e.g. atmospheric delays). On the other hand, the non-common errors are specific to a particular geographical location, and are distinc for two receivers, even with small antennae separation. This difference is important since the common-error will be eliminated in the differential GPS and RTK processing for short and medium baseline length.

Table 2.2
Summary of GNSS signal measurement errors

Errors on the signal and the position determination		**Common-mode error**	**Removed in short baseline**
$I_{k,P}^{p}(t)$	Ionosphere delays	X	X
$T_{k}^{p}(t)$	Troposphere delays	X	X
$dt^{p}(t)$	Satellite clock error		X
$dt_{k}(t)$	Receiver clock error		X
$d_{P}^{p}(t)$	Satellite hardware phase delays		X
d^{p}	Satellite clock drift		X
$d_{k,P}(t)$	Receiver hardware phase delays		X
	Ephemeris errors		X
	Satellite Attitude Effects	X	X
	Site displacements Effects	X	X
$dM_{k,P}^{p}(t)$	Multipath		
ε_{P}	Measurement noise		

The ephemeris errors are present in the satellite-receiver distance ρ. It is related to the satellite position error computed using these ephemeris. The satellite attitude and site displacement effects are too small in RTK for baseline below 200 km to figure in the main equations. They will be removed using IGS products in PPP applications (Kouba and Héroux 2001).

In the next sections, the atmospheric and ephemeris errors will be detailed, followed by some of the non-common mode errors as multipath.

2.3 Details of common errors for all the observations

2.3.1 Troposphere delays

The troposphere is the lowest portion of Earth's atmosphere and is mainly composed of dry gases (N2 and O2) and 'wet' gases (primary water vapor) below 4 km, and all of it is below about 12 km from sea surface. The refractive index of the troposphere is slightly greater than unity, which gives rise to a velocity decrease and thus a delay of travel time for the GPS signal. The tropospheric delay can be divided into two main categories, dry and wet delay.

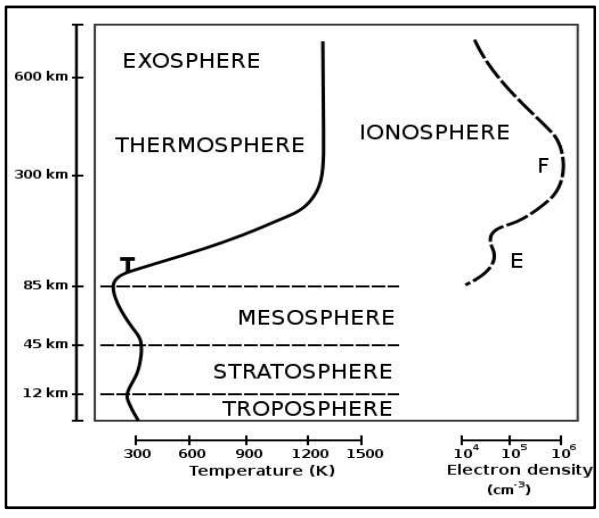

Figure 2.2 Atmospheric layers of the earth.
from (http://en.wikipedia.org/wiki/Ionosphere)

The troposphere is a non-dispersive element for radio wave, which makes it insensitive to the frequency of the GPS signals. The total tropospheric delay can be computed using dry and wet zenith delays and mapping functions for different satellite elevation angle:

$$T = T_{z,d} m_d(el) + T_{z,w} m_w(el) \tag{2.16}$$

Where :

T	is the total tropospheric delay,
$T_{z,d}$	is the zenith dry delay,
$T_{z,w}$	is the zenith wet delay,
m_d	is the mapping function for dry delay,
m_w	is the mapping function for wet delay,
el	is the elevation angle of selected satellite.

The simplest mapping function will be T=1/sin(*el),* which is consistent with a flat Earth but will not be really accurate. The model detailed in (Misra and Enge 2006) can be used instead:

$$\begin{aligned} m_d(el) &= \frac{1}{\sin(el) + \dfrac{0.00143}{\tan(el) + 0.0445}} \\ m_w(el) &= \frac{1}{\sin(el) + \dfrac{0.00035}{\tan(el) + 0.017}} \end{aligned} \tag{2.17}$$

The zenith delays T_z for the wet and dry delays, can be expressed using the Saastamoimen model (Saastamoinen 1972), an empirical model which needs ambient atmospheric pressure, temperature and relative humidity level around the receiver measurements:

$$T_{z,d} = 0.002277(1 + 0.0026\cos 2\phi + 0.00028H)P_0$$
$$T_{z,w} = 0.002277(\frac{1255}{T_0} + 0.05)e_0 \quad (2.18)$$

Where:

$T_{z,d}$	is the zenith dry delay [m],
$T_{z,w}$	is the zenith wet delay [m],
T_0	is the ambient temperature at the receiver position [Kelvin],
P_0	is the ambient total pressure at the receiver position [millibar],
e_0	is the partial pressure due to water vapor at the receiver position [millibar],
ϕ	is the latitude of the receiver [degres],
H	is the orthometric heights of the receiver[m].

In theory, the hydrostatic component of the delay can be predicted in the zenith at the millimeter level. However, the highly variable nature of atmospheric water vapor means that the accuracy of the non-hydrostatic delay is at the centimeter, or even decimeter level in absolute mode, and need further development to be correctly evaluated, for example with estimation process (Collins and Langley 1997).

2.3.2 Ionosphere delays

The ionosphere is located about 50 km to about 1000 km above the Earth and is a region of ionized gases (free electrons and ions). The ionization is caused by the sun's radiation, particularly the extreme ultraviolet (EUV) wavelengths, and the state of the ionosphere is determined primarily by the intensity of the solar activity. Observations have shown that the Sun has a maximum activity cycle of 11 years and that the last maximum occurs during years 2000-2001. The current cycle is near its end and the magnitude of the new cycle is anxiously anticipated (Kunches 2008). The next perturbation should be in 2011-2012 and GNSS receivers should be ready for that.

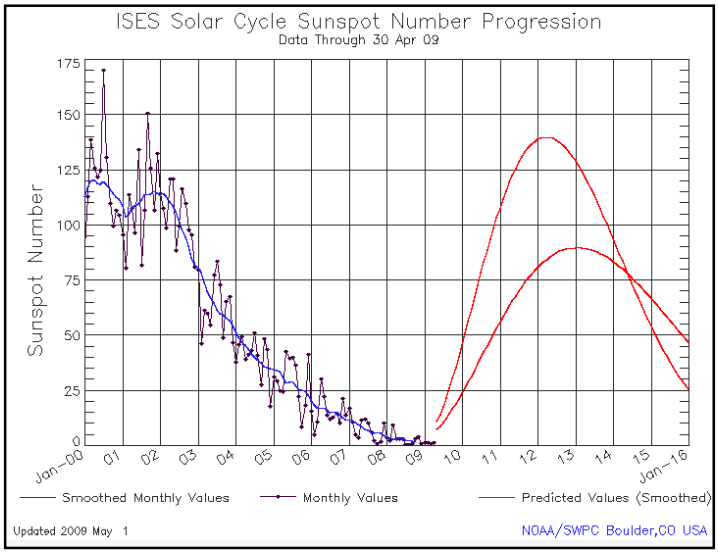

Figure 2.3 Predicted solar activities.
from (noaanews.noaa.gov)

The amount of the GPS signal distortion through the ionosphere depends of the Total Electron Content (TEC), which is defined as the number of electrons in a tube of $1m^2$ cross section extending from the receiver to the satellite:

$$TEC = \int_{k}^{p} n_e(l)dl \tag{2.19}$$

Where $n_e(l)$ is the variable electron density along the signal path l, and the integration is from the satellite p to the receiver k.

The principal disturbances of the GPS signals caused by the layers of the ionosphere are group delay of the signal modulation, carrier phase advance, Doppler shift or phase scintillation (Grejner-Brzezinska, Wielgosz et al. 2006). The TEC in the ionosphere can vary rapidly in time during the course of a day, and under severe geomagnetic disturbances, it can display rapid and significant changes over very short periods of time. As a consequence, the ionosphere stays one of the main sources of errors for single positioning, where it can induce several meters errors in the GPS measurements. In RTK, the ionosphere delay is removed in

short baseline, since the errors stay correlated, but it can be a limiting factor in successful long baseline applications (Kim and Langley 2005).

The phase delay $\Delta\tau_p$ of the GPS signals passing through ionosphere depends of the TEC and their associated frequency:

$$I_\varphi = -I_P = c\Delta\tau_P \tag{2.20}$$

$$\Delta\tau_P = -\frac{40.3TEC}{cf^2} \tag{2.21}$$

Where:

I_φ, I_P	is the phase and pseudo-range ionosphere delay respectively,
$\Delta\tau_P$	is the phase delays of the signal [s],
TEC	is the Total Electronic Content,
f	is the associated carrier frequency [Hz],
c	is the speed of light in vacuum [m/s].

As a consequence, the simplest way for determining the ionosphere delay of the GPS signal is to use L1 and L2 frequency when available, forming the ionosphere-free measurement, using (2.6):

$$\begin{aligned} P_{IF} &= \frac{f_{L1}^2}{f_{L1}^2 - f_{L2}^2}P_{L1} - \frac{f_{L2}^2}{f_{L1}^2 - f_{L2}^2}P_{L2} \\ I_{L1} &= \frac{f_{L1}^2}{f_{L1}^2 - f_{L2}^2}(P_{L1} - P_{L2}) \\ I_{L2} &= \frac{f_{L2}^2}{f_{L1}^2 - f_{L2}^2}(P_{L2} - P_{L1}) \end{aligned} \tag{2.22}$$

Where:

P_{IF} is the iono-free pseudo-range measurement [m],

I_{L1}, I_{L2} is the L1 and L2 ionospheric delay respectively [m],

f_{L1}, f_{L2} is the L1 and L2 frequency respectively [Hz],

P_{L1}, P_{L2} is the L1 and L2 pseudo-range respectively [m].

Unfortunately, if the ionospheric delay is removed in the iono-free code measurement, this measurement is 3 times noisier than the pseudo-range measured at L1 and L2 as it will be highlighted in section 5.2.2.

When the L2 frequency is not available, the user can use the broadcast signal to determine the ionospheric delay. The model, referred as the Klobuchar model, represents the zenith delay as a constant value at nighttime and a half-cosine function in daytime (ARINC Engineering Services 1993). But it is assumed that this process removes only 40% of the errors.

In RTK technique, another method to eliminate the ionospheric delay for the carrier-phase and the pseudo-range is to estimate this delay in an estimation process. This method has the advantage of getting rid of the noise introduced by the iono-free measurement. This method has been successfully introduced and used in the work of (Odjik 2000; Alves, Lachapelle et al. 2002) and (Kim and Langley 2005). Details of this method will be examined for the long-baseline problem and it will be used in the RTK algorithm.

Table 2.3
Errors related to atmospheric delays in absolute mode

	Ionosphere	**Troposphere**	
		Dry delay	Wet delay
Variability	High (ionosphere scintillations)	Low	High
Zenith delay	1 – 10 meters	~ 1 m	~ 1 m
Modeling	~ 60 % (broadcast)	~ 80 %	~ 40 %

2.3.3 Satellite ephemerides errors and its impact on positioning

The satellites position can be computed in real-time using the broadcast ephemerides in the navigation message, which contains the orbital parameters of each satellite. These ephemerides are predicted 24/48 hours in advance by the ground segment and updated every 2 hours to the user. A set of data is usually valid for 4 hours to account for an upload failure. The broadcast satellite ephemeris give the satellite position with a standard deviation in the errors of approximately 1.1 meters with a 0 mean (Warren and Raquet 2003).

The other solution is to use the International GPS Service (IGS) products, which provide different satellite ephemerides, depending on the precision of the satellite's position and clock and the latency of the solution (from near real-time to 13 days delays) (IGSproducts 2008). The most precise ephemerides are the final ephemerides, and the precision is less than 5cm for the satellite precision and less than 0.1ns for the satellite clock error.

Table 2.4
Approximate relation between ephemerides errors dr and
baseline error db from (Leick 2003)

Baseline [km]	**dr [m]**	**db [cm]**
1	20 2	0.1 0.01
10	20 2	1 0.1
100	20 2	10 1

If the precision of the satellite position and clock is a major concern for the PPP solution, in differential techniques, the errors are cancelled for short baseline. In long baseline, the effects of ephemerides errors become relevant only for baselines higher than 100 km. Table 2.4 indicates the effects of the ephemerides errors to the baseline precision.

2.3.4 Other common-mode error

The other common-mode errors that have to account for in a PPP processing and which are cancelled during differentiation are:

1) Satellite Altitude Effects:
a) Satellite Antenna Offsets: the separation between the GPS satellite center of mass and the phase center of its antenna.
b) Phase wind-up: change in carrier phase due to the rotation of satellite or receiver antenna around its vertical axis. Removed in differentiating.
2) Site displacements Effects (relative to ITRF position):
a) Solid Earth Tides: the periodic vertical and horizontal site displacement of the 'solid' earth due to gravitational forces. Unaffected for baseline < 100 km.
b) Ocean loading: identical to solid earth tides, except it results from ocean tides loading. More important in coastal regions but is negligible when differencing.
c) Earth Rotation Parameters (ERP): sub-daily ERP variations (modeled in IGS products).

For more details of the corrections needed for PPP, the reader should consult (Kouba and Héroux 2001)

2.4 Details of non-common errors for all observations

2.4.1 Multipath error

The multipath is a non-common error because it can differ between two receivers in a close area. The multipath is the phenomenon associated with the multiple paths that a signal can take before reaching the antenna. These paths lead to one or more reflections of the signal, delayed and usually weaker than the original one, before reaching the antenna. The measurement becomes the sum of all the reflected signals and leads to significant errors. A reflected signal by more than 1.5 chips of C/A code would be suppressed automatically in the

correlation process because the auto-correlation process for the C/A code is nearly 0 for delays more than 1.5 chip (Misra and Enge 2006).

Attenuating multipath is one of the major concerns nowadays, because reducing its impact can lead to a major increase of GPS/GNSS applications. From indoor positioning to accurate urban positioning, the challenges are vast. Apart from putting the antenna away from the reflectors, there exist different methods to attenuate multipath. One of them will be to use special omnidirectional antenna, like a choke-ring antenna. Development of new correlators (Vision correlator, Narrow correlator) can also lead to significant improvements.

In a software way, it is possible to attenuate multipath by modeling their effect in the estimation process. Assigning an error to the measurements in relation to the multipath can reduce its impact in the estimation process and thus to the quality of the positioning. Generally, an elevation-based stochastic model reduces the multipath effect, because the multipath depends on the elevation angle of the satellites. Recent methods show that a C/N_o based stochastic model is more appropriated and better reflects the multipath dependency (Lau and Cross 2005).

The multipath is still a major issue and the error associated with it can lead to a 5 or 10 meter errors in the position, even with special antenna and control measurements.

2.4.2 Receiver noise

Receiver noise refers to the noise of the measurements. The receiver is always affected by random measurement noise, covering the RF radiations sensed by the antenna, noise introduced by the hardware (antenna, amplifiers, cables) and signal quantization. There are also delays and distortions in the lock loops of the receiver. As a result, the structure of the signal is masked by noise, especially if the signal to noise-ratio is low. . The Table 2.5 presents the noise of the different measurements. The C/A code measurements noise can be reduced using carrier-smoothing processing (Hwang, Mcgraw et al. 1999).

Table 2.5
Receiver noise for C/A code and phase measurements

	Receiver noise
Code phase (C/A)	0.25 – 0.5 m
Carrier phase	0.005 – 0.01 cycle

2.5 Expression of double difference measurements

The principle of double difference is a technique to eliminate the common-error mode between two receivers and different satellites. A reference station is used, with known position, which transmits in real-time its measurements to a user's receiver, or 'rover'. When the carrier phase is used and the ambiguities resolved, the combination of the measurements in real-time from the fixed reference station and the moving rover is referred as RTK. The mathematical expression of the double difference is now detailed.

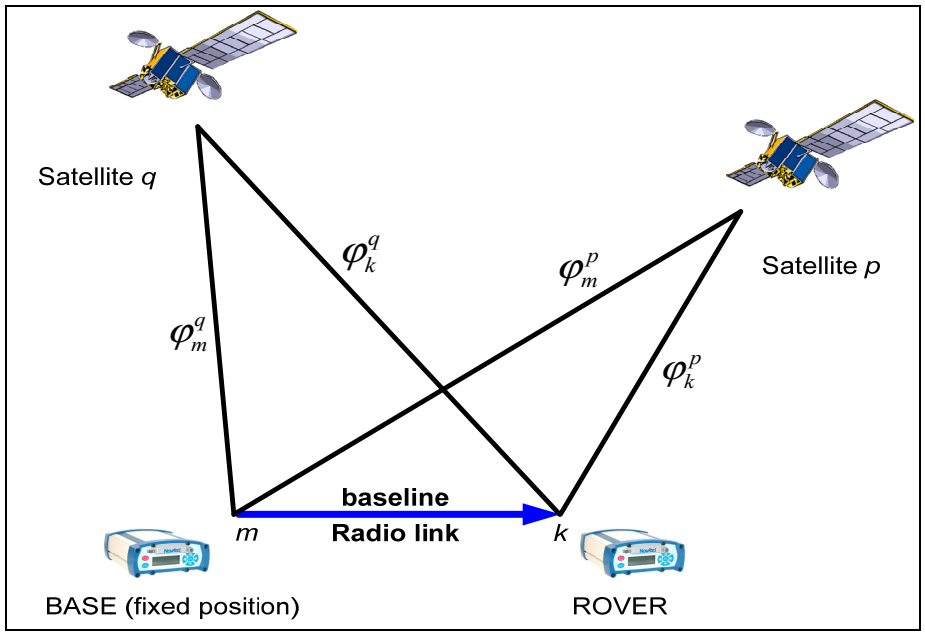

Figure 2.4 Method of double difference between two receivers k and m and two satellites p and q for the ADR measurements.

Usually, one receiver is considered as base and is fixed at a known position, and the other receiver will be the rover. It receives information from the base to compute the desired baseline position. First a Single Difference (SD) is made between the measurements of the two receivers for the same satellite. By making the single difference, most of the satellite related error can be removed, as the ephemeris errors, hardware delays and part of the atmospheric errors. The expression of the carrier-phase measurements p and p for the receiver k and m is detailed in section 2.2.4.

$$\varphi_{km}^{p}(t) = \varphi_{k}^{p}(t) - \varphi_{m}^{p}(t)$$
$$\varphi_{km}^{p}(t) = \frac{f}{c}[\rho_{k}^{p}(t) - \rho_{m}^{p}(t)] + fdt_{k} + fdt_{m} + N_{km}^{p} + \frac{f}{c}T_{km}^{p} - \frac{f}{c}I_{km}^{p} + \varepsilon_{km,\varphi}^{p} \quad (2.23)$$

Where:

φ_{km}^{p}	is the carrier-phase SD between receiver k and receiver m [cycles],
$\rho_{k}^{p}, \rho_{m}^{p}$	are the distances between satellite p and receivers k and m, respectively, [m].
N_{km}^{p}	is the single difference ambiguity [cycles],
T_{km}^{p}, I_{km}^{p}	are the single difference troposphere and ionosphere error [m],
dt_{k}, dt_{m}	are the receivers' clock bias [s],
$\varepsilon_{km,\phi}^{p}$	is the residual errors [m].

Then, the error related to the receiver, as clock's bias, are eliminated by differencing all single difference to the reference single difference, which is made with the satellite of the higher elevation angle, i.e. the reference satellite:

$$\varphi_{km}^{pq}(t) = \varphi_{km}^{p}(t) - \varphi_{km}^{q}(t)$$
$$\varphi_{km}^{pq}(t) = \frac{f}{c}[(\rho_{k}^{p}(t) - \rho_{k}^{q}(t)) - (\rho_{m}^{p}(t) - \rho_{m}^{q}(t))] + N_{km}^{pq} + \frac{f}{c}T_{km}^{pq} - \frac{f}{c}I_{km}^{pq} + \varepsilon_{km,\varphi}^{pq} \quad (2.24)$$

Where:

φ_{km}^{pq}	is the carrier-phase double difference,
ρ_k^p, ρ_m^p	are the distance between satellite p and receiver k and m respectively,
ρ_k^q, ρ_m^q	are the distance between satellite q and receiver k and m respectively,
N_{km}^{pq}	is the double difference ambiguity,
T_{km}^{pq}, I_{km}^{pq}	are the double difference troposphere and ionosphere errors,
$\varepsilon_{km,\phi}^{pq}$	is the carrier-phase residual errors.

The same procedure can be done with the pseudo-range and the Doppler measurements, using the expression of the measurements and related errors, as in section 2.3.4. The final double difference observations for the estimation process are:

$$\varphi_{km}^{pq}(t) = \frac{1}{\lambda}\rho_{km}^{pq} + N_{km}^{pq} + \frac{1}{\lambda}T_{km}^{pq} - \frac{1}{\lambda}I_{km}^{pq} + \varepsilon_{km,\phi}^{pq} \tag{2.25}$$

$$P_{km}^{pq}(t) = \rho_{km}^{pq} + T_{km}^{pq} + I_{km}^{pq} + \varepsilon_{km,P}^{pq} \tag{2.26}$$

$$\dot{\varphi}_{km}^{pq}(t) = \dot{\rho}_{km}^{pq} + \dot{T}_{km}^{pq} - \dot{I}_{km}^{pq} + \dot{\varepsilon}_{km,\varphi}^{pq} \tag{2.27}$$

Where:

φ_{km}^{pq}	is the double difference carrier-phase [m],
P_{km}^{pq}	is the double difference pseudo-range [m/s],
$\dot{\varphi}_{km}^{pq}$	is the double difference Doppler,
ρ_{km}^{pq}	is the double difference satellite-receiver true range [m],
$\dot{\rho}_{km}^{pq}$	is the double difference true Doppler range[m/s],
I_{km}^{pq}	is the double difference ionosphere errors [m],
λ	is the frequency wavelength,
ε_{km}^{pq}	represents the residual errors, mainly refers as multipath and random noise.

For example, if the rover and the base have the same eight satellites in view with valid data, seven double difference measurements for each observation is produced. The atmospheric errors will be mostly removed in short baseline. If the troposphere errors are also removed in long baseline by proper modeling, the ionosphere errors will need specific estimation process.

The quality and the precision of these measurements are important for the position solution in the RTK algorithm. They will be used in the Kalman filter to estimate the user's position in an estimation process. The next chapter will present in detail the Kalman filter algorithm and how the double difference observation will be used to obtain a real-time position.

CHAPITRE 3

ROBUST KALMAN FILTER FOR REAL-TIME HIGH PRECISION POSITION ESTIMATION

In the previous chapter, three different observations have been detailed. These observations provide the satellites-receivers distances, which are needed to compute the position of the user and its velocity. As it has been seen, these distances have some identified errors, like atmospheric delays or clock biases. Even if all these errors would be perfectly modeled, some noises stay present in the observations, Gaussian receiver noise, for example. In that case, an estimation technique is required.

The Kalman filter is a recursive estimation process. It will estimate, in an optimal way, the noisy system parameters. In the present case, these parameters will be mainly the baseline position, the rover velocity and the ambiguities. Having the measurements at time k and the previous parameters state vector, the next parameters state vector can be found. The linear system is defined as:

$$x_{k+1} = f(x_k) + u_k \qquad Q = E(u_k u_k^T) \tag{3.1}$$

$$y_k = g(x_k) + w_k \qquad R = E(w_k w_k^T) \tag{3.2}$$

Where:

x_k	is the unknown parameter state vector at time k,
y_k	is the observation vector at time k,
f	is the process function,
g	is the observation function,
u_k	is the process noise at time k represented by the matrix Q,
w_k	is the observation noise at time k represented by the matrix R.

The stochastic model is referring to the noise u_k and w_k. Evaluating this noise in a robust and adaptive manner is a major challenge for optimal Kalman filtering. The other important point is to define the functional model, referring to the process function f and the observation function g.

This chapter describes all the challenging aspects of Kalman filter for an optimum RTK algorithm. Details of the functional model and stochastic model will be explained, as well as an innovative robust method, and ambiguity resolution technique. First of all, a real-time satellite selection and observations management is presented. It is presented as to be the first step to develop the robust Kalman filter system.

3.1 Satellite management in the Kalman filter

3.1.1 Satellite selection criterions

The selection of the satellites in view is of primary importance in order to compute an accurate position. A minimum number of 4 satellites are necessary to resolve the parameters of the navigation equation in a classic single receiver solution (for the three baseline coordinates and for the receiver time). In RTK, it has been seen that the use of only 4 satellites can lead to divergence at some point and 5 satellites are minimally required to have a stable solution and an estimation of the ambiguities.

The selection of satellites for the solution in real-time is made upon classic criteria, like a minimum elevation angle of 5^o, a C/No ratio above 48 dB and basic valid observations criteria (like non-zero value) for the pseudo-range, the carrier phase and the Doppler frequency. With the Novatel receiver, the parameter Lock Time (LT) is used to detect cycle-slip and valid satellites. It indicates the time a satellite has been tracked by the receiver. Above 10s, this satellite is considered stable and the probability of cycle-slip will be less important. In that case, it is added in the solution in a progressive way. Satellites which are lost or invalid for a period of time are removed from the solution without any disturbances.

For the solution, the RTK algorithm takes as much satellites which fit these criteria as possible. This means sometimes the Kalman filter can reach up to 10 satellites in the solution. Using the L1 and L2 frequencies, the number of observations is doubled. This method will provide the best solution available, using as much information as possible. The main drawbacks will be the computation issue, particularly when new satellite configurations will arise. In that case, an efficient selection of satellites will be necessary. A satellite selection will considerably vary in time, and for long periods, an efficient real-time satellite management is necessary.

For long period of observations, a dynamic Kalman filter techniques is used, which adapts its structure to the actual number of satellites used in the solution. Technique of matrices substitution is also used, when a satellite is added or removed from the selection. At each epoch, or time of observations, the satellite selection is performed. If a satellite is added or removed from the solution, the associated Kalman filter matrices are modified in consequence. For example, if a satellite is added in the solution, a new row and corresponding line is added and initialized in the Kalman filter matrices. This technique helps the stability of the filter and lowers the computation burden. It also keeps track of the stochastic assignment of the other remaining satellites.

3.1.2 Stochastic model assignment of the satellite receiver measurements

It is very important in a Kalman filter to have good functional and stochastic models. The stochastic model indicates the expected quality of the satellite measurements during the time of processing. A correct and realistic stochastic assignment will lead to an optimal Kalman filtering. On the contrary, bad stochastic assignments may lead to inaccurate estimation or even a divergence in the filter. It could also have a major impact in the ambiguity resolution.

GNSS measurements, removed from systematic errors, are considered as measurements with independent Gaussian noise. It will be not true if there is strong multipath, for example. The

values of variance for the measurements are the same as in section 2.4.2 and represent the variance of the receiver noise:

$$\sigma_P{}^2 = 0.5 \quad [m^2] \tag{3.3}$$

$$\sigma_\varphi{}^2 = 0.0001 \quad [cycles^2] \tag{3.4}$$

$$\sigma_D^2 = 0.0001 \quad [Hz^2] \tag{3.5}$$

Where:

σ_P is the pseudo-range standard deviation on L1,

σ_φ is the carrier phase standard deviation,

σ_D is the Doppler standard deviation.

The measurements variance-covariance matrix in the Kalman filter is usually represented by the matrix R. It is the matrix form of the measurements noise described as w_k in equation (3.2). In the RTK algorithm, the three different measurements are used, each one with two different frequencies. With n satellite in view, the vector of observations will be a 6(n-1) element vector and its associated covariance matrix R a 6(n-1)*6(n-1) element matrix:

$$R = \begin{bmatrix} \sigma^2_{P,L1} & 0 & 0 & 0 & 0 & 0 \\ 0 & \sigma^2_{P,L2} & 0 & 0 & 0 & 0 \\ 0 & 0 & \sigma^2_{\varphi,L1} & 0 & 0 & 0 \\ 0 & 0 & 0 & \sigma^2_{\varphi,L2} & 0 & 0 \\ 0 & 0 & 0 & 0 & \sigma^2_{D,L1} & 0 \\ 0 & 0 & 0 & 0 & 0 & \sigma^2_{D,L2} \end{bmatrix} \tag{3.6}$$

But these measurements noise are related to single measurements. As the RTK algorithm uses double difference measurements instead of single measurement, the noise of the measurements are correlated. The Kalman filter is not using measurements, but rather ‘observations’, which is an important aspect of the RTK algorithm (see section 2.4).

First, by differencing each satellite between 2 receivers, a single difference is formed. However, the result is an observation two times noisier:

$$\sigma^2_{SDP,L1} = 2\sigma^2_{P,L1} \tag{3.7}$$

Where:

$\sigma^2_{SDP,L1}$ is the standard deviation of the single difference pseudo-range measurements on L1,

$\sigma^2_{P,L1}$ is the standard deviation of pseudo-range measurements on L1.

Then, the single-difference measurements are differentiated, using a reference satellite, which has the highest elevation angle. By doing so, the final double difference observations are obtained. To do so, the matrix D is used to achieve this process (example for 5 satellite and 4 double difference):

$$D = \begin{bmatrix} 1 & -1 & 0 & 0 & 0 \\ 1 & 0 & -1 & 0 & 0 \\ 1 & 0 & 0 & -1 & 0 \\ 1 & 0 & 0 & 0 & -1 \end{bmatrix}, \quad DD = D \cdot SD \tag{3.8}$$

Where:

DD is the double-difference measurements vector,

SD is the single-difference measurements vector,

D is the double differencing operation matrix.

By applying the covariance propagation (Leick 2003), the final L1 pseudo-range observation standard deviation can be obtained:

$$R'_{P,L1} = \sigma^2_{SDP,L1} \cdot D \cdot D^T \tag{3.9}$$

$$R'_{P,L1} = \sigma^2_{P,L1} \begin{bmatrix} 4 & 2 & 2 & 2 \\ 2 & 4 & 2 & 2 \\ 2 & 2 & 4 & 2 \\ 2 & 2 & 2 & 4 \end{bmatrix} \tag{3.10}$$

At the end, the covariance matrix of the observations is a highly correlated matrix for each observation. It can be guessed easily with intuition but it is represented here in a formal way by variance computation. The final matrix R for all observations will be a block-diagonal matrix:

$$R = \begin{bmatrix} R'_{P,L1} & 0 & 0 & 0 & 0 & 0 \\ 0 & R'_{P,L2} & 0 & 0 & 0 & 0 \\ 0 & 0 & R'_{\varphi,L1} & 0 & 0 & 0 \\ 0 & 0 & 0 & R'_{\varphi,L2} & 0 & 0 \\ 0 & 0 & 0 & 0 & R'_{D,L1} & 0 \\ 0 & 0 & 0 & 0 & 0 & R'_{D,L1} \end{bmatrix} \tag{3.11}$$

Let's suppose that each satellite has the same uncorrelated standard deviation or variance. To improve the stochastic assignment, it will be better to assign a specific variance to each satellite, depending on its signal-to-noise ratio C/N_o and its elevation angle. This weighting scheme allows a more reliable model to the noise associated with each satellite. The measurement standard deviation of a satellite, with respects to its C/N_o and elevation angle, will be (Liu 2002):

$$\sigma' = \sigma \cdot [1 + \alpha^{\frac{-el}{el_0}}] \cdot \beta^{\frac{c}{c_0}} \tag{3.12}$$

Where:

σ	is the standard deviation of the associated observations,
el	is the satellite elevation angle,
el_0	is the reference satellite elevation angle,

c	is the satellite C/N_o,
c_0	is the reference satellite C/N_o,
α , β	are parameters from 0 to 1.

The reference satellite signal-to-noise ratio and reference elevation angle are the elevation angle and the C/No expected from tables, for different standard deviation. The parameters α and β are determined empirically. α represent the additional noise of the measurement when the satellite is at the horizon. With this weighting scheme, the satellites with low elevation angle and low C/No will be considered much noisier and thus will have less impact in the estimation process for the position solution. A more sophisticated stochastic model, using long observation periods and equipments characteristic can be found in (Kim and Langley 2001). Other information of this sensitive field of stochastic modeling can be find in (Keefee, Pettovelo et al. 2006) and (Wang 2000).

3.2 Development of the improved Kalman filter

3.2.1 State vector, the functional model and associated variance

The fundamental objects to be defined in a Kalman filter are the state vector, the observation vector and the link between them. The state vector represents the parameters to be estimated by the estimation process. The observation vector will represent the measurements. The state parameters will be estimated using the observations and their stochastic assignment.

In the proposed new RTK Kalman filter, the state vector consists of position and velocity of the rover, and all the ambiguities of the double difference carrier phase. This means that for n satellite in view, the vector X will have 6+(n-1) elements. The ionosphere can also be added and estimated in long baseline applications. The related model will be described in section 5.1. These are the parameters estimated in the Kalman filter:

$$X = \begin{bmatrix} x & y & z & \dot{x} & \dot{y} & \dot{z} & N_{km}^{pq} & \dots \end{bmatrix}^T \tag{3.13}$$

Where:

x, y, z	are the three baseline components,
$\dot{x}, \dot{y}, \dot{z}$	are the three rover velocity components,
N_{km}^{pq}	are the double difference carrier-phase ambiguities,

The functional model represents the discrete time evolution of the state vector through the process. For the position and the velocity parameters, it is computed using a constant velocity model where:

$$\ddot{x} = u_k \tag{3.14}$$

Where:

$\ddot{x}$	is the receiver acceleration.
u_k	is the acceleration white noise.

This model is well suited for dynamic receiver and can be used for RTK application (Uratani, Sone et al. 2003). But to obtain the functional model in the Kalman filter algorithm, this model has to be adapted to the discrete time (Zarchan and Musoff 2005).

$$X_{k+1} = F \cdot X_k \tag{3.15}$$

$$\begin{bmatrix} x_{k+1} \\ y_{k+1} \\ z_{k+1} \\ \dot{x}_{k+1} \\ \dot{y}_{k+1} \\ \dot{z}_{k+1} \\ N_{km,k+1}^{pq} \\ .. \end{bmatrix} = \begin{bmatrix} 1 & 0 & 0 & t_s & 0 & 0 & 0 & .. \\ 0 & 1 & 0 & 0 & t_s & 0 & 0 & .. \\ 0 & 0 & 1 & 0 & 0 & t_s & 0 & .. \\ 0 & 0 & 0 & 1 & 0 & 0 & 0 & .. \\ 0 & 0 & 0 & 0 & 1 & 0 & 0 & .. \\ 0 & 0 & 0 & 0 & 0 & 1 & 0 & .. \\ 0 & 0 & 0 & 0 & 0 & 0 & 1 & .. \\ .. & .. & .. & .. & .. & .. & .. & .. \end{bmatrix} \begin{bmatrix} x_k \\ y_k \\ z_k \\ \dot{x}_k \\ \dot{y}_k \\ \dot{z}_k \\ N_{km,k}^{pq} \\ .. \end{bmatrix} \tag{3.16}$$

Where:

X_k is the state vector at instant k

F is the transition matrix.

The associated process noise matrix is represented by Q in the Kalman filter. It is the variance of the functional model represented by u_k in equation (3.1). For the baseline position and the rover velocity, the process noise is associated with the constant velocity model. As it can be seen in (3.16), carrier phase ambiguities are considered as a fixed parameter through time. Its associated process noise will be low, i.e around $1e^{-12}$. Increasing this number will add more variability to the parameters in the estimation process. The ionosphere model is detailed in section 5.1 for long baseline applications.

$$Q = \begin{bmatrix} \sigma_x^2 & 0 & 0 & 0 & 0 & 0 & 0 & .. \\ 0 & \sigma_y^2 & 0 & 0 & 0 & 0 & 0 & .. \\ 0 & 0 & \sigma_z^2 & 0 & 0 & 0 & 0 & .. \\ 0 & 0 & 0 & \sigma_{\dot{x}}^2 & 0 & 0 & 0 & .. \\ 0 & 0 & 0 & 0 & \sigma_{\dot{y}}^2 & 0 & 0 & .. \\ 0 & 0 & 0 & 0 & 0 & \sigma_{\dot{z}}^2 & 0 & .. \\ 0 & 0 & 0 & 0 & 0 & 0 & \sigma_{N_{km}^{pq}}^2 & .. \\ .. & .. & .. & .. & .. & .. & .. & .. \end{bmatrix} \tag{3.17}$$

For the functional model, the process noise will be assigned as:

$$\sigma_x{}^2 = 1e^3 \quad [m^2], \qquad \sigma_{\dot{x}}{}^2 = 1e^3 \quad [m^2/s^2] \tag{3.18}$$

$$\sigma_N{}^2 = 1e^{-12} \quad [cycles^2] \tag{3.19}$$

Where:

σ_a^2 is the variance of the acceleration process,

σ_N^2 is the variance of the ambiguities estimation process,

σ_I^2 is the variance of the ionosphere estimation process.

It is interesting to notice that in order to make an efficient and stable Kalman filter and avoid the effect of error in the stochastic process estimation, the user can assign a very large value to the process noise. In the proposed RTK algorithm, a value of $1e^3$ is used and the filter relies only on the measurements noise (Wang 2000).

3.2.2 Observation model

The observations are all the measurements included in the Kalman filter. The developed RTK will use all the pseudo-range measurements, all the ADR and Doppler measurements also, and this for each selected double difference. At the end, there is 2*[3(n-1)] observations vectors, where n is the number of selected satellites. The observation vector is usually referred as Y in the Kalman filter and have all the observations detailed in section 2.6:

$$Y = \begin{bmatrix} P_{km,L1}^{pq} & P_{km,L2}^{pq} & \varphi_{km,L1}^{pq} & \varphi_{km,L2}^{pq} & D_{km,L1}^{pq} & D_{km,L2}^{pq} \end{bmatrix}^T \tag{3.20}$$

Where:

$P_{km,L1}^{pq}, P_{km,L2}^{pq}$ are the L1 and L2 double difference pseudo-range observation,

$\varphi_{km,L1}^{pq}, \varphi_{km,L2}^{pq}$ are the L1 and L2 double difference carrier phase observation,

$D_{km,L1}^{pq}, D_{km,L2}^{pq}$ are the L1 and L2 double difference Doppler frequency observation.

To link the observations measurements to the state space vector, it is proposed the use of a simple form of linear equations involving the parallelism of the satellite line of sight between two close receivers. This assertion will not be true in long baseline situation as it will be discussed in section 5.1.3. But this technique works well for short baseline scenarios and has the advantages of low computation while keeping the Kalman filter linear.

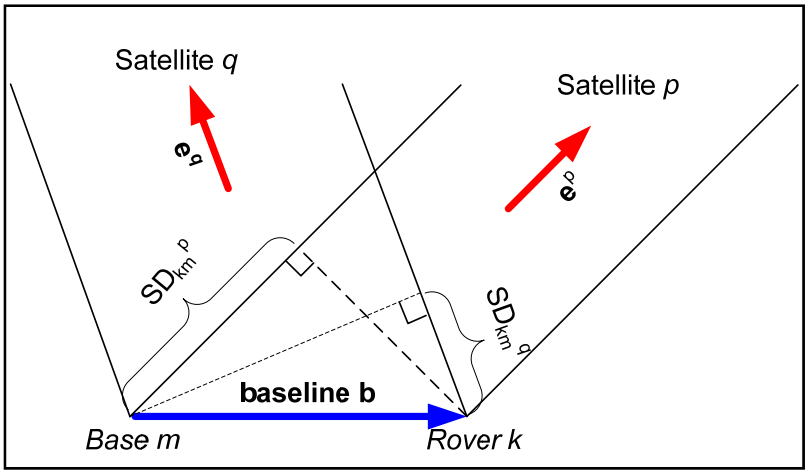

Figure 3.1 Geometrical view of the double difference measurement in the observation model.

As seen in Figure 3.1, the Single Difference (SD) is expressed as:

$$SD_{km}^{p} = \vec{e}^{\,p} \cdot \vec{b} \tag{3.21}$$

Where:

SD_{km}^{p}	is the single difference distance between receiver k and m for satellite p,
$\vec{b}$	is the baseline vector,
$\vec{e}^{\,p}$	is the p satellite line of sight unit vector.

Using two single differences with satellite p and q, the double difference distance DD_{km}^{pq} is obtained

$$DD_{km}^{pq} = SD_{km}^{p} - SD_{km}^{q} = (\vec{e}^{\,p} - \vec{e}^{\,q}) \cdot \vec{b} \tag{3.22}$$

Finally, using the equations (2.25), (2.26) and (2.27) of the double difference measurements expression, the relation between the observations vector and the state space vector for the carrier phase becomes:

$$\varphi_{km,L1}^{pq} = \frac{1}{\lambda}\vec{h}\cdot\vec{b} - \frac{1}{\lambda}I + N \tag{3.23}$$

Where:

$$\vec{h} = \vec{e}^{\,p} - \vec{e}^{\,q} \tag{3.24}$$

And for all observations, in general:

$$Y = HX \tag{3.25}$$

With:

$$H = \begin{bmatrix} h_x & h_y & h_z & 0 & 0 & 0 & 0 & .. \\ h_x & h_y & h_z & 0 & 0 & 0 & 0 & .. \\ \frac{1}{\lambda_1}h_x & \frac{1}{\lambda_1}h_y & \frac{1}{\lambda_1}h_z & 0 & 0 & 0 & 1 & .. \\ \frac{1}{\lambda_2}h_x & \frac{1}{\lambda_2}h_y & \frac{1}{\lambda_2}h_z & 0 & 0 & 0 & 1 & .. \\ 0 & 0 & 0 & h_x & h_y & h_z & 0 & .. \\ 0 & 0 & 0 & h_x & h_y & h_z & 0 & .. \end{bmatrix} \tag{3.26}$$

Where:

$$h_x = (\vec{e}^{\,p} - \vec{e}^{\,q})\cdot\vec{b} \tag{3.27}$$

$$\lambda_1 = \frac{c}{f_1} \tag{3.28}$$

Expanding the final observation equation, the observation model becomes:

$$\begin{bmatrix} P_{km,L1}^{pq} \\ P_{km,L2}^{pq} \\ \varphi_{km,L1}^{pq} \\ \varphi_{km,L2}^{pq} \\ dop_{km,L1}^{pq} \\ dop_{km,L2}^{pq} \end{bmatrix} = \begin{bmatrix} h_x & h_y & h_z & 0 & 0 & 0 & 0 & .. \\ h_x & h_y & h_z & 0 & 0 & 0 & 0 & .. \\ \frac{1}{\lambda_1}h_x & \frac{1}{\lambda_1}h_y & \frac{1}{\lambda_1}h_z & 0 & 0 & 0 & 1 & .. \\ \frac{1}{\lambda_2}h_x & \frac{1}{\lambda_2}h_y & \frac{1}{\lambda_2}h_z & 0 & 0 & 0 & 1 & .. \\ 0 & 0 & 0 & h_x & h_y & h_z & 0 & .. \\ 0 & 0 & 0 & h_x & h_y & h_z & 0 & .. \end{bmatrix} \begin{bmatrix} x \\ y \\ z \\ dx \\ dy \\ dz \\ N_{km}^{pq} \\ .. \end{bmatrix} \tag{3.29}$$

With the observations model and the functional model, and their associated stochastic assignment, all the elements are present to perform an optimal estimation with a recursive Kalman filter.

3.2.3 Recursive equations of the Kalman filter

The Kalman filter is a recursive least-square estimator. The covariance matrix P of the state vector is updated at each epoch and is computed using only the previous epoch. There are 3 main steps in a conventional Kalman filter:

- Estimation:

$$\begin{aligned} X_{est} &= F \cdot X \\ P_{est} &= (F \cdot P \cdot F^t) + Q \end{aligned} \tag{3.30}$$

- Computation:

$$\begin{aligned} DD_{est} &= H \cdot X_{est} \\ K &= P_{est} \cdot H \cdot (H \cdot P_{est} \cdot H^t + R)^{-1} \\ res &= DD_{est} - DD \end{aligned} \tag{3.31}$$

- Update:

$$\begin{aligned} P &= P_{est} - K \cdot H \cdot P_{est} \\ X &= X_{est} + K \cdot res \end{aligned} \tag{3.32}$$

The residues res is an important parameter. It is refer as the difference between the actual observations DD and the estimated one. With the computed Kalman gain K, it is use to perform the correction on the estimated parameters vector $X_{est.}$ For more information about

these essential Kalman filter equations and their computations, the reader can refer to (Simon 2006).

During the estimation process, the variance-covariance (vc) of the estimated state space parameters in the Kalman filter is represented in the P matrix. This matrix is computed at each epoch after the update process. It is the best indicators of the precision of the state parameters in the estimation process, after a certain time of convergence.

$$P=\begin{bmatrix} \sigma_x^2 & \sigma_{xy}^2 & \sigma_{xz}^2 & \sigma_{xdx}^2 & \sigma_{xdy}^2 & \sigma_{xdz}^2 & \sigma_{xN}^2 & .. \\ \sigma_{yx}^2 & \sigma_y^2 & \sigma_{yz}^2 & \sigma_{ydx}^2 & \sigma_{ydy}^2 & \sigma_{ydz}^2 & \sigma_{yN}^2 & .. \\ \sigma_{zx}^2 & \sigma_{zy}^2 & \sigma_z^2 & \sigma_{zdx}^2 & \sigma_{zdy}^2 & \sigma_{zdz}^2 & \sigma_{zN}^2 & .. \\ \sigma_{dxx}^2 & \sigma_{dxy}^2 & \sigma_{dxz}^2 & \sigma_{dx}^2 & \sigma_{dxdy}^2 & \sigma_{dxdz}^2 & \sigma_{dxN}^2 & .. \\ \sigma_{dyx}^2 & \sigma_{dyy}^2 & \sigma_{dyz}^2 & \sigma_{dydx}^2 & \sigma_{dy}^2 & \sigma_{dydz}^2 & \sigma_{dyN}^2 & .. \\ \sigma_{dzx}^2 & \sigma_{dzy}^2 & \sigma_{dzz}^2 & \sigma_{dzdx}^2 & \sigma_{dzdy}^2 & \sigma_{dz}^2 & \sigma_{dzN}^2 & .. \\ \sigma_{Nx}^2 & \sigma_{Ny}^2 & \sigma_{Nz}^2 & \sigma_{Ndx}^2 & \sigma_{Ndy}^2 & \sigma_{Ndz}^2 & \sigma_N^2 & .. \\ .. & .. & .. & .. & .. & .. & .. & .. \end{bmatrix} \tag{3.33}$$

By assigning a large value to the estimated covariance of the state parameters in P, the algorithm will not consider the estimated value as reasonable. This can be done in the initialization of the process, to avoid wrong first estimation or anomalous state. This can also speed up the convergence time, especially concerning the ambiguity state, which is very sensitive to associated covariance.

Managing the stochastic model of the Kalman filter is a very important aspect of its stability and accuracy. In the developed RTK algorithm, the stochastic model works. But for specific applications, like very high dynamic scenarios, or shadowed environments and constant low signal to noise ratio, some improvement could be done. In the next section, a robust scheme is developed for the RTK algorithm using stochastic management.

3.2.4 Robust management of the observations

Global robustness can be added in the Kalman filter to correct non-usual errors as satellite failure or incorrect observations. These errors introduce biases in the measurements than can induce large errors in the solution. To prevent the RTK solution from this kind of anomaly, an adaptive stochastic method using a robust M-estimation approach has been introduced in the developed software (Delaporte, Landry et al. 2008). This method uses a weighting function to adapt and correct the contribution of the updated parameters in the Kalman filter. It has already been successfully applied for stand-alone positioning (Rao, MN.S.Swam et al. 2004) and has been adapted here for RTK positioning. The M-estimation method minimizes the sum of a function of the residuals:

$$\sum_{i=1}^{n} g(res_i) = \sum_{i=1}^{n} g(DD_{est} - DD) \tag{3.34}$$

Where

DD_{est}	is the estimated double difference observation vector,
DD	is the observed double difference,
res_i	is the Kalman filter residual of observations i,
g	is the M-estimator function.

The choice of the M-estimator function is related to the statistical distribution of the residuals vector. It is the matrix W which is a function of each of the residual observation Y_i of all selected satellite

$$W(res_i) = \begin{cases} 1 & if \quad |res_i| < a \\ a & if \quad a < |res_i| < d \\ \dfrac{a}{d}\exp\left(1 - \dfrac{res_i^2}{d^2}\right) & if \quad |res_i| > d \end{cases} \tag{3.35}$$

The parameters a and d are evaluated for each matrix with the variance of the residual's measurements. The measurement's histogram is used to determine the correct values of the outliers. As the distribution of the covariance matrix of Gaussian measurements is a chi-square distribution, one may use this statistical test to detect impulsive update in the Kalman filter.

The factor a is estimated as the medium value of the outliers in the histograms method. The outlier represents the value outside the normal range. For the Novatel receiver, a medium value for a of 5 for the pseudo-range has been founded, and 0.5 for the ADR and the Doppler. According to simulations and analysis of the residuals, $d = 2a$ has been chosen in the implementation. This parameter is empirical and can be changed for different test.

Using this W matrix, the robust processing will reduce the residues which have spike and outliers. At the same time, it will associate a higher value to its estimated noise. This is done in the computation process in the Kalman filter using equations (3.36) and (3.38) before the gain matrix K computation.

$$Y = W \cdot Y \tag{3.36}$$

$$R' = W^{-1} \cdot R \cdot W^{-1} \tag{3.37}$$

By removing the unwanted outliers and adding corresponding noise to the associated measurements, this weighting matrix W allows the Kalman filter to resist to the influence of impulsive errors without degradations in the solution. This basic robust method could be improved to determine other unexpected errors in the measurements, as multipath or interference.

3.3 Ambiguity resolution of the carrier phase

3.3.1 Using the dual-frequency ADR to combine ambiguities

In the Kalman filter, it is important to evaluate the double difference ambiguity to reach the carrier phase full range precision. The double difference ambiguities can take different forms, considering whether it stays as integer value or real values. There are different forms of combination of the double difference ambiguity, using L1 and L2 ambiguity.

Those ambiguities combinations could be considered as new ambiguities with different wavelength, which can lead to more reliable estimation. Here are detailed different combination of dual frequency and their associated wavelength. Only the iono-free combination transforms the integer property of the DD ambiguities into a real one but is free of ionosphere bias, as seen in equation 2.20.

Iono-free (19cm or 1575 MHz but non-integer):

$$N_{km,IF}^{pq} = \frac{f_{L1}^2}{f_{L1}^2 - f_{L2}^2} N_{km,L1}^{pq} - \frac{f_{L2}^2}{f_{L1}^2 - f_{L2}^2} N_{km,L2}^{pq} \approx 2.546 N_{km,L1}^{pq} - 1.984 N_{km,L2}^{pq} \tag{3.38}$$

$$\varphi_{km,IF}^{pq} = 2.546\varphi_{L1} - 1.984\varphi_{L2} \tag{3.39}$$

Wide-lane (86.2 cm or 347.82 MHz):

$$N_{km,WL}^{pq} = N_{km,L1}^{pq} - N_{km,L2}^{pq} \tag{3.40}$$

$$\phi_{WL} = \varphi_{L1} - \varphi_{L2} \tag{3.41}$$

Narrow-lane (10.70 cm or 2.8 GHz):

$$N_{km,NL}^{pq} = N_{km,L1}^{pq} + N_{km,L2}^{pq} \tag{3.42}$$

$$\phi_{WL} = \varphi_{L1} + \varphi_{L2} \tag{3.43}$$

The wide-lane combination brings longer wavelength to the ambiguity, but with more associated noise. It is then easier to determine the correct ambiguity cycles related to it. Using a widelane ambiguity can speed up the convergence of the filter. But as seen for the iono-free measurement, the drawback is that the noise associated to the double difference measurements will be higher. It could be a good step for the Kalman filter convergence.

In the contrary, the narrow-lane DD ambiguity will be shorter, but the associated noise will be diminished. When the Kalman filter reach a good convergence point using residues observation, the filter can switch to the narrow-lane DD ambiguity and then improve the accuracy. These methods of mixing ambiguity are not exploited here for the RTK algorithm but could be easily implemented in the algorithm in the future, especially with the new constellations arising. Performance and evaluation could be done compared to single frequency ambiguity resolution.

3.3.2 Overview of the resolution of the double difference ambiguity

In the Kalman filter process, the carrier phase ambiguities are first estimated as real values. It is called ‘float’, as they vary during the estimation process. But the ambiguities are integer values, and should be considered like this to take full advantage of the precision of the carrier phase. That is why at some point in the estimation process, the carrier-phase ambiguities in the Kalman filter have to be fixed to obtain high precision positioning.

To fix the ambiguities, it is necessary to first have the correct integer value, and this is the most difficult task in the RTK techniques. To do so, there are two main steps: finding potential ambiguities and validate the correct one with a high probability. One cycle of error in one ambiguity could lead to a precision error of the corresponding cycle (0.19 meters for L1), which is not acceptable.

The easiest way to have an approximation of the double difference ambiguity is to use the pseudo-range measurement. Indeed, if the pseudo-range is an approximation of the distance

between satellite and the receiver, the round up of the difference between the ADR and the corresponding pseudo-range should lead to an estimate of the correct ambiguity. For example, for the L1 frequency:

$$N_{km,L1}^{pq} = round(\frac{1}{\lambda_{L1}}(P_{km,L1}^{pq} - \lambda_1 \phi_{km,L1}^{pq})) \tag{3.44}$$

Of course, this approximation has the noise associated to the pseudo-range. The standard deviation of the estimate is about 5 cycles. This error can be reduced by making an approximation over several minutes of observation.

This method is called 'Integer Rounding' (IR) and evaluates ambiguities one at the time. The double difference ambiguity can also consider as a set. Using the correlation between them, the algorithm is able to evaluate the correct ambiguities. The most known techniques are 'Integer Least Squares' (ILS) and 'Integer Bootstrapping' (IB) (Teunissen 2002). They offer better performance than IR and the ILS method is considered as optimal.

One of the most interesting and widely used techniques for finding the correct ambiguities is the LAMBDA method (Least-squares AMBiguity Decorrelation Adjustements) developed by the university of Delft and introduced for the first time in 1993 by P.J.G Teunissen (Teunissen 1993). It uses a decorrelation and an integer least-squares process. It is widely used in research because of its easy computational aspects and reliability. It is also very well documented and the source code is accessible through internet. This is the technique and part of the TUdelft package used here for the new proposed RTK algorithm.

3.3.3 Overview of the LAMBDA method

The ambiguity resolution method using LAMBDA works in 4 step (Jonge and Tiberius 1996; Joosten 2001):

1. First, obtaining the float ambiguity resulting of the Kalman filter process. The ambiguities are still considered real values. Their associated covariance matrices have also to be found.
2. In the second step, a decorrelation and a search process is used to find the 2 best ambiguity sets. This is the main part of the LAMBDA method.
3. Then, validate the best ambiguity set, if possible.
4. At the end, incorporate the fixed ambiguity in the estimation process to strengthen the model.

The model defined to find the ambiguity uses the observations vector and the state space vector and will be described here as in the general LAMBDA literature. But indications are provided to make the correspondence between the model proposed in the thesis. The general model is:

$$y = A\,a + B\,b + \varepsilon \tag{3.45}$$

Where:

y	is the observation vector (the vector DD),
a	is the baseline vector (the vector X),
b	is the vector of double difference ambiguity (N),,
A	is the design matrix for the baseline coordinate (H_X),
B	is the design matrix for the ambiguity terms (H_N),
ε	is the vector of unmodelled effect and measurements noise.

The model used is slightly different than the conventional one since a linear model is used for the observation. The state vector comprised the a and b vectors together and the observation matrix will be a concatenation of the B and A matrices. Apart from the notation, the research of ambiguities will be exactly identical.

The goal is to find the double difference ambiguity term that minimizes (3.45), which can be expressed as:

$$\min_{a,b} \left\| y - A \cdot a - B \cdot b \right\|^2_{Q_y^{-1}} \tag{3.46}$$

Q is the variance-covariance matrix of the state space parameters. In the developed RTK algorithm, it is referred to the P matrix and is provided by the Kalman filter update process.

It can be developed using orthogonal decomposition (Teunissen 2002) as

$$\left\| y - A \cdot a - B \cdot b \right\|^2_{Q_y} = \left\| \hat{e} \right\|^2_{Q_y} + \left\| \hat{a} - a \right\|^2_{Q_{\hat{a}}} + \left\| \hat{b}(a) - b \right\|^2_{Q_{b|\hat{a}}} \tag{3.47}$$

where:

$$\left\| \hat{e} \right\|^2_{Q_y} = \left\| y - A \cdot \hat{a} - B \cdot \hat{b} \right\|^2_{Q_y} \tag{3.48}$$

$$\hat{b}(a) = \hat{b} - Q_{\hat{b}\hat{a}} Q_{\hat{a}}^{-1} (\hat{a} - a) \tag{3.49}$$

and

$\hat{a}$	is the float ambiguity vector.
$\hat{b}$	is the estimated baseline vector.
a	is the true integer ambiguity.
b	is the true baseline.
Q	is the associated vc matrix of the parameters (corresponding to P).

The term (3.47) will be a minimum if the last term in the right-hand side is set to zero and the second term is minimal. In a classic norm, the ambiguity search is now resumed at the minimization of :

$$\left\| \hat{a} - a \right\|^2_{Q_{\hat{a}}} = (\hat{a} - a)^T Q_{\hat{a}}^{-1} (\hat{a} - a) \tag{3.50}$$

And the search space of the ambiguities has to be defined, using the constant boundary χ:

$$\Omega_a = \left\{ a \in Z^n \mid (\hat{a} - a)^T Q_{\hat{a}}^{-1} (\hat{a} - a) \leq \chi^2 \right\} \tag{3.51}$$

Where:

$\hat{a}$	are the estimated float ambiguities,
a	are the true ambiguities,
$Q_{\hat{a}}$	is the estimated covariance matrix of the ambiguities,
χ	is the threshold of the search space.

The search space has a shape of an ellipsoid, due to the correlation of the double difference ambiguities. It is centered on â, its shape is governed by the variance-covariance $Q_{\hat{a}}$, and its size is determined by χ. The threshold χ has to be as small as possible but large enough for the search space to contain at least 2 candidates for validation (*see* section 3.3.2).

In order to decrease the number of grid points to search, the LAMBDA method propose a decorrelation step which transform the ellipsoid shape of the ambiguity search (left on Figure 3.2) to a more spherical shape (right on Figure 3.2). The Z-transformation consists mainly in transforming the $Q_{\hat{a}}$ matrix in a more diagonal one (Q_z), and changing state space. It is clearly visible in the Figure 3.2 than the domain of search using vertical and horizontal axes will be much more optimal in the spherical shape than in the ellipsoid shape (15x15 grids against 3x3 grids, in this example).

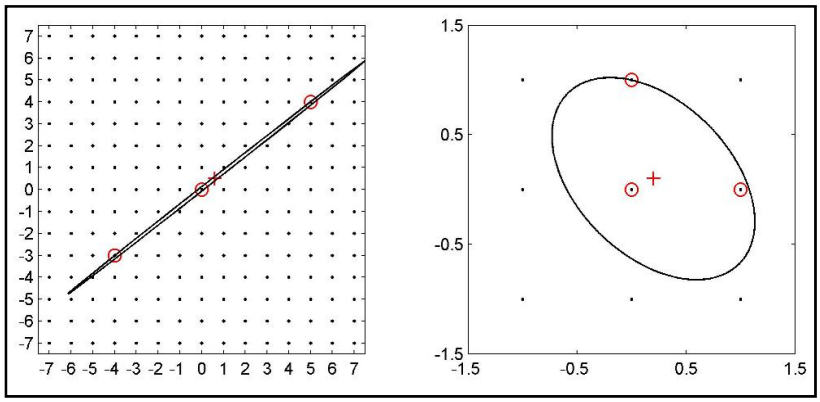

Figure 3.2 Transformation of the ellipsoid search space using Z-transformation.
(from Delft University)

Using this Z-transformation, a discrete version of the Laplace transform, to the float ambiguities and the corresponding vc-matrix, the search space of the ambiguities become:

$$\Omega_z = \left\{ z \in Z^n \mid (\hat{z} - z)^T Q_{\hat{z}}^{-1} (\hat{z} - z) \leq \chi^2 \right\} \tag{3.52}$$

The transformation preserves the integer nature of the ambiguities and reduces drastically the computation. Now the iterative scheme can be used to search for candidates. Using the decomposition of the matrix Q_z, after several computations (Joosten 2001), equation (3.52) is expanded as:

$$\sum_{i=1}^{n} \frac{(\hat{z}_{i|I} - z_i)^2}{\sigma_{i|I}^2} \leq \chi^2 \tag{3.53}$$

Where:

$\sigma_{i|I}$ is the diagonal element of Q_z and conditional standard deviation of the associated ambiguities.

$\hat{z}_{i|I}$ is the conditioned least-square estimated ambiguity.

Using the sum-of-square structure, one can finally set up the n intervals which are used for the search. The sequential intervals are given as:

$$\begin{aligned} (\hat{z}_1 - z_1)^2 &\leq \sigma_1^2 \chi^2 \\ (\hat{z}_{2|1} - z_2)^2 &\leq \sigma_{2|1}^2 (\chi^2 - \frac{(\hat{z}_1 - z_1)^2}{\sigma_1^2}) \end{aligned} \tag{3.54}$$

Once the double difference ambiguities z have been found, the inverse Z-transformation is necessary to find back the correct double difference ambiguities a. These ambiguities can be

referred to any frequencies or combination of ambiguity as long as they are referred as integer.

The search procedure will output the two best candidates of the ILS method $\breve{a}_1$ and $\breve{a}_2$, which fits the intervals in (3.54), and their associated residual square norm vector:

$$\begin{aligned} \breve{a}_1 : R_1 &= \left\| \hat{a} - \breve{a}_1 \right\|^2_{Q_{\hat{a}}} \\ \breve{a}_2 : R_2 &= \left\| \hat{a} - \breve{a}_2 \right\|^2_{Q_{\hat{a}}} \end{aligned} \tag{3.55}$$

Having found these two candidates, the next step is to validate them as the correct ambiguities.

3.3.4 Validation method for the fixed ambiguities

The LAMBDA method has been explained in details in the previous section and the fixed ambiguities have been found using the ILS estimator after a decorrelation step. But to incorporate the fixed ambiguities in the Kalman filter, a validation test is needed. The ambiguities found in the LAMBDA method may not be valid and an incorrect fix can lead to substantial errors.

An easy way to validate the first candidate of the LAMBDA method is to use the ratio test, with *c* as the validation threshold:

$$accept \quad \breve{a}_1 \quad if: \quad \frac{\left\| \hat{a} - \breve{a}_1 \right\|^2_{Q_{\hat{a}}}}{\left\| \hat{a} - \breve{a}_2 \right\|^2_{Q_{\hat{a}}}} \leq c \tag{3.56}$$

The ratio test shows that if the square norm of the first candidate is far apart from the square norm of the second candidate, it is most likely that it is the correct ambiguity. In other words, if the first candidate has always better performance than the other one, there is a high chance

that it is the correct one. With the ratio test, a fixed tolerance value is used, as it is made in most of the experiments on the ambiguity resolution. A compromise has to be made and the tolerance value c is usually set to 0.4. Moreover, the proposed ambiguities will be considered valid if the same ambiguity set pass the ratio test a certain number of times.

The problem is that the ratio test will not test the correctness of the fixed ambiguities but rather the correctness of the LAMBDA method. A lot of research has been made by the University of Delft to asset a correct theoretical background to the LAMBDA method and especially the validation procedure. Larger classes of integer estimator have been introduced other than the ILS or IB class. The Integer Aperture (IA) and Best Integer Equivariant (BIE) are larger class of integer estimator with better performance in terms of validation. Especially, the IA estimator validates the fixed ambiguities considering the fail, success or undecided rate of the candidates (Verhagen 2005). But all these methods have very high computational aspects and are not well designed for real-time applications for now.

The LAMBDA method is a very powerful method to find the correct ambiguities. In order to do that, a well designed functional and stochastic model, and an appropriate estimation of all the different errors involved in the solution (ionosphere, multipath, orbit errors etc…) is needed. If the model is well suited to the proposed application, the Kalman filter will provide precise float ambiguities and associated covariance. In that way, the performance of the LAMBDA method will be optimal.
The lower bound of the probability of correct fix (PCF) using the integer boot-strapping and their conditional standard deviation $\sigma_{i/I}$ can also be sued. It is presented in (Keefee, Pettovelo et al. 2006):

$$PCF \quad \geq \quad P(\breve{a} = a_{true}) = \prod_{i=1}^{n} \; [2 \cdot \psi(\frac{1}{2\sigma_{i|I}}) - 1] \tag{3.57}$$

With the area under the normal probability density function (PDF) of the float ambiguity defined as:

$$\psi(x) = \frac{1}{\sqrt{2\pi}} \int_{-\infty}^{x} \exp(-\frac{1}{2} n^2) \cdot dn \qquad (3.58)$$

This lower bound can give a good approximation of the validity of the fixed ambiguity.

The next section will briefly summaries the new proposed RTK algorithm.

3.4 Global summary of the complete RTK technique

The Figure 3.3 presents the overall RTK algorithm, with the flow of computations and data until the final PVT (Position Velocity Time) solution. The RTK algorithm exists in a C version and in a Matlab version. The figure summarizes the C version, which is a completely independent real-time RTK positioning solution, working with two Novatel receivers. The Matlab version is used for new developments and new technique. These versions work also with the developed GNSS receiver, but with small modifications in the observations management. The two versions are still in development for new perspective and other applications, like INS or new frequencies development.

The square represents the different algorithm process and the arrow shows the flow of data. Every data can be accessed or recorded in real-time. One can see that the RTK algorithm works with real-time RS-232 link or with post-process files, like pdc file for Novatel.

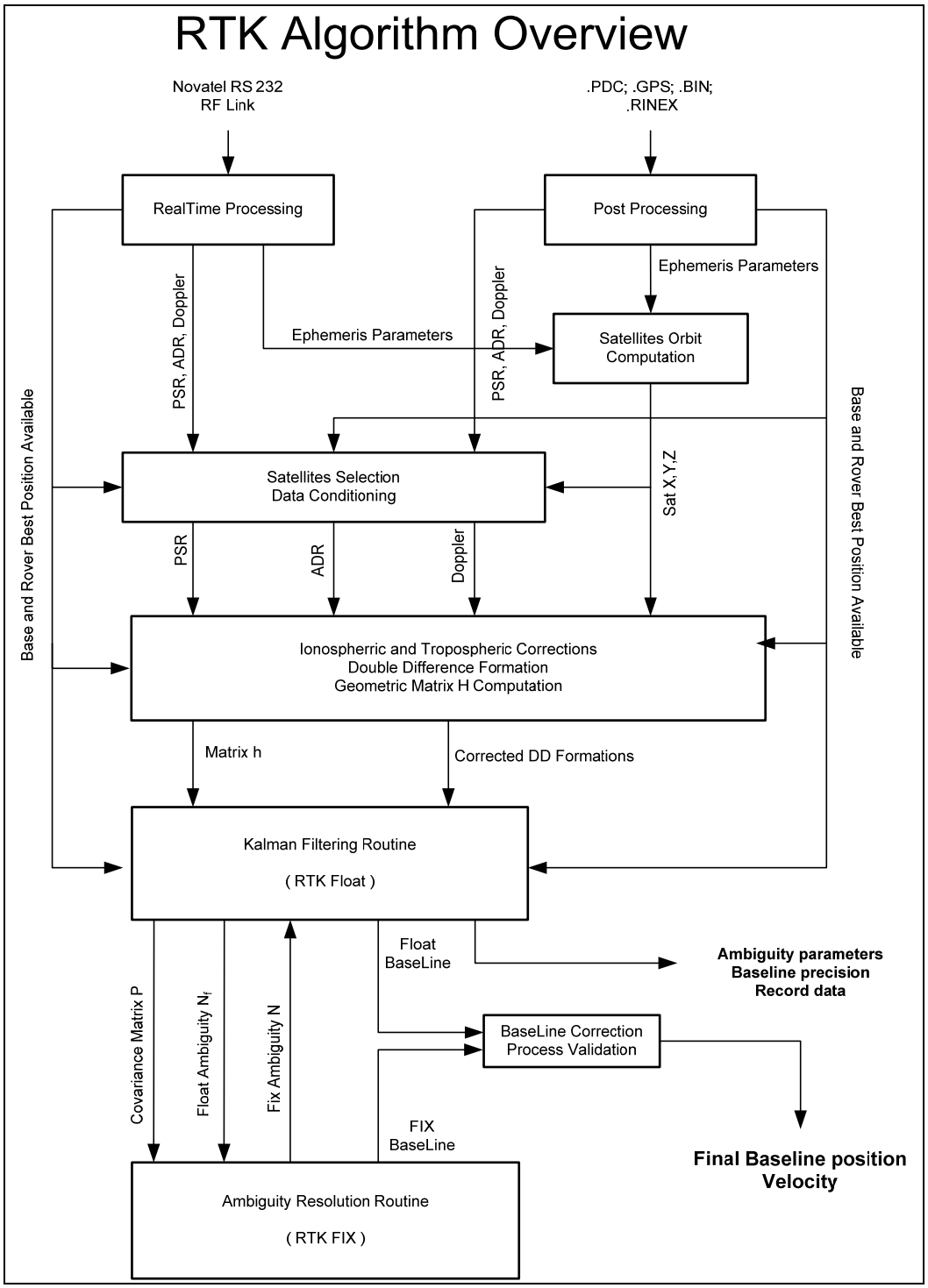

Figure 3.3 Overview of the global Kalman filter procedure for the RTK algorithm.

CHAPITRE 4

ALGORITHM VALIDATION FOR SHORT BASELINE RTK USING LACIME-NRG GNSS AND NOVATEL RECEIVERS

4.1 Introduction

This chapter will present the main results of the developed RTK software for short baseline test. These results will validate the theory explained through the last two chapters, concerning the observations analysis and the Kalman filter theory. Data coming from static and dynamic tests will be processed, in float mode (real value ambiguities) and in fixed mode (fixed integer DD ambiguities). The RTK algorithm will be used with two different receivers, the GNSS receiver developed at the LACIME-NRG laboratory and the Novatel receiver.

The Novatel receiver is a commercial Novatel DL4-plus receiver. It features L1 and L2 frequencies and allows complete access of measurements through the use of multiple logs, in real-time or in post-process mode. On the other hand, the GNSS receiver is a FPGA-based GPS/Galileo receiver for the L1 frequency. This software based receiver has multiple advantages compared to a commercial receiver. It is reprogrammable, fully adaptive, and allows complete access and control to all the internal parameters and signals of a GNSS receiver. It is the perfect tool for research and development on new technology in the GNSS domain.

In the LACIME laboratory, two Novatel receivers and one GNSS receiver are available. To perform RTK positioning using the developed algorithm, two different configurations are used:

- **The Novatel configuration**: one Novatel receiver is used as the base and the other Novatel receiver is used as the rover.
- **The GNSS configuration**: the GNSS receiver is used as the rover and one Novatel receiver is used as the base

These two configurations will be used to analyze the RTK algorithm performances, and in the same way, to analyze the performance of the developed GNSS receiver compared to the commercial Novatel receiver.

There are two main sections in this chapter. In the first section, the performance of the RTK algorithm will be analyzed for static mode, using both configurations. The RTK algorithm performs millimeter standard deviation precision on the static baseline position and rapid ambiguity resolution (less than 10 s) for both configurations. This is very encouraging for further development of the GNSS receiver.

In the second section, the RTK algorithm will be performed for a dynamic test using only the Novatel configuration. To analyze the precision of the algorithm, the post-process Waypoint solution will be used. Waypoint is a commercial post-processing software by Novatel. The RTK algorithm shows the same position precision and overall performance as the Waypoint solution.

4.2 Static analysis and performance of the GNSS receiver

4.2.1 Static double difference measurements precision

The static analysis of the observations is a first step to analyze the errors of the GPS signals. Two receivers are fixed at a known location, receiving GPS signals from all satellites in view. Double difference observations are made, and then compared to the true double difference reference, computed using the true receiver's position and the computed satellite position. The obtained difference is often called the *residuals*. The test setup will use first the GNSS receiver as rover (GNSS configuration), and then the Novatel receiver as rover (Novatel configuration). For the both cases, the base receiver is a Novatel receiver.

In order to use simultaneously the GNSS rover and the Novatel base, the observation measurement times have to be synchronized. Indeed, the Novatel receiver corrects

automatically his internal clock bias and synchronizes its measurements to the GPS time. The GNSS receiver has its own clock bias and its measurements are not adjusted to the GPS time. To perform double difference observations, the time of the GNSS measurements has to be adjusted to the GPS time. To do so, a simple extrapolation is made:

$$P_{GNSS}(t_{GPStime}) \approx P_{GNSS}(t_{GNSS}) + \Delta t \cdot DOP_{GNSS}(t_{GPStime}) \quad (4.1)$$

$$\Delta t = t_{GPStime} - t_{GNSS} + dt_{GNSS}(t_{GPStime}) \quad (4.2)$$

Where:

$P_{GNSS}(t_{GNSS})$	is the GNSS pseudo-range at time of GNSS measurements t_{GNSS},
$P_{GNSS}(t_{GPStime})$	is the GNSS pseudo-range at the GPS time,
$DOP_{GNSS}(t_{GPStime})$	is the Doppler measurements at the GPS time,
$dt_{GNSS}(t_{GPStime})$	is the GNSS clock bias at GPS time,
Δt	is the time delay between the time of GNSS measurements and GPS time.

The LACIME-NRG GNSS receiver clock bias dt_{GNSS} is computed internally in the GNSS receiver by a simple Kalman filter once the position solution is made. It is an important issue to correctly synchronize the GNSS receiver time and to perform a double difference with the Novatel receiver base in real-time. The carrier phase is so precise that a bias of a few ms in the interpolation can induce a major drift in the solution.

Once the measurements are synchronized between receivers, the residuals are computed using the double difference measurements and the true double difference satellite receiver's distance. They are analyzed in

Figure 4.**1** for the pseudo-range observations and the ADR observations. The residuals are presented for the GNSS configuration and the Novatel configuration, sharing the same antenna for the rover and the same base. The carrier phase has been removed from their expected ambiguity for more clarity.

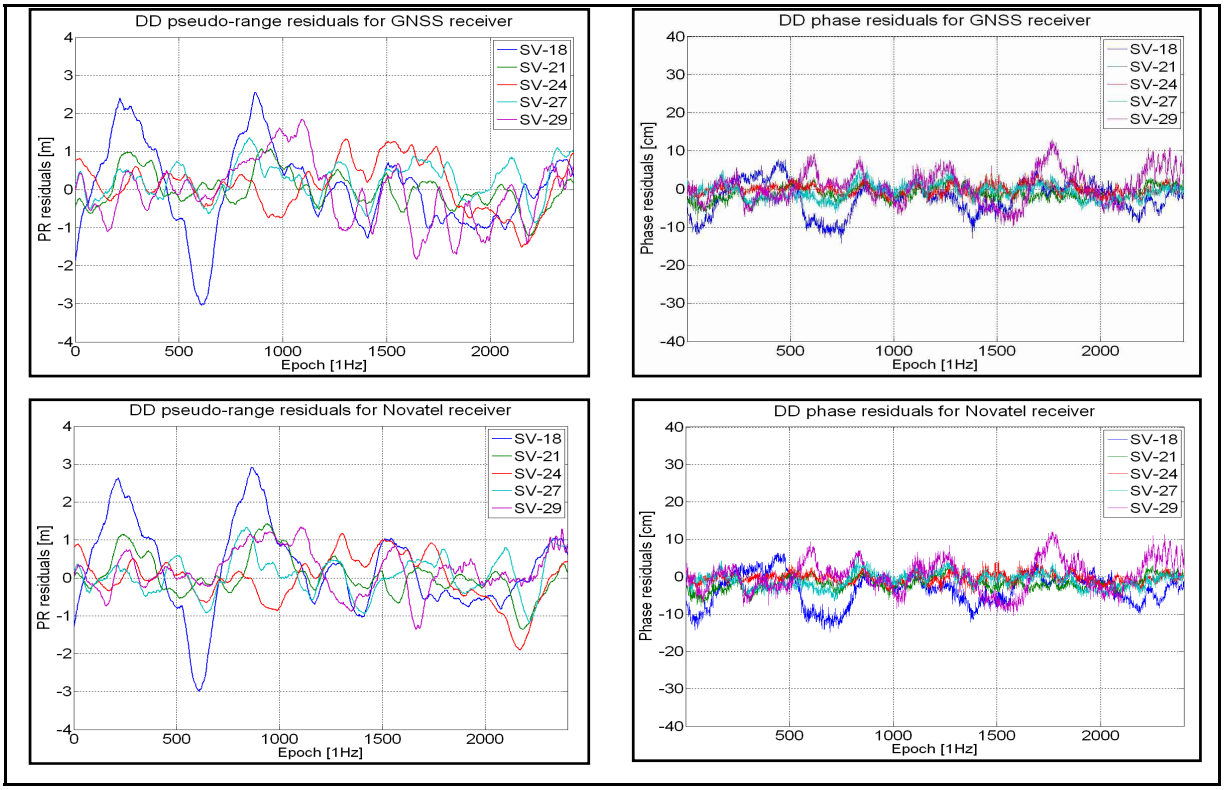

Figure 4.1 Analysis of measurements double difference residuals for the GNSS-Novatel and Novatel-Novatel pair of rover-base in static mode, using known baseline position.

What is the most striking in these figures and the Table 4.1 is the similarity between the two configurations. The patterns are identical for the carrier phase and very similar for the pseudo-range. This resemblance can be explained by the use of the same base station and of course the use of the same antenna for the rover. The small difference in pseudo-range may be explained by a difference in the carrier-smoothing process used by Novatel.

The precision of the carrier phase is the most interesting part of the developed RTK solution. Once the ambiguities are resolved, the positioning is only based on the carrier-phase measurements. As shown in Table 4.1, the residuals of the GNSS configuration are very similar to the ones of the Novatel configuration. As a consequence, the RTK solution precision is expected to be similar.

Table 4.1
Standard deviation of Pseudo-range and carrier phase measurement for
GNSS and Novatel Double difference, and related medium elevation angle

	Pseudo-range mean [cm] and standard deviation[m]									
	SV 15-18		SV 15-21		SV 15-24		SV 15-27		SV 15-29	
Novatel configuration	2.7	1.16	5.5	0.53	10.7	0.64	10.2	0.51	19.3	0.56
GNSS configuration	8.9	1.12	14	0.46	25.5	0.62	32.3	0.47	10.8	0.80
	Carrier-phase mean [cm] and standard deviation [cm]									
	SV 15-18		SV 15-21		SV 15-24		SV 15-27		SV 15-29	
Novatel configuration	1.2	4.2	2.3	1.9	3.3	1.4	-0.7	2.0	4.1	4.3
GNSS configuration	2.1	4.2	1.8	1.8	4.2	1.4	-3.9	2.0	9.6	4.3
	Medium elevation angle (reference SV15 : 75)									
	SV 18		SV 21		SV 24		SV 27		SV 29	
Medium elevation angle [degree]	30.1		29.6		56.2		36.7		26.6	

The residuals will be considered as the measurements noise. As seen in the previous chapters, in short baseline scenario, the common error are removed in the RTK algorithm. The remaining errors are mainly composed of the measurements noise, and in some cases the multipath, but in our case, it was free of multipath. Towards the results of the Table 4.1, the reference standard deviation of the double difference pseudo-range and carrier-phase measurements take the values:

$$\sigma_P = 0.7 \quad [m] \tag{4.3}$$

$$\sigma_\varphi \approx 0.02 \quad [m] \quad \approx 0.1 \quad [cycles] \tag{4.4}$$

These results can be compared to the theoretical values for such a short baseline configuration in Table 4.2. These values are in the same range for the GNSS and Novatel configurations.

Table 4.2
General User Range Error analysis of GPS measurements in short baseline

	Pseudo-range	**Carrier-phase**
Measurement noise	0.25 – 0.5 m	1 – 2 mm
Ephemerides errors	0.001 m	0.001 m
Atmospheric error	0.001 m	0.001 m
Multipath	~0 - 0.4 m	~0 - 0.1 m
Total	0.30 – 0.9 m	0.005 – 0.2 m

This technique is an interesting way of analyzing the different errors in the measurements for double difference scenarios. More studies can be done on specific non-common or common mode errors, like multipath. This analysis could lead to more accurate noise determination and modeling in control environment.

4.2.2 Float Solution results for GNSS and Novatel configuration

The developed RTK algorithm works in simulated real-time mode, with a post process algorithm. It means that the algorithm works epoch after epoch to find the best satellite set and estimate the position at each epoch, without looking ahead. As in the previous section, the two configurations will be used to analyze the performance of the RTK algorithm and the GNSS receiver.

The results are for static positioning, where the antenna are located at the rooftop of the school building as shown in Figure 4.2. The baseline is approximately 15 meters long, which is considered a very short baseline. The same antenna is mounted on the Novatel receiver and the GNSS receiver, allowing the receivers to share the same RF measures.

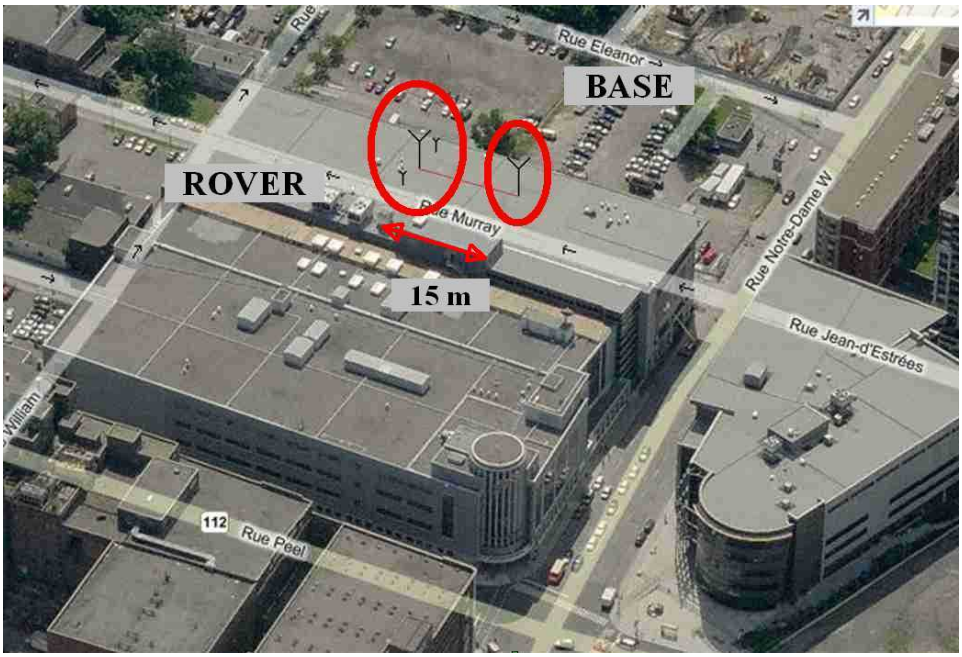

Figure 4.2 Static configuration of the antennas on the ETS rooftop. (from Microsoft bird view)

First, the float solution is presented. This solution keeps the ambiguity as real value in the Kalman filter instead of constrained-integers by the LAMBDA method. The float solution gives a good idea of the solution precision when there is no ambiguity resolution. The data have been recorded on March 19th 2009 and the figures represent a time span of 1 hour. Figure 4.3 and

Figure 4.**4** present the static RTK solution precision for the two configurations.

The Figure 4.5 presents the number of satellite used in the solution and the associated DOP. It shows that the GNSS receiver takes more time to compute a solution in the beginning of the process. This is mainly because the algorithm has to wait for a first internal solution to obtain the GNSS clock bias. It shows also that the GDOP is much related to the satellite selection. Change in one satellite in the selection can cause change in the GDOP up to 0.5.

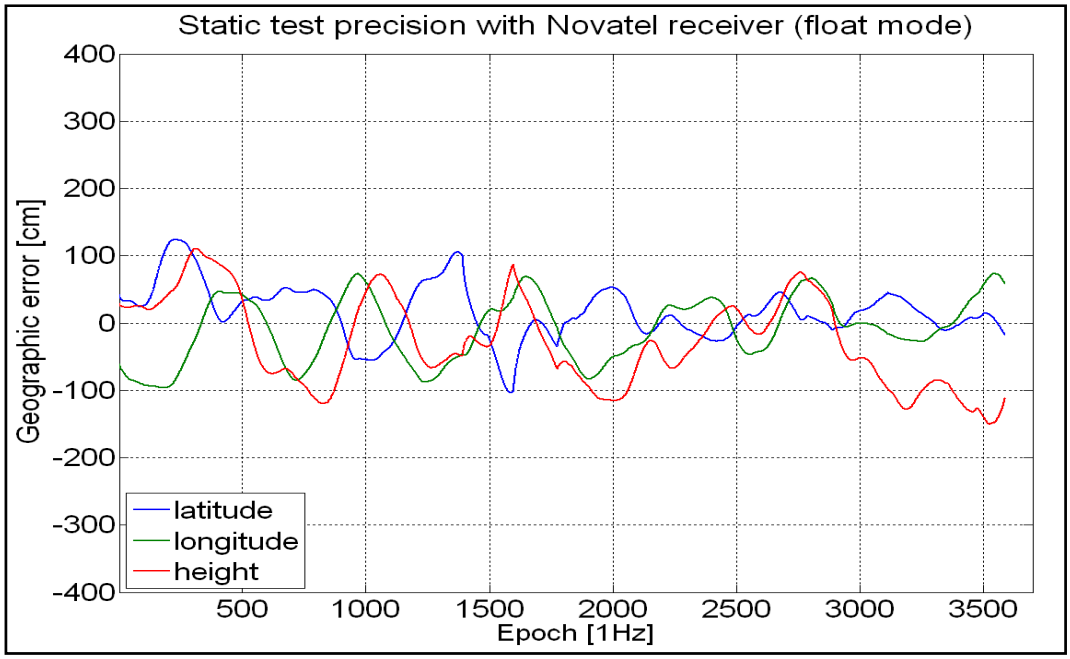

Figure 4.3 Geographic error of the position using the RTK software in float mode with the Novatel configuration for short baseline static test at ETS.

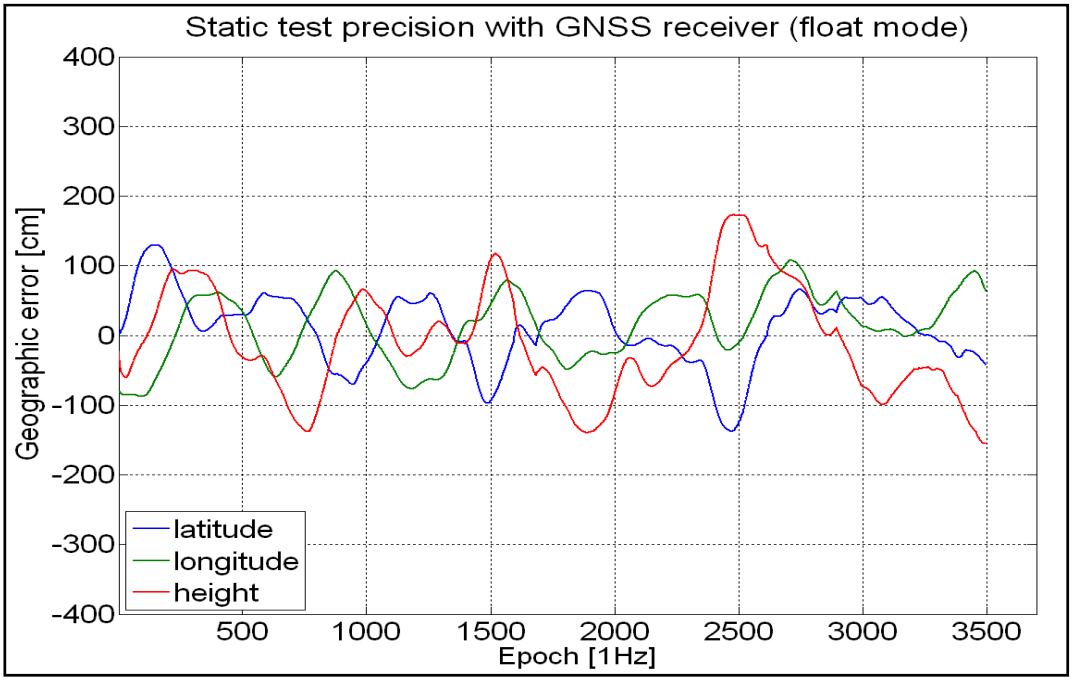

Figure 4.4 Geographic error of the position using the RTK software in float mode with the GNSS configuration for short baseline static test at ETS.

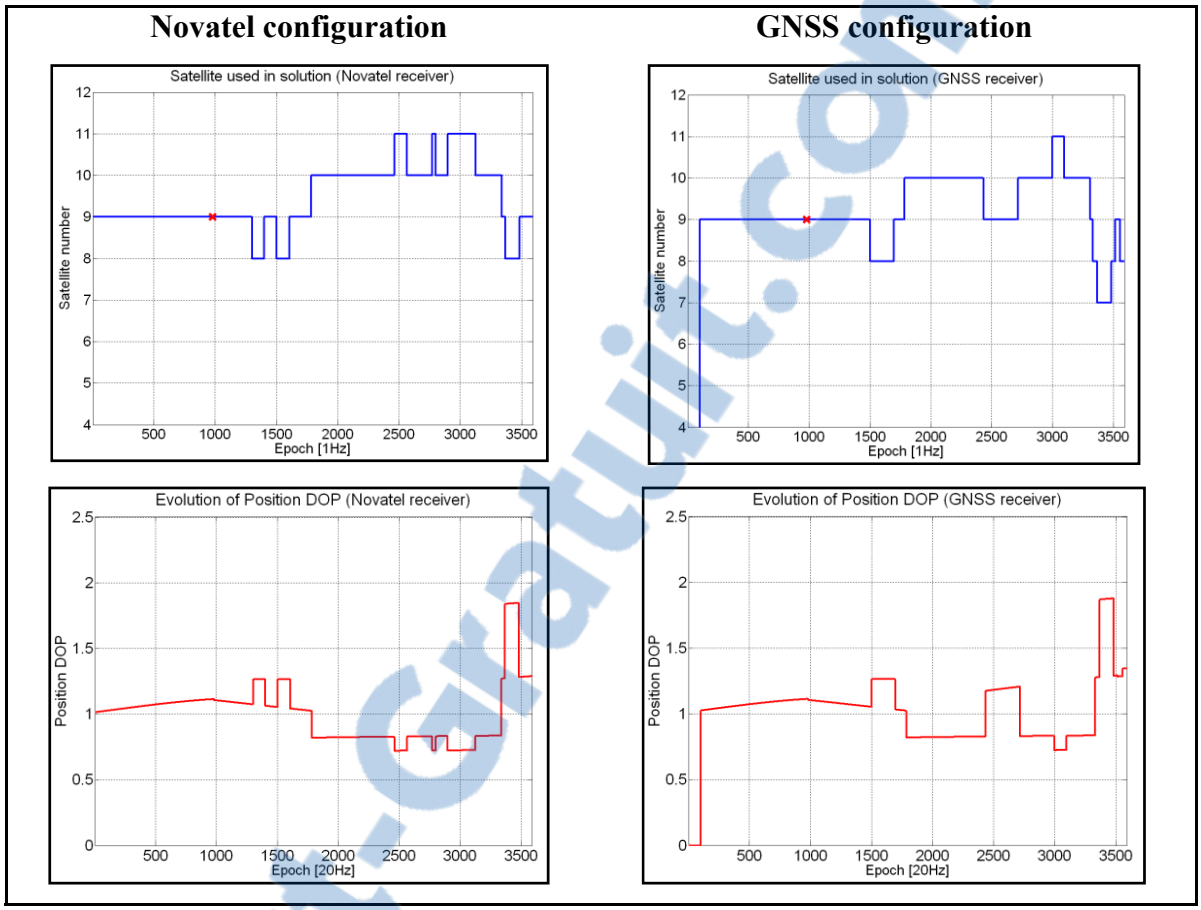

Figure 4.5 Number of GPS satellites used in the RTK solution and the associated PDOP for the Novatel and GNSS configuration.

For the same test scenario and the same base data set, the results in Table 4.3 show that the GNSS receiver is less precise than the Novatel receiver in float mode. It shows clearly this difference, with a GNSS solution presenting slightly higher standard deviation in the geographic axes.

This difference can be explained with the Figure 4.5, which presents the number of satellites used in both solutions and its associated PDOP. The figure shows that the GNSS PDOP is slightly higher, thus providing less accurate solution. It appears that the GNSS receiver did not track exactly the same GPS satellites than the Novatel receiver. This is due to a different channel management and acquisition technique. The Novatel is a more robust and fast GPS receiver than the developed GNSS receiver.

Table 4.3
Standard deviation (std) of the FLOAT solution for the two configurations:
the Novatel configuration and the GNSS configuration using known position.

	std LAT	**std LONG**	**std HEIGTH**
Novatel configuration	39.8 cm	47.5 cm	65.9 cm
GNSS configuration	51.5 cm	49.2 cm	78.3 cm

This float solution gives an interesting first look of the GNSS configuration performance. The LACIME-NRG universal GNSS receiver reacts similarly as the Novatel receiver in terms of solution precision with the RTK algorithm. But the GNSS performance could be improved with a faster tracking acquisition and channel management, to match the Novatel receiver performance.

4.2.3 Ambiguity resolution results and fixed solution analysis

This section will now present the fixed solution. This solution is the same as the float solution, but with the use of ambiguity resolution during processing. In the developed algorithm, when the float solution has its ambiguity resolved, it becomes the fixed solution. The LAMBDA method is used to find the correct integer ambiguities and to constrain the vector X in the Kalman filter.

In a static short baseline mode, the ambiguity will easily be resolved. These nice results come from the complete removal of the atmospheric errors and some systematic errors (e.g.) clock bias, due to the double difference and the proximity of both receivers. If the stochastic model is well suited for the test, the ambiguity will be resolved quickly, and the solution will show centimeter precision.

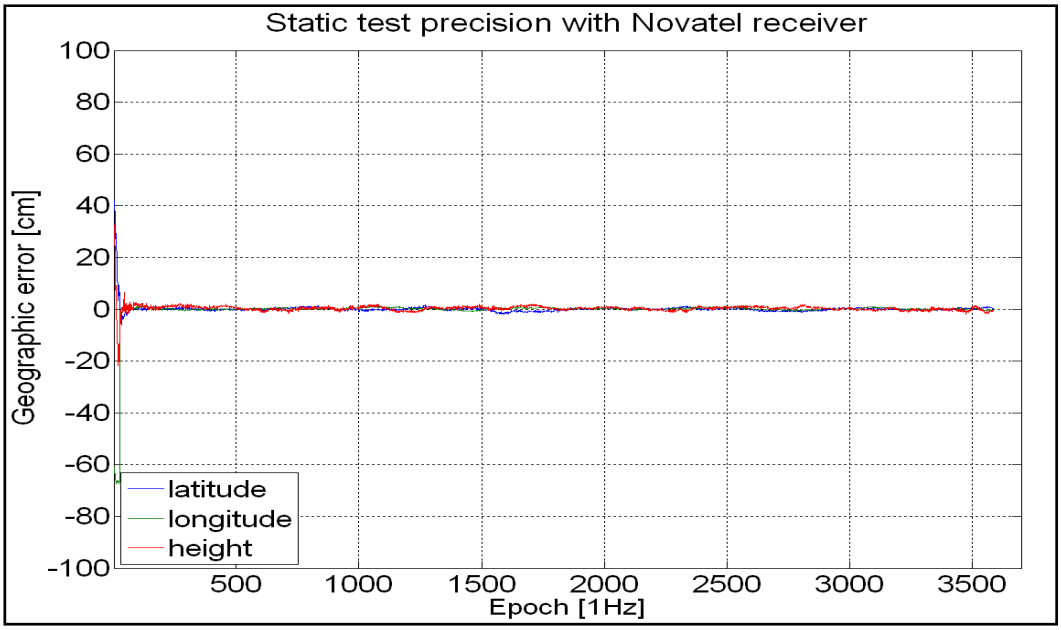

Figure 4.6 Geographic error of the position using the RTK software in fixed mode with the Novatel configuration for short baseline static test at ETS.

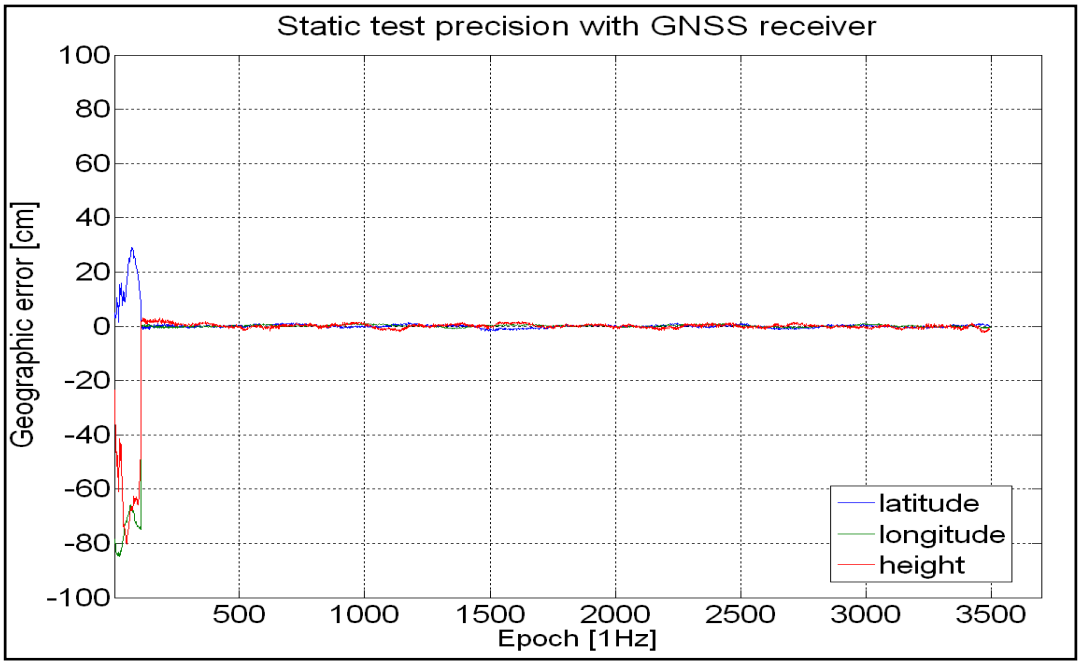

Figure 4.7 Geographic error of the position using the RTK software in fixed mode with the GNSS configuration for short baseline static test at ETS.

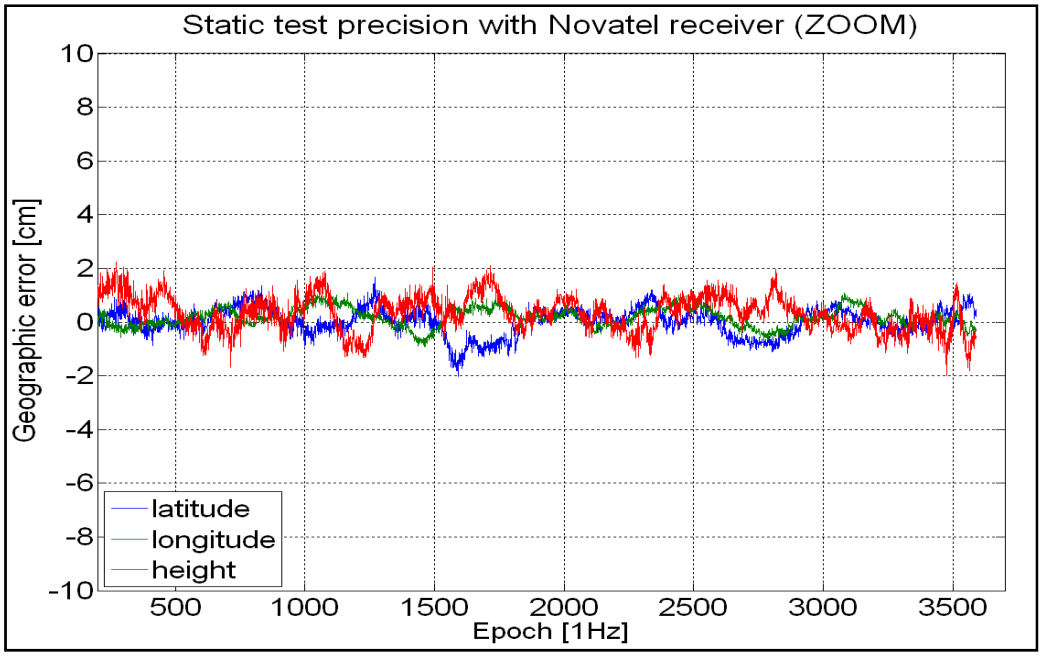

Figure 4.8 Zoom of the geographic error of the position in fixed mode with Novatel configuration for short baseline test at ETS.

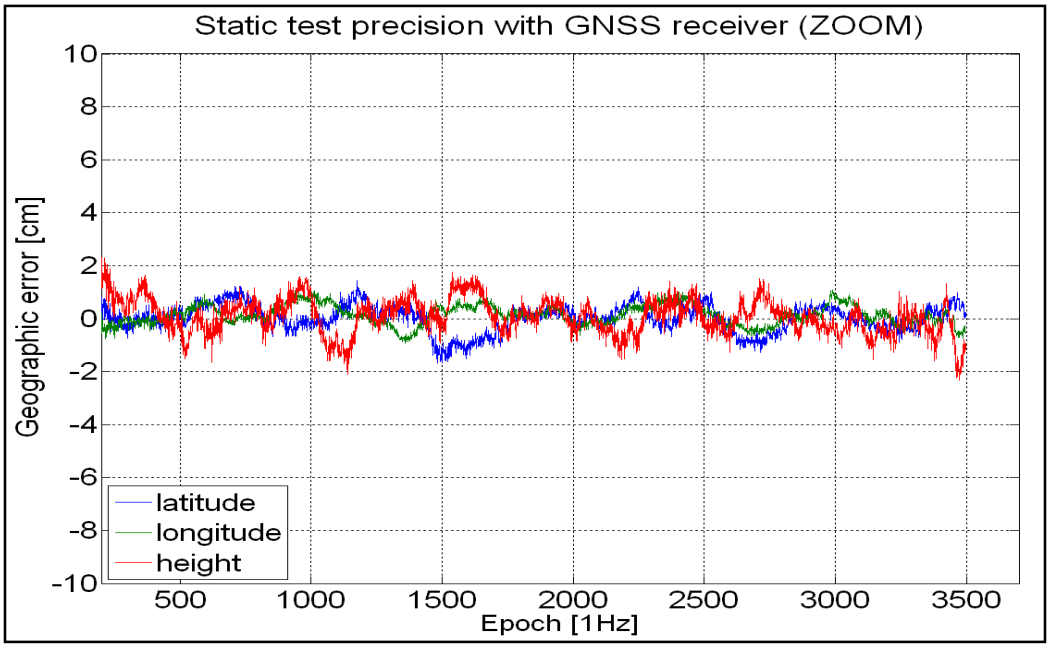

Figure 4.9 Zoom of the geographic error of the position in fixed mode with GNSS configuration for short baseline test at ETS.

Once the ambiguities are resolved, the solution will remain fixed all the time, except in case of general satellite cycle-slip or missing epoch. Special techniques could be performed in order to keep the ambiguities valid during such events. For example, in a static mode, once the fixed solution found and the position is obtained, the ambiguity can be recovered anytime using this reference known position. Surveyors usually use reference points in the field to obtain a fixed solution in a fast and reliable way.

The Figure 4.6 and Figure 4.7 show the fixed solution error for the two configurations. One can observe clearly the point of convergence, when the ambiguities are resolved after less than 1 minute, but it is more obvious in the GNSS configuration. The next figures show the same solution but with a zoom on the fixed solution, after ambiguity resolution.

Table 4.4
Standard deviation of the fixed solution errors for the Novatel and the GNSS configurations, and the difference between the two configurations solution.

Standard deviation	**Latitude**	**Longitude**	**Height**
Novatel	0.4 cm	0.4 cm	0.9 cm
GNSS	0.5 cm	0.4 cm	0.6 cm
Difference	0.2cm	0.1cm	0.3cm

The results are very interesting. First, it shows the precision of the static session using the RTK algorithm. When the ambiguities are fixed, the solution precision is below 1 cm for the Latitude, Longitude and Height axes (LLH). This is the expected precision for a short baseline static RTK solution. The height always shows higher deviation due to the GPS constellation geometry.

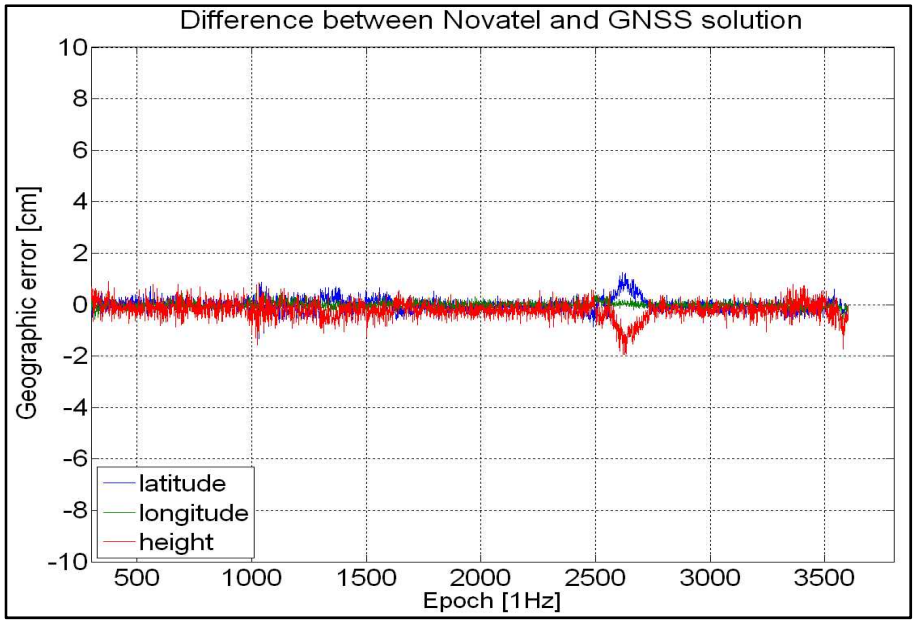

Figure 4.10 Solution difference between the Novatel and the GNSS configuration using the same RTK algorithm for the static test at ETS.

Figure 4.10 shows the difference between the Novatel configuration solution and the GNSS configuration solution. The difference between the two configurations is very low for the three geographic axes. The differences are due to the different satellite selection between the two configurations, and also to the measurements noise.

Table 4.5
Ambiguity success rate and Time to First Fix

	Time first fix	**% success**
Novatel configuration	14 s	99.4%
GNSS configuration	186 s	94.7%

The ambiguity resolution statistics presented in Table **4.5** show the time before the first ambiguity resolution fixed and the percentage of correct ambiguity resolution for the two configurations. This percentage takes into account the time the solution looses a satellite and need the ambiguity to be re-evaluated. The GNSS receiver shows lower results. This is due to a different channel management in the GNSS receiver and to the delay having the receiver

bias for synchronization. The Novatel receiver performs also carrier phase ambiguity estimation that could accelerate the Time to First Fix. The pourcentage of error represented the ambiguities that have been incorrectly validated.

In this section, the performances of the developed RTK algorithm were analyzed. In static short baseline, this powerful algorithm shows millimeter precision for the user position compared to the estimated reference position, for the Novatel and the GNSS configuration. The LACIME-NRG universal GNSS receiver shows similar performance than the Novatel receiver. Improvements in the GNSS could be made in channel management and data logs. It could speed up the ambiguity resolution process and allow more flexibility in position solution.

4.3 Analysis of the kinematic mode with both Novatel receivers (short baseline)

4.3.1 Experimental procedure

On the 15th july 2007, dynamic tests with Novatel receivers have been performed to record raw measurements for the RTK software. Two Novatel receivers have been used, one as the base station and one as the rover. The two antennas were Novatel model XLR704. The rover antenna was mounted on the top of a car as shown on Figure 4.11 and the base was fixed.

Figure 4.11 Installation set-up for the kinematic test recording (cars and receivers).

Figure 4.12 Trajectory of the dynamic test.
(From Google map view)

In this chapter, the raw measurements are recorded at 20 Hz. The trajectory of the car is presented in Figure 4.12. It includes low dynamic and static scenarios.

4.3.2 Float and fixed solution results

This section presents two solutions using float and fixed mode of the RTK algorithm. The solution is compared to the Novatel post-processing software named Waypoint. The fixed mode use the LAMBDA method and the validation method explained in section 3.3**.** The ambiguities are resolved as integers, and then fixed in the Kalman filter. The precision of the carrier phase is fully used, thus providing solution precision at the centimeter level.

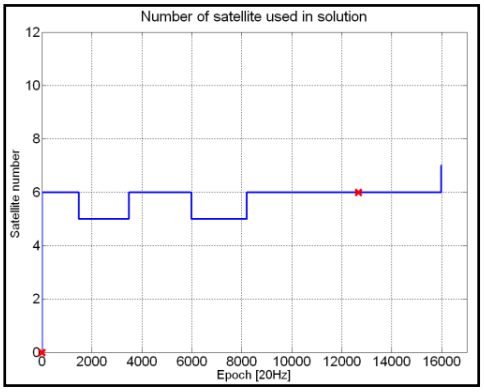

Figure 4.13 Number of satellites used in the RTK solution for the kinematic test.

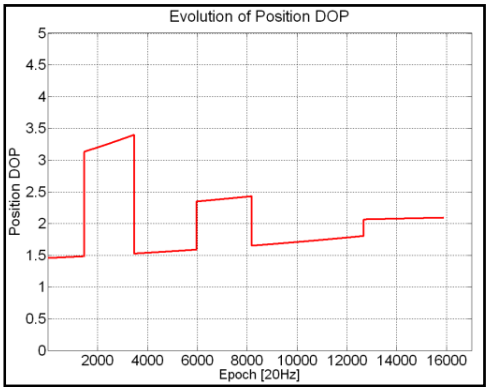

Figure 4.14 Evolution of Position DOP in the RTK solution for the kinematic test.

Figure 4.13 and Figure 4.14 show respectively the number of satellites used in the solution and the associated position DOP (PDOP) of the satellite geometry. As it is clearly explained in (Misra and Enge 2006), the DOP is directly related to satellite geometry and thus the position precision. It is a good indicator for a-priori position errors. The PDOP is calculated as follow:

$$PDOP = \sqrt{H'_{11} + H'_{22} + H'_{33}} \tag{4.5}$$

$$H' = H^t H \tag{4.6}$$

Where:

$PDOP$	is the Position Dilution Of Precision.
H	is the observation matrix (as detailed in section 3.2.2).
H'_{ii}	stands for the i diagonal element of H', here the 3 position axes.

In a standard estimation technique, the 3-D Root Mean Square (RMS) error of the user position can be defined as:

$$RMS_{3-D\ error} = \sigma \cdot PDOP \tag{4.7}$$

Where:

$RMS_{3-D\ error}$	is 3-D Root Mean Square (RMS) error of the position.
$PDOP$	is the Position Dilution Of Precision.
σ	is the User Range Error standard deviation.

The float mode in Figure 4.15 shows clearly more variations than the fixed mode. Nevertheless, the float mode is more precise than a classic stand alone solution and even a GPS-WAAS solution specifically on altitude. The fixed solution in Figure 4.16 shows little standard deviation in the position and impressive small errors. The majority of the remaining errors are localized in the height domain, as shown in Table 4.3. The evolution of the standard deviation is pretty much constant, as detailed in Figure 4.15 and Figure 4.16.

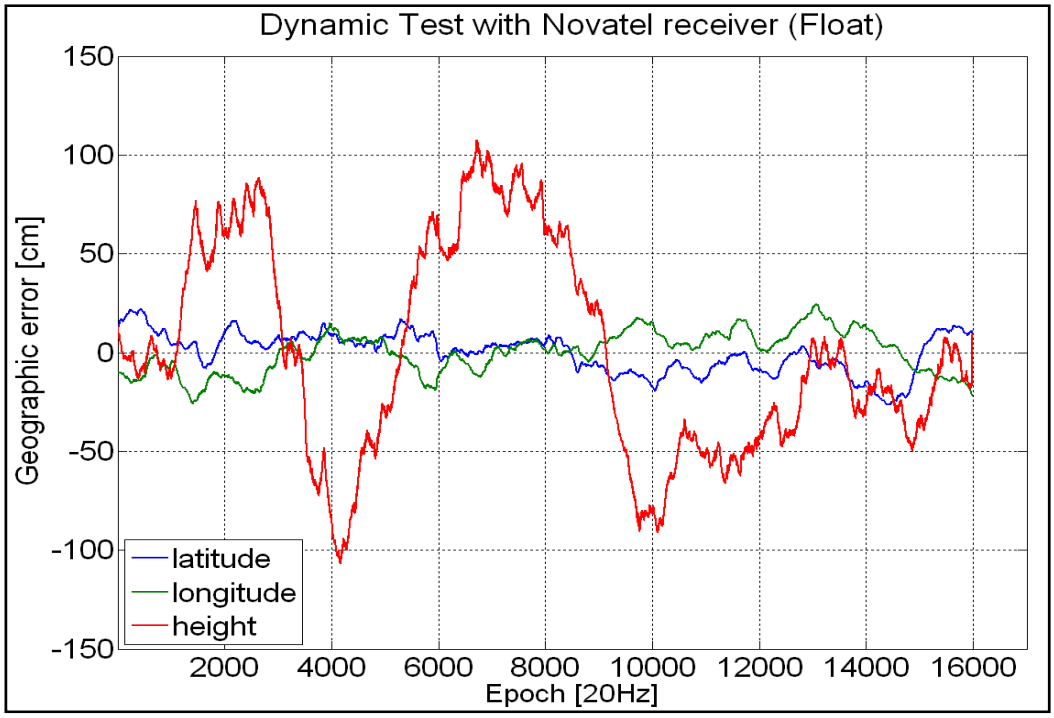

Figure 4.15 Position error for the float solution in the dynamic test, using Novatel configuration, compared to the Waypoint solution.

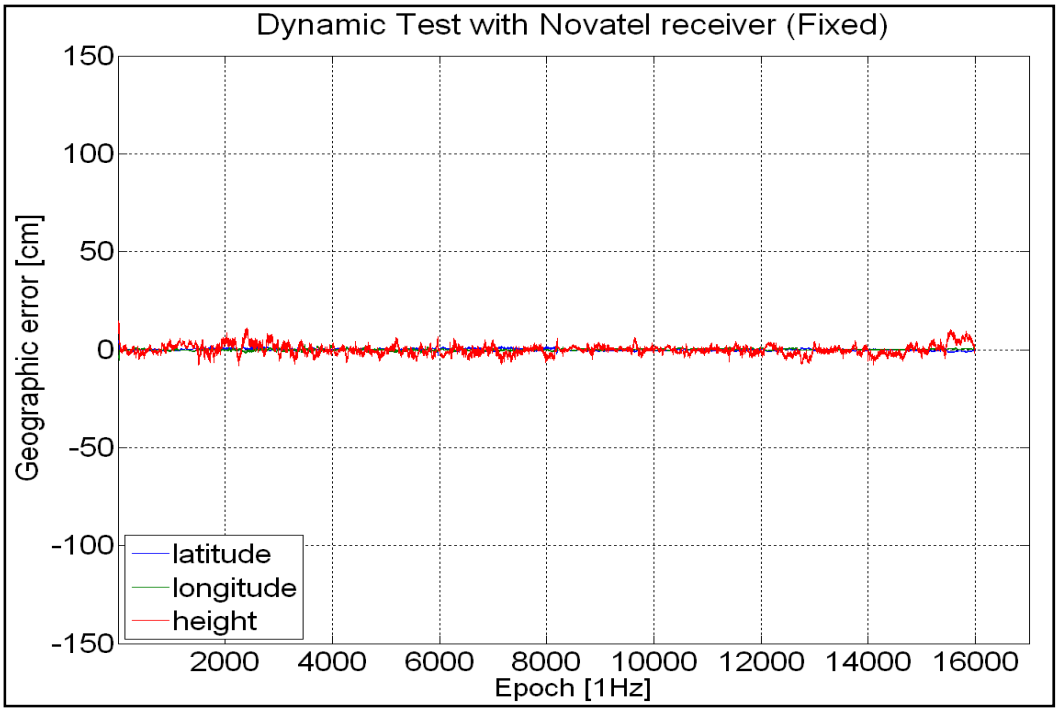

Figure 4.16 Position error for the fixed solution error in dynamic test, using Novatel configuration compared to the Waypoint solution.

Table 4.6
Standard deviation of the solution for the LLH axes

	std LAT	**std LONG**	**std HEIGTH**
Float mode	10.1 cm	10.6 cm	52.5 cm
Fixed mode	0.5 cm	0.5 cm	2.5 cm

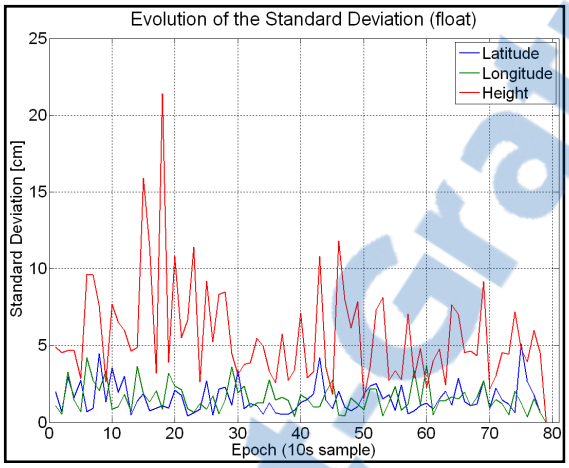

Figure 4.17 Evolution of the standard deviation of the position errors for the float solution in dynamic test.

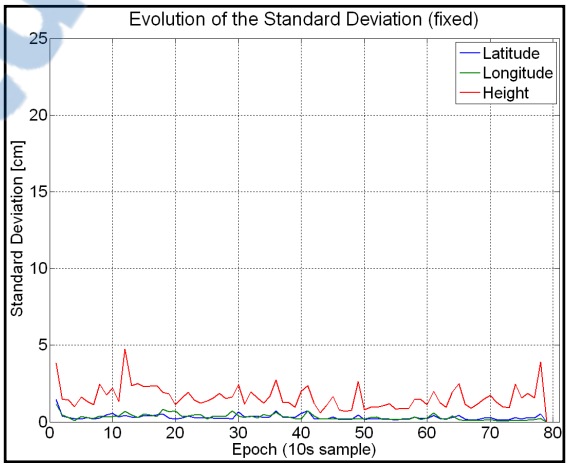

Figure 4.18 Evolution of the standard deviation of the position errors for the fixed solution in dynamic test.

These performances are sensibly the same as in static mode. In a static mode, one can consider the fixed position as the absolute reference, even if some unknown bias is present. In this dynamic mode, the position solution is compared with the Waypoint solution, which is not the true reference. Some errors will be inherent to the data and presented in both solution, which the difference doesn't detect. As a consequence, it is important to take the performance results with caution since it is a relative error analysis with Waypoint solution which is not the perfect one. Figure 4.17 and Figure 4.18 represent the evolution of the standard deviation but does not correspond to the overall test. This is because the float solution has deviation errors varying slowly in time.

Figure 4.19 presents the standard deviation of the Waypoint post-processing solution. The order of magnitude of the Waypoint solution is the same as the RTK solution precision compared to Waypoint. It is now easy to conclude that the RTK developed algorithm has the same precision as the Waypoint solution for that case. But the RTK solution works in real-time mode, without post-processing algorithm. It is very interesting to have such a solution for real-time applications, like embedded GPS receiver in car or airplane. If more details on the dynamic solution precision are needed, a scenario with an exact reference trajectory has to be made and compared with the RTK algorithm solution.

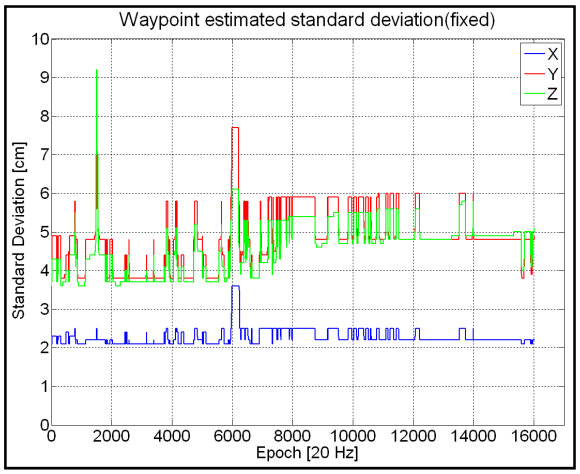

Figure 4.19 Waypoint estimated standard deviation of the position error for the dynamic test.

4.3.3 Velocity error of the dynamic solution

This section takes a look at the velocity estimation of the rover. There are many ways to calculate the precise velocity of a rover using RTK technique. The developed RTK algorithm estimates the velocity of the rover using the Doppler measurement and a state estimation in the Kalman filter. This solution provides a good approximation of the velocity but it is limited by the precision of the Doppler measurements.

Other method will be needed to estimate the velocity using directly the position and differentiate it through time using simple single epoch method. Other method can be applied,

using spline approximation or high order derivation, but this is not the process done here. The reader can refer to (Cannon, Lachapelle et al. 1997) for further information. Figure 4.20 shows the rover velocity in Latitude and Longitude axis (similar to East-North axis). The maximum velocity reaches 9 m/s (32.4 km/h).

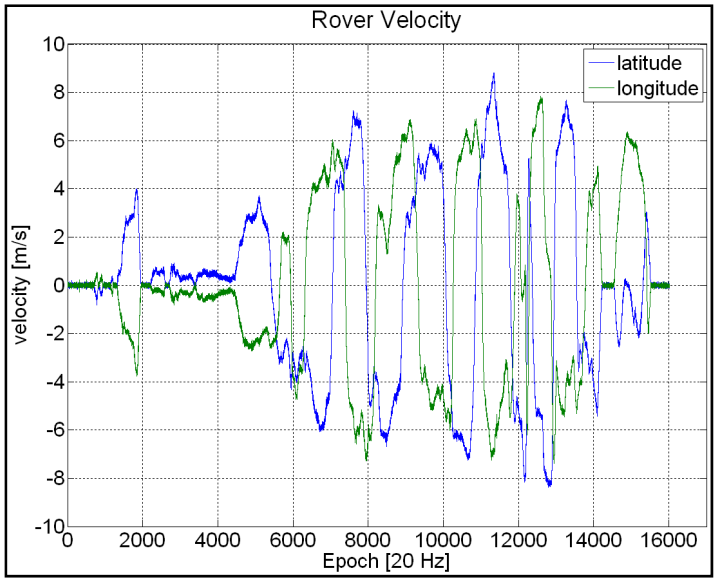

Figure 4.20 Velocity of the Novatel receiver mounted on the car during the dynamic test.

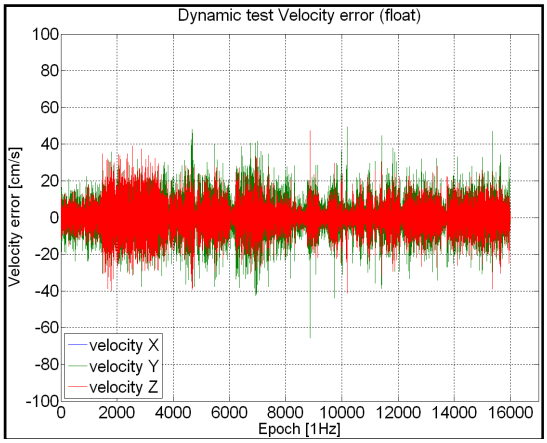

Figure 4.21 Errors of the rover velocity using the float solution in dynamic compared to Waypoint.

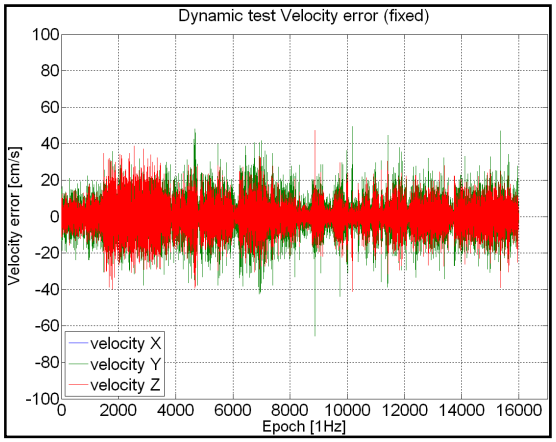

Figure 4.22 Errors of the rover velocity using the fixed solution in dynamic compared to Waypoint.

Table 4.7
Standard deviation of the velocity solution for the two modes

Standard deviation	vel X	vel Y	vel Z
Float mode	2.7 cm/s	9.3 cm/s	7.8 cm/s
Fixed mode	2.7 cm/s	9.3 cm/s	7.8 cm/s

The Doppler measurement is almost as precise as the carrier phase measurements for relative motion and contains the same information between two consecutive epochs. As a consequence, the fixed solution compared to the float solution will not improve the velocity precision in the RTK algorithm. The process is a standard constant velocity model. If further improvement is needed, another Markov model could be used.

4.3.4 Ambiguity resolution

This section will present the results of the RTK algorithm on ambiguity resolution. This result shows that the ambiguity resolution worked perfectly during all the process with 99% of success rate. The precision is at the centimeter level compared to the post-process solution generated by Waypoint.

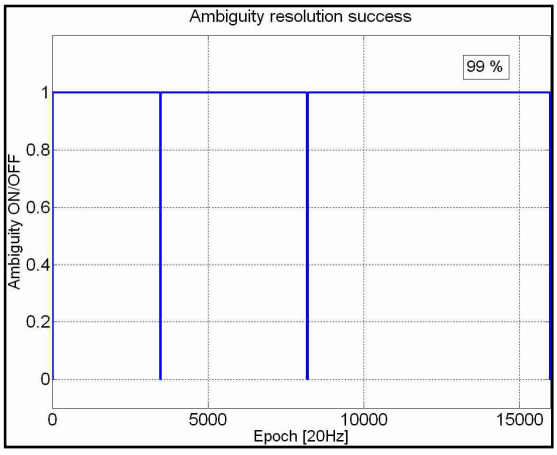

Figure 4.23 Ambiguity resolution success rate during dynamic test.

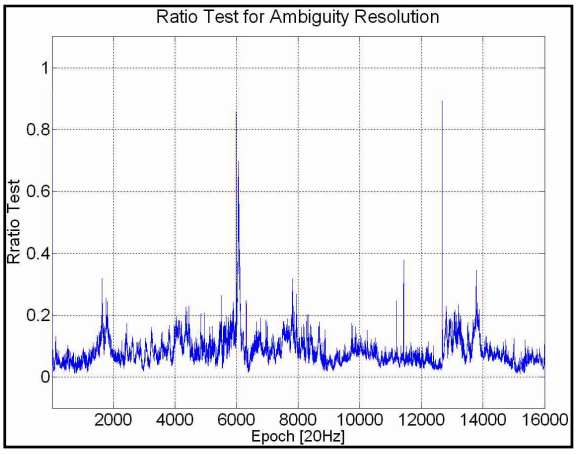

Figure 4.24 Evolution of the ratio test during dynamic test.

The ratio test is used to validate the ambiguity candidates as detailed in section 3.3. When the ratio is below 0.4 for a period of 20 epochs (1 second here), the ambiguity candidate is validated and is integrated in the Kalman filter. Figure 4.24 shows that the ratio test is below 0.4 for the major part of the process, allowing an excellent ambiguity resolution. The spikes in ambiguity resolution success rate happen when a new satellite incorporates the solution. The ratio test have sudden jump when a satellite leaves the solution. These results come from the stochastic management of the RTK software for satellite changes in the solution.

Table 4.8
Ambiguity success rate and Time to First Fix for dynamic short baseline test

	Time first fix	**% success**
Ambiguity Resolution	14 epoch (<1s)	99.89%

When a new satellite arises in the solution, a new ambiguity resolution is processed for that new satellite but the ambiguities already found are preserved. During that time, the ratio test has brief spikes as seen in Figure 4.23. But the Kalman filter quick convergence allows a fast ambiguity resolution of the new satellite. The results in Table 4.8 show very good results for a dynamic test. The ambiguities are almost instantaneously resolved.

The RTK algorithm is a fully functional centimeter precision position algorithm, for both static and dynamic test. The results presented in this section are valid for short baseline, since the distance between the base and the rover never exceeds 10 km. As a consequence most of the errors are completely removed. This will not happen when the baseline increases, as most of the errors of the GPS signals will not be removed anymore. The ambiguities will be more difficult to resolve and the classic RTK precision will not be met.

In the next chapter, the corrections and the model used to remove these non-common errors in medium and long baseline scenarios will be presented. Accurate model can improve the precision and allow correct ambiguities resolution, thus leading to the same centimeter precision as in short baseline.

CHAPITRE 5

CORRECTIONS FOR MEDIUM AND LONG BASELINE RTK AND RESULTS

Long baseline RTK situation is obtained when the distance between the base and the rover is larger than 80 km. The medium baseline can be defined when a baseline distance is between 20 and 80 km.

The non-common errors, mainly atmospherics and ephemeris errors, will be totally removed in short baseline using double difference measurements, due to the common location of the receivers. When the distance between the base and the rover reaches more than 10 km, these non-common and systematic errors (e.g. atmospheric errors) start to be decorrelated and need to be evaluated in the solution algorithm. They will affect the ambiguity resolution and validation, and will increase the solution errors and variance.

The difference between medium and long baseline is linked to the importance of the non-common erros in the RTK solution. Medium baseline presents less challenges toward error modeling and ambiguity resolution. There is still a low correlation between these errors, making the estimation more easier. On the other hand, long baseline is a lot more challenging for the RTK users. The non-common errors are mostly decorellated, thus implying the use of improved method that will be proposed in this study.

In this chapter, two scenarios will be considered. One is a static medium baseline test, which will be used to validate the embedded ionospheric model. With this proper modeling, the solution precision will be close to the short baseline one. The other test is a high dynamic long baseline scenario where the rover-baseline distance can reach up to 140 km. This test will be interesting to validate the continuity of the new RTK algorithm in a long baseline situation and to analyse the solution precision and degradation.

5.1 Presentation of the ionosphere modeling estimation for medium and long baseline scenario

As it has been detailed in chapter 2, the ionosphere can be modeled in different ways. With a single receiver, SBAS corrections or broadcast modeling can remove most of the ionosphere errors using L2 frequency. But in RTK, the solution is more precise than in single- receiver mode, since the measurements are free of much of the common mode error like satellites and receivers clock biases. The ionosphere will be one of the remaining errors and will need to be adequately estimated to reach the centimeter precision, especially in a long baseline situation.

The iono-free estimation method, detailed in chapter 2, is a theoretical model which is proven to remove most of the ionosphere errors in a multipath free environment (Grejner-Brzezinska, Wielgosz et al. 2006). It uses the dual-frequency carrier-phase measurements, and needs the ambiguity to be resolved. It will be used in a short baseline scenario or in a fixed ambiguity resolution situation. In that case, the iono-free corrections can be applied as long as continuous carrier tracking is maintained.

On one hand, the ionospheric errors have to be estimated to find the correct carrier-phase ambiguities, and on the other hand, the correct carrier-phase ambiguities have to be found to evaluate the ionospheric errors in the iono-free model. This explains why the methods to evaluate the carrier-phase ambiguity and the ionospheric errors at the same time are required. An *ionosphere-nullification* technique has been proposed with success by Don Kim and R. Langley (Kim and Langley 2005). The idea is to evaluate the ionospheric errors and the ambiguities at the same time in a recursive estimation method, until a minimum variance has been found. The other classic method is to model the ionospheric errors as parameters in the Kalman filer.

The *ionosphere weighted* method have been introduced by (Teunissen 1997) and (Odjik 2000), followed by (Liu and Lachapelle 2002) and (Alves, Lachapelle et al. 2002). It has also been used for multiple frequency carrier phase ambiguity resolution (Julien, Alves et al. 2004). This method has shown interesting results and good matching with the current

development. This is the reason why it is presented here as a development in the proposed RTK real-time algorithm for the medium and long baseline scenarios.

5.1.1 Ionosphere error state in the weighted ionosphere estimation.

The weighting ionosphere technique estimates the double difference ionosphere error I_{km}^{pq} for every satellite pair at each epoch, directly in the state space vector X, using also an ionosphere pseudo-observation. This pseudo-observation is added in the measurement vector Y. The state space vector X becomes:

$$X = [x \quad y \quad z \quad \dot{x} \quad \dot{y} \quad \dot{z} \quad N_{km}^{pq} \quad .. \quad I_{km}^{pq} \quad ..]^T \tag{5.1}$$

Where:

I_{km}^{pq}	is the double difference ionosphere error,
N_{km}^{pq}	is the double difference carrier-phase ambiguity vector,
(x, y, z)	is the baseline vector component in ECEF axes,
(dx, dy, dz)	is the receiver velocity component in ECEF axes.

The ionosphere error is defined as a classic random walk process:

$$\begin{aligned} I_k &= I_{k-1} + w_k \\ E\{w_k^2\} &= E\{(I_k - I_{k-1})^2\} \\ &= E\{I_k^2\} + E\{I_{k-1}^2\} - 2E\{I_k I_{k-1}\} \\ &= 2\sigma_{iono}{}^2 \end{aligned} \tag{5.2}$$

Where:

I_k	is the double difference ionosphere errors at time k,
w_k	is the ionosphere error associated noise,
σ_{iono}	is the ionosphere estimated covariance.

The associated matrix Q of the state covariance has to be modified according to the new state space vector, with the (n-1) new double difference ionospheric error states at each epoch.

The ionosphere process variance is baseline dependant (Liu and Lachapelle 2002). When the baseline is long, the double difference ionospheric errors are more likely to fluctuate heavily, especially in high ionospheric activities. On the other hand, when the baseline is short, the ionospheric error will remains constant and near zero over time.

$$E\{w_k^2\} = 2\sigma_{iono}^2(1 - e^{-2\frac{d}{D}}) \tag{5.3}$$

Where:

σ_{iono}	is the ionospheric double difference error process variance,
d	is the baseline distance,
D	is the first-order distance correlation.

This model allows the ionospheric error to be baseline dependant. A value of 1500 km for D is taken, as specified in (Liu and Lachapelle 2002). This value is an empirical one and can be adjusted by researchers in future works.

The ionospheric error is considered as the remaining errors of the observables (pseudo-range and carrier-phase). For each double difference observation, the corresponding ionospheric error is modeled as a state in the Kalman filter space vector. The Doppler measurement is not used for simplicity. The ionospheric error state is directly related to the observables as:

$$P_{km,L1}^{pq}(t) = \rho_{km}^{pq}(t) - I_{km,L1}^{pq}(t) \tag{5.4}$$

$$P_{km,L2}^{pq}(t) = \rho_{km}^{pq}(t) - \frac{f_{L1}^2}{f_{L2}^2} I_{km,L1}^{pq}(t) \tag{5.5}$$

$$\varphi_{km,L1}^{pq}(t) = \frac{1}{\lambda_{L1}} \rho_{km}^{pq}(t) + N_{km,L1}^{pq} + \frac{1}{\lambda_1} I_{km,L1}^{pq}(t) \tag{5.6}$$

$$\varphi_{km,L2}^{pq}(t)=\frac{1}{\lambda_2}\rho_{km}^{pq}(t)+N_{km,L2}^{pq}+\frac{1}{\lambda_2}\frac{f_{L1}^2}{f_{L2}^2}I_{km,L1}^{pq}(t) \tag{5.7}$$

Where:

ρ_{km}^{pq}	is the DD satellite (pq)-receiver (km) geometric distance [m],
$P_{km,L1}^{pq}, P_{km,L2}^{pq}$	are the DD pseudo-range measurements on L1 and L2, respectively [m],
$\varphi_{km,L1}^{pq}, \varphi_{km,L2}^{pq}$	are the DD ADR measurements on L1 and L2, respectively [cycles],
$I_{km,L1}^{pq}$	is the L1 DD ionospheric errors [m],
$N_{km,L1}^{pq}, N_{km,L2}^{pq}$	are the L1 and L2 DD ambiguities, respectively [cycles],
$\lambda_{L1}, \lambda_{L2}$	are the L1 and L2 wavelengths, respectively [m],
f_{L1}, f_{L2}	are the L1 and L2 frequencies, respectively [s^{-1}].

The geometry-free model, which determine the satellite-receiver distance instead of the relative receiver position is not used in this case, as it is in some studies on ionosphere weighted estimation (Liu and Lachapelle 2002), (Alves, Lachapelle et al. 2002). Instead, we expand the satellite-receiver range using the baseline position. As a consequence, the matrix H is changed to account for ionospheric error in the relation between the baseline vector and the observation.

$$H=\begin{bmatrix} h_x & h_y & h_z & 0 & 0 & 0 & 0 & -1 \\ h_x & h_y & h_z & 0 & 0 & 0 & 0 & -\frac{f_{L1}^2}{f_{L2}^2} \\ \frac{h_x}{\lambda_{L1}} & \frac{h_y}{\lambda_{L1}} & \frac{h_z}{\lambda_{L1}} & 0 & 0 & 0 & 1 & \frac{1}{\lambda_{L1}} \\ \frac{h_x}{\lambda_{L2}} & \frac{h_y}{\lambda_{L2}} & \frac{h_z}{\lambda_{L2}} & 0 & 0 & 0 & 1 & \frac{1}{\lambda_2}\frac{f_{L1}^2}{f_{L2}^2} \\ 0 & 0 & 0 & h_x & h_y & h_z & 0 & 0 \\ 0 & 0 & 0 & h_x & h_y & h_z & 0 & 0 \\ 0 & 0 & 0 & 0 & 0 & 0 & 0 & 1 \end{bmatrix} \tag{5.8}$$

Where:

(h_x, h_y, h_z) is the relative satellite-receiver line of sight vector,

λ, f is the corresponding wavelength and frequency.

One can see that this model allows the estimation of the ambiguities and the ionospheric errors at the same time. This model can be enough but the main drawback is that it introduces (n-1) more parameters to be estimated. This is the reason why pseudo-ionosphere observation are introduced in the ionosphere weighted method, to provide new observations and improve the filter stability.

5.1.2 Ionosphere pseudo-observations in the weighted ionosphere model

The ionosphere observations have been introduced in the algorithm with values close to zero. But these null pseudo-observations have an associated dispersive standard deviation error. If the variance of the pseudo-observation is high, the validity of the null values will be highly inaccurate, thus forcing the filter to estimate the real value. On the other hand, if the variance of the pseudo-observable is near zero, the null value of the ionosphere error is highly probable, thus keeping the ionosphere error as a null value, like in the short baseline case.

These two cases are commonly referred to the *ionosphere-fixed* and the *ionosphere-float* models, respectively (Odjik 2000). The combined solution of these two models is called the *ionosphere-weighted* model, and allows the model to adapt itself to its current baseline situation. It brings flexibility to the global RTK positioning algorithm, depending on the baseline distance and its associated ionosphere errors, as well as the time of convergence.

The observations vectors of the Kalman filter becomes:

$$Y = \begin{bmatrix} P_{km,L1}^{pq} & P_{km,L2}^{pq} & \varphi_{km,L1}^{pq} & \varphi_{km,L2}^{pq} & dop_{km,L1}^{pq} & dop_{km,L2}^{pq} & 0 \end{bmatrix}^T \quad (5.9)$$

In the *ionosphere-float* model, the pseudo-observations have a standard deviation of zero, thus keeping the ionosphere errors as null, like in short baseline scenario. In the *fixed-ionosphere* model, the pseudo-observations have a standard deviation of infinity or a high value for practical reasons. This model is equivalent to an ionosphere free solution, and is interesting for fixed solution with integer carrier phase ambiguities.

The weighted model is a generalization of the two extremes, where the ionospheric dispersion is stochastically tuned in accordance to the baseline length (Liu and Lachapelle 2002) In the developed RTK algorithm, a baseline dependant stochastic model is taken, in the same way as the ionosphere error covariance in equation (5.3).

$$\sigma_{iono}^{2}{}' = 2\sigma_{iono}^{2}(1 - e^{-2\frac{d}{D}}) \tag{5.10}$$

Where:

$\sigma_{iono}^{2}{}'$	is the weighted ionosphere covariance error,
σ_{iono}^{2}	is the reference ionosphere covariance error,
d	is the baseline distance,
D	is the reference baseline distance .

The covariance is introduced in the matrix R, which represents the covariance of all measurements. This model has been proved rather accurate by previous research, especially for the linearity of the baseline dependant parameters (Odjik 2000) and (Liu and Lachapelle 2002).

When a new satellite enters the system, a low value is assigned to the corresponding ionosphere variance. Indeed, the filter has to consider zero value ionosphere error as valuable, in order to integrate the new observations. The filter convergence and stability will be greatly improved.

5.1.3 Other non-common errors corrections

The tropospheric errors are well modeled by the Saastamoinen model detailed in section 2.3.1. Other model can be integrated, in order for example to model the wet zenith delays to increase the performance in long-baseline mode, as in (Collins and Langley 1997).

When the baseline length increases, the ephemerides have to be carefully adjusted. The satellite position cannot longer use the same emission time for the base and the rover, because of the significant difference in the satellite-receiver distance and thus, time of emission. The difference can introduce more than 20 cm error in the estimation processing (Table **2**.**4**).

Moreover, the linear observations model which is used for the relation between the satellite geometry and the baseline in section 3.2.2 is no longer valid. The parallelism of the satellite-receiver line-of-sight is not 'true' anymore. The only way to resolve this problem is to switch to an extended Kalman filter process (Simon 2006), where the observation matrix is linearized. This model was helpful at the beginning for computation purpose in short baseline but cannot be ignored in other scenarios.

To do so, instead of the matrix H defined in section 3.2.2, the use of the derivative of the navigation equation towards the base position is implemented but the position of the rover could be used also:

$$H = \begin{bmatrix} \frac{\delta g_{dd}}{\delta x} & \frac{\delta g_{dd}}{\delta y} & \frac{\delta g_{dd}}{\delta z} \end{bmatrix} \tag{5.11}$$

$$H = \begin{bmatrix} \frac{-(x-x_s)}{\rho} & \frac{-(y-y_s)}{\rho} & \frac{-(z-z_s)}{\rho} \end{bmatrix} \tag{5.12}$$

Where:

(x, y, z)	is the rover position,
(x_s, y_s, z_s)	is the satellite position,
g	is the observation function from (3.2),
ρ	is the receiver satellite distance.

In the state space vector of the Kalman routine, the baseline position is no longer used as a state. The difference in rover position relative to the base, epoch by epoch, will be rather represented. As a consequence, the satellite-receiver distance has to be evaluated to compute the residues in the Kalman filter update:

$$Y = DD - (DD_c + HX_{est}) \tag{5.13}$$

Where:

DD	is the measurement's observations.
DD_c	is the computed satellite-receiver distance with the estimated position.
H	is the linearized observation matrix.
X_{est}	is the estimated state space vector.

At the end of the Kalman filter procedure, the rover position is updated using:

$$position_{k+1} = position_k + X_{k+1} \tag{5.14}$$

In this way, the errors coming from satellite receiver parallelism in the previous linear model are not modeled anymore in the observation matrix for longue baseline distance.

5.2 Static validation of the ionosphere weighting scheme for medium baseline

5.2.1 Experimental procedure and methodology

To validate the proposed RTK algorithm in medium baseline, a static medium baseline test is used. The data were recorded simultaneously with two Novatel DL-4 receivers. The rover was installed in the Canadian national park of OKA on October 2008 (Figure 5.1). The base was placed on the ETS rooftop. The baseline between the base and the rover is approximately 40 km (Figure 5.2) and the height difference is 12 meters.

Figure 5.1 Static rover antenna installation for the medium baseline test.

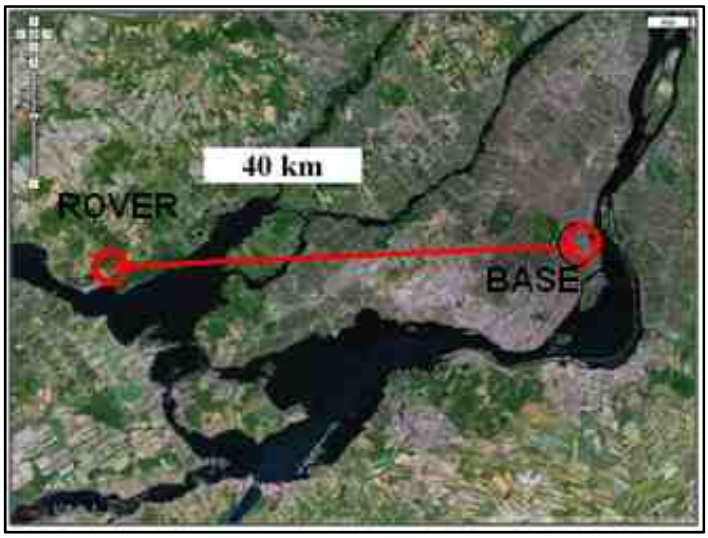

Figure 5.2 Satellite view of the baseline distance for the medium baseline test.
(from Google Map view)

The RTK algorithm uses the intelligent satellite selection of section 3.1 to manage the reference satellite selection, and the satellite coming in and out of the solution. The corresponding satellite double difference phase ambiguities are managed in a robust way during the process. The elevation angle cut-off is set at 15 degrees and the minimum Novatel's Lock Time (LT) is set at 20 epochs, and the data are recorded at 1Hz.

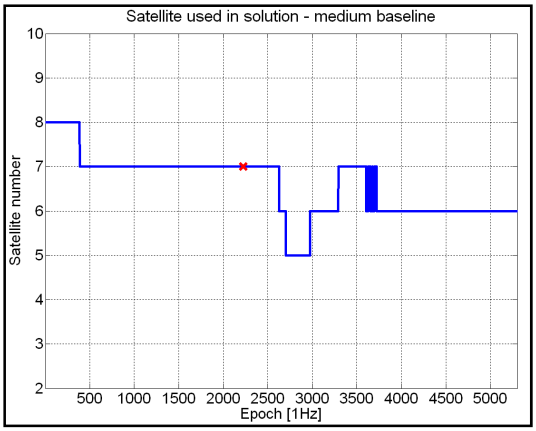

Figure 5.3 Number of satellites in use during medium baseline test.

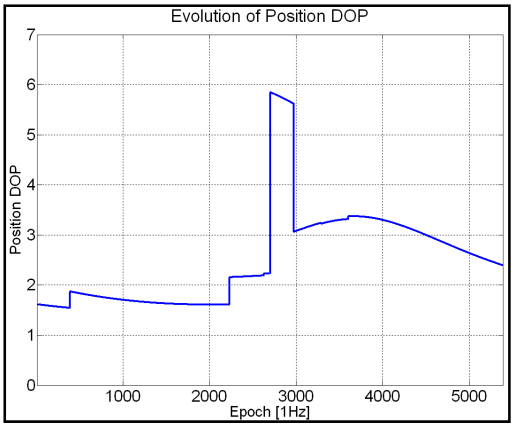

Figure 5.4 Evolution of Position DOP during medium baseline test.

Figure 5.3 presents the satellite's selection during the process. A red cross represents a change in satellite reference. The associated PDOP of the solution is represented in Figure 5.4. One can observe the spike of the PDOP solution between epoch 2400 and 3000, when the number of satellite becomes as low as five.

5.2.2 Ionosphere estimation of the medium baseline solution

The RTK solution is performed with two different ionospheric corrections method: the iono-free and the ionosphere-weighted methods. The iono-free estimation using dual frequency is enabled when the carrier phase ambiguities are resolved. These ionospheric errors are theoretically considered as the 'true' ionospheric errors (1^{st} order), since the ionosphere delays are frequency dependent. In this way, the real-time weighted ionospheric estimation can be compared to this post-process iono-free estimation.

As shown in Figure 5.5 and Figure 5.6, the ionosphere weighted model finds the same pattern of ionosphere estimation as the iono-free method. This confirms the accuracy of the implemented weighted ionospheric scheme and the associated variance. As a consequence, the ionosphere weighted method can be used in real-time. The brief spike in Figure 5.6 is due to the change in satellite reference.

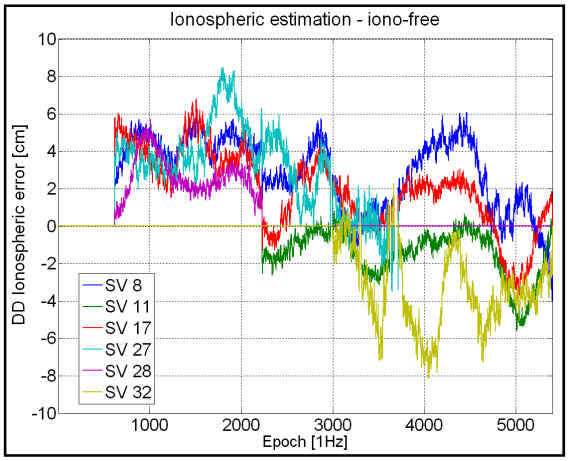

Figure 5.5 DD ionospheric error estimation using iono-free solution.

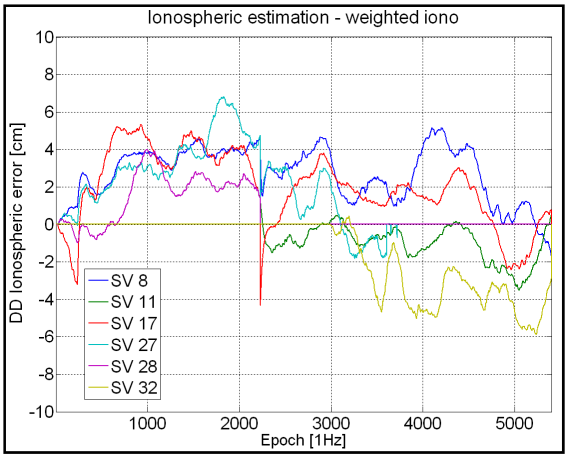

Figure 5.6 DD ionospheric error estimation using iono-weighted solution.

Table 5.1
Ionosphere standard deviation (1σ) for the iono-weighted and iono-free solution for each DD satellite and the associated satellite elevation angle

[cm]	SV 8	SV 11	SV 17	SV 27	SV 28	SV 32
Iono-free	1.0	1.3	2.1	2.2	1.1	2.1
Iono-weighted	0.9	0.9	2.0	2.1	1.4	1.6
Mean elevation	*43*	*61*	*39*	*20*	*70*	*19*

As expected, the ionosphere errors are noisier in the iono-free method than in the ionosphere weighted method, as it can be seen in Table 5.1 and Figure 5.20. This noise is associated with the linear carrier-phase combination of the two frequencies in the iono-free measurement. This measurement is noisier than the single frequency one (Misra and Enge 2006):

$$\sigma_{iono-free} = \sigma_{L1/L2}\sqrt{2.546^2 + 1.546^2} \approx 3\sigma_{L1/L2} \tag{5.15}$$

Where:

$\sigma_{L1/L2}$ is the L1 and L2 measurements variance.

The ionosphere error variance is elevation-dependant, particularly for satellite elevation angle below twenty degrees.

The weighted ionosphere model has the advantage to find the ionosphere estimate even without the ambiguity resolution. The introduction of the ionospheric parameters in the Kalman filter introduces a smooth and accurate estimation, no matter what location of the rover receiver, which is particularly interesting for medium to long baseline situation.

This technique allows more flexibility and accuracy for the GPS RTK users. The weighted ionosphere model is a solid and concrete method to remove the ionospheric errors in dynamic environment where the iono-free method cannot be enabled.

5.2.3 Solution precision using two different ionospheric corrections

In this section, the result's analysis of the improved RTK algorithm solution for the two methods of ionospheric correction will be presented. The classic iono-free correction and the developed weighted ionosphere method are presented in section 2.3.2 and section 5.1 respectively. The solution is compared to the mean static position computed by Waypoint post processing software.

The standard solution (without ionospheric corrections) of the RTK algorithm will show lower ambiguity resolution results in medium baseline. The absence of accurate ionospheric corrections has direct consequences on the measurements precision and on the ability to resolve the phase ambiguities. Ionospheric correction has to be enabled, like broadcast model or SBAS corrections.

In this project, the LAMBDA method is used. It is a robust method and it is able to find the corresponding carrier-phase ambiguities after a certain period of filter convergence in the medium baseline test. When the ambiguities are fixed and validated, the ionospheric errors will be evaluated using iono-free technique and the solution precision will reach the centimeter level.

On the other hand, when the weighted ionosphere method is used, the ambiguities are resolved quicker, due to a better filter convergence and an adequate ionospheric estimation. In this case, when the ambiguities are resolved, the solution precision looks similar to the solution using iono-free corrections, but less noisy.

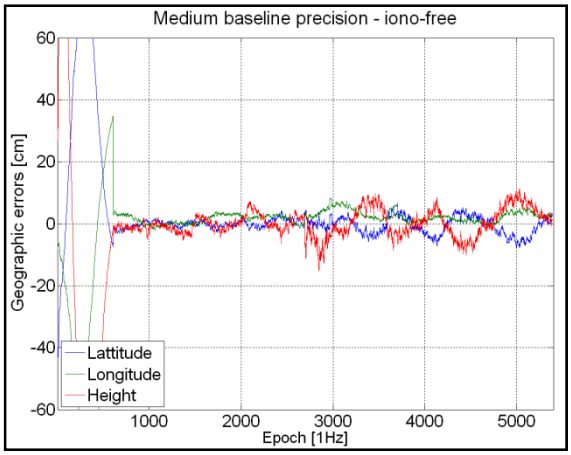

Figure 5.7 Position precision using iono-free method in the medium baseline test compared to Waypoint

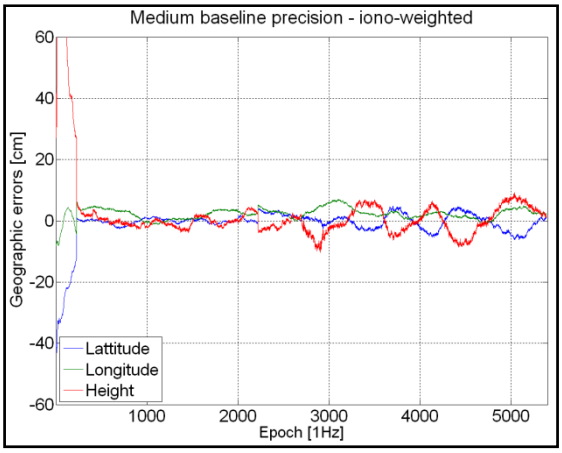

Figure 5.8 Position precision using iono-weighted method in the medium baseline test compared to Waypoint.

The Table 5.2 presents the standard deviation of the fixed solution for the two methods using the two ionospheric estimation methods.

Table 5.2
Standard deviation of the iono-free and iono-weighted solution for the geographic axes compared to the mean Waypoint solution

	std LAT	**std LONG**	**std HEIGTH**
iono_free	2.4 cm	1.7 cm	4.1 cm
weighted iono	2.1 cm	1.7 cm	3.6 cm

As it can be seen in Figure 5.7 and Figure 5.8, once the ambiguities are fund, the two solution errors present the same precision pattern. The weighted ionosphere model helps the filter to converge and enables a better and faster ambiguity resolution, due to adequate ionospheric error estimation.

The global results of both solutions are less precise than a short baseline scenario. This is expected and is due to the inaccuracy of different non-common mode error corrections, like troposphere or satellite positions. This solution precision is still at the centimeter level in fixed mode.

5.2.4 Ambiguity resolution performance

The ambiguity estimation performance of the ionosphere weighted algorithm will be analyzed here, by looking at the LAMBDA ratio test. This ratio test, described in section 3.3.4, is used to validate the carrier-phase ambiguity candidate of the LAMBDA method.

To examine the ratio test, the ambiguity resolution is deactivated. The solution stays in float mode and the ratio test is recorded epoch by epoch. In this way, the ratio test is analyzed epoch after epoch, like in a real-time implementation. In fixed mode, the ratio test stays around 0 just after the first ambiguity resolution, despite of the validity of the ambiguity candidates. This methodology is similar to resolving the ambiguities at any time in the process. This is a good way to analyze the performance of the ambiguity resolution in real-time.

Figure 5.9 and Figure 5.10 present the ratio test for the two methods. In the developed RTK algorithm, the ambiguity validation criterion is usually fixed at 0.4. When the ratio test is below 0.4 for 20 epochs, the ambiguity is considered valid and fixed in the solution, otherwise the ambiguity is rejected.

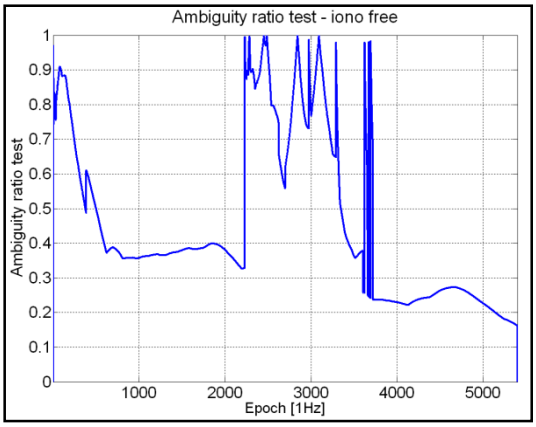

Figure 5.9 LAMBDA ratio test using the iono-free method in the medium baseline test.

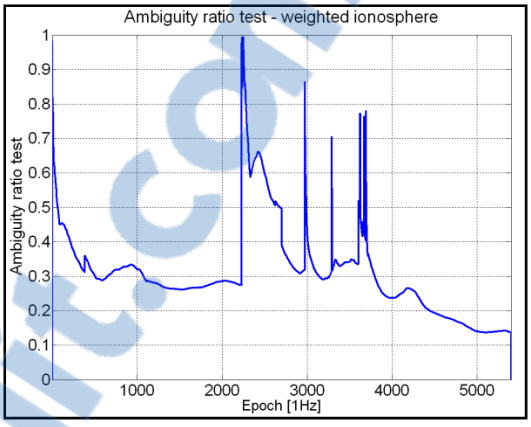

Figure 5.10 LAMBDA ratio test using the weighted ionosphere method in the medium baseline test.

As it can be seen, the ionosphere weighted method presents interesting and promising results. The ratio test mean is below 0.4 for much of the process, and presents 85% of ambiguity resolution. The ratio test is not valid during satellite change and when the ambiguity resolution is restarted. During that time, a period of convergence of the filter is necessary to lower this ratio test. On the other hand, due to a lack of rapid convergence and ionosphere estimation, the other method presents lower results. The ambiguity resolution is not possible during 33% of the process, keeping the solution in float mode.

Table 5.3
Ambiguity success rate and Time to First Fix using iono-free modeling

	Time to first fix	**% success**	**mean ratio**
Iono-free	11 min	66%	0.46
Iono-weight	4 min	85%	0.31

This result certainly shows that the ionosphere estimation is a critical parameter for the carrier ambiguity resolution. In the medium baseline test, the double-difference ionospheric errors computed with the weighted ionosphere method seem below the carrier cycle length (19cm), as seen in Figure 5.6. The ionospheric error will have impact on the convergence time of the solution and the rapidity of the ambiguity resolution. But since the ionospheric errors are below carrier phase ambiguity cycle length, it will not apply major errors in the

ambiguity resolution. On the contrary, in long baseline, the ionosphere errors will have major impacts in ambiguity resolution. In that case, the ionosphere weighted technique is preferred to resolve this problem and improve RTK accuracy.

5.3 Analysis of long baseline high dynamic test

5.3.1 Experimental procedure

This section presents a high dynamic test made by Gedex in October 2004 in the region of Toronto. The data are obtained from two Novatel DL-4 GPS receivers, one located on an airplane, flying with high dynamic and one base located at the airport. The raw measurements were recorded at 20 Hz.

Figure 5.11 Initial position and starting point of the airplane.
(from Google map view)

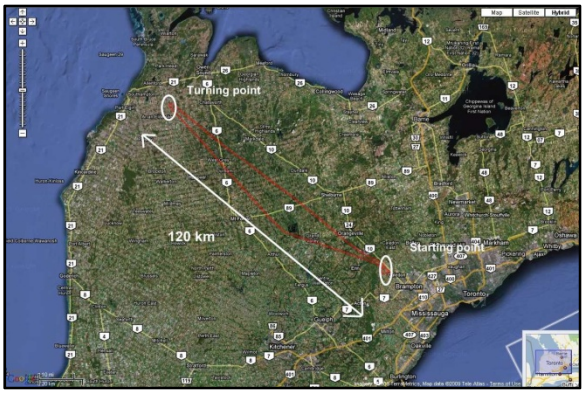

Figure 5.12 Trajectory of the airplane during long baseline test.
(from Google map view)

Figure 5.11 and Figure 5.12 give a representation of the test environment (starting point) and the full trajectory of the airplane in the region of Toronto. The trajectory time length was less than 1½ hours (93000 epochs at 20Hz). The test is considered as a long baseline trajectory since the airplane go as far as 100 km away from the base station, as seen in Figure 5.15.

Figure 5.16 and Figure 5.14 show that the rover goes as fast as 80 m/s (288 km/h) during the trajectory and flight at an altitude of 1000 meters. It is interesting to note that at the turning

point, in the middle of the process, the velocity is totally reverse for the three axes. This maneuver can have impacts on the velocity and position estimation during post-processing of the RTK long baseline algorithm.

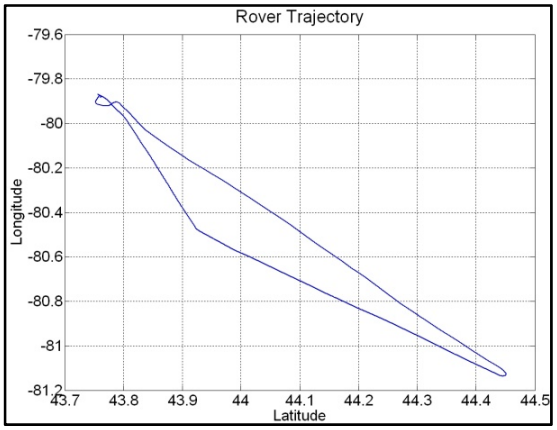

Figure 5.13 Trajectory of the airplane in geographic axes.

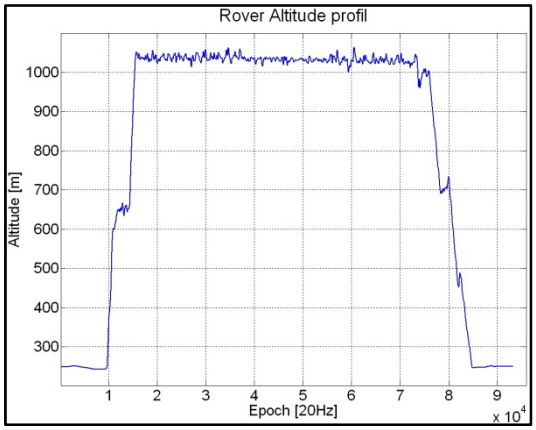

Figure 5.14 Altitude profil of the airplane during flight.

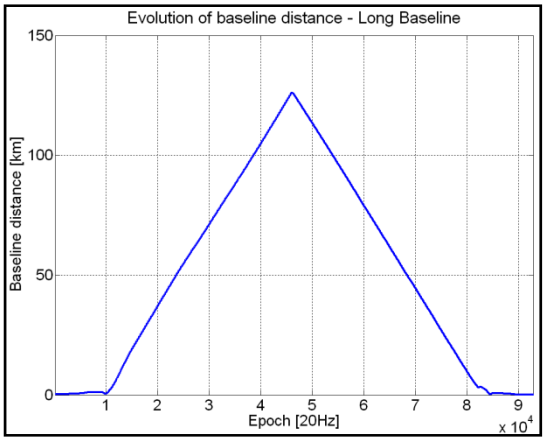

Figure 5.15 Evolution of the baseline distance during the long baseline test.

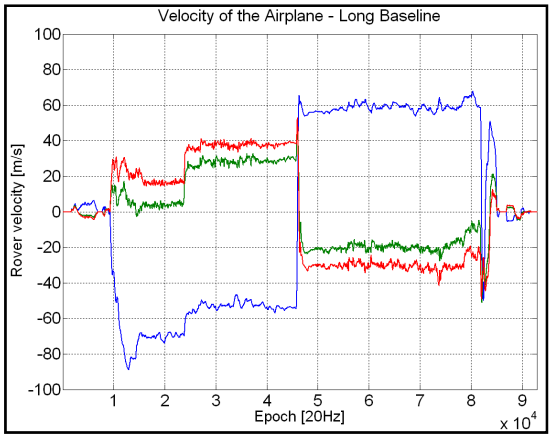

Figure 5.16 3D velocity of the airplane during long baseline test.

Figure 5.17 and Figure 5.18 present the number of satellite used in the solution and its associated PDOP. According to the results, there is no major change in satellite selection, except at the long baseline point (around epoch 46000), which is also the airplane turning point, where the number of satellite decreases to 5. At this point, the PDOP has a relatively high value of 3.

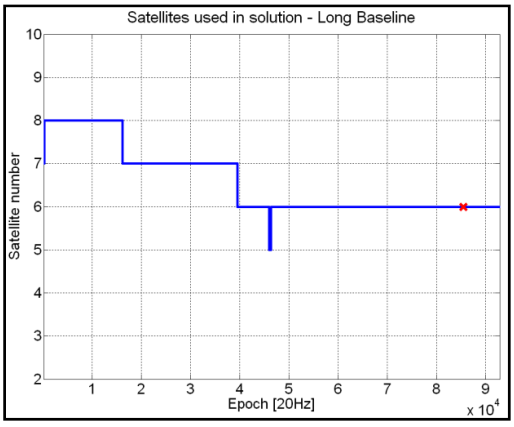

Figure 5.17 Number of satellites used during long baseline test.

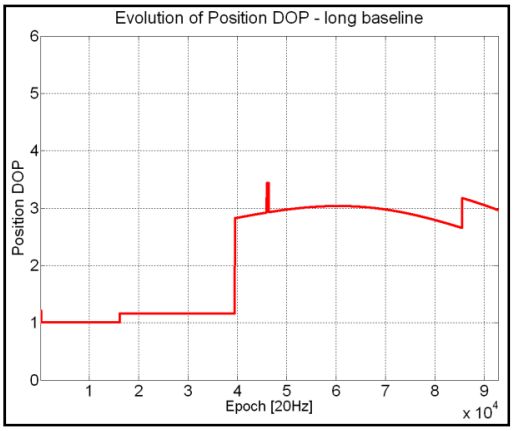

Figure 5.18 Evolution of the Position DOP during long baseline test.

5.3.2 Atmospheric errors estimation using the ionosphere weighted model

The tropospheric errors are modeled using the Saastamoinen equations presented in section 2.3.1, both for hydrostatic and non-hydrostatic delays.

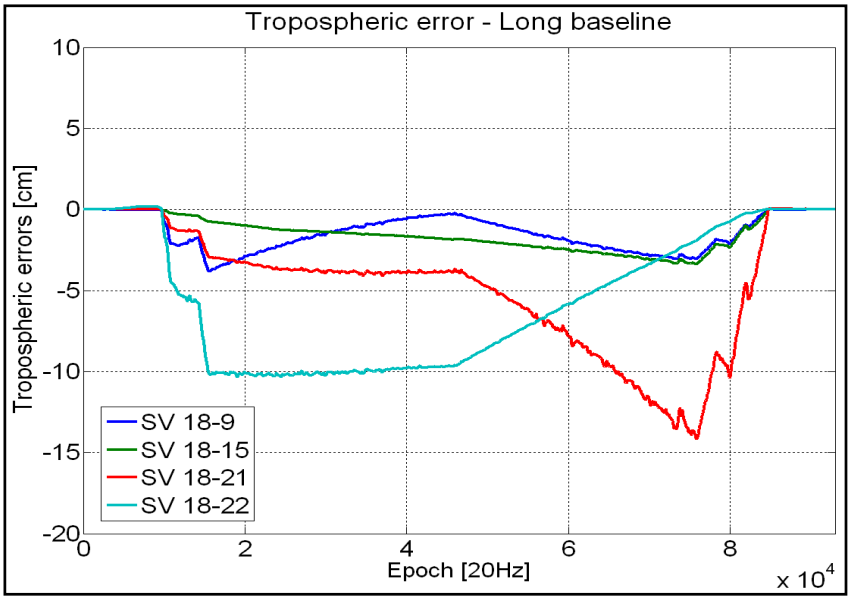

Figure 5.19 Double difference troposheric errors modeling for the long baseline test using Saastamoinen model.

As presented in Figure 5.19, the double difference tropospheric errors increase with the baseline length for every satellite. The errors can reach 15 centimeters and need to be modeled to improve the ambiguity resolution.

The ionosphere is estimated using the proposed weighted ionosphere technique during all the process. The ionosphere pseudo-observable has a linear baseline dependant variance. As a consequence, the ionosphere errors variance will be considered low in the early stage of the test, when the baseline remains short. When the airplane is flying, the receivers' baseline increases and the ionospheric errors variance increases proportionally.

Figure 5.21 presents the ionosphere estimation for 4 different satellites which are stable during the process. The ionosphere estimation could have been estimated using the iono-free method since the ambiguities are resolved all along the test but it is interesting to see that the ionosphere weighted model performs accurately in the same way.

Table 5.4
Standard deviation of the DD ionospheric errors during process

	SV 18-14	**SV 18-15**	**SV 18-21**	**SV 18-22**
Ionosphere errors std	1.6 cm	0.8 cm	1.1 cm	0.8 cm
Ionosphere errors ppm	0.32 ppm	0.16 ppm	0.22 ppm	0.15 ppm
Mean elevation angle	32	31	47	58

The ionosphere errors are computed in ppm for the long baseline point. This ionospheric errors seems low compared to the range of standard deviation proposed in (Liu and Lachapelle 2002), which range from 0.8ppm to 3 ppm (1 ppm corresponds to 1 dm deviation for 100 km of baseline). For example, 0.5 ppm of ionospheric error corresponds to 50cm of errors in a 100 km baseline scenario. In the present situation and as summarized in the Table 5.4, the standard deviation corresponds to approximately 0.1 to 0.5 ppm. These results may be due to quiet solar activities and low TEC in the atmosphere during this year period.

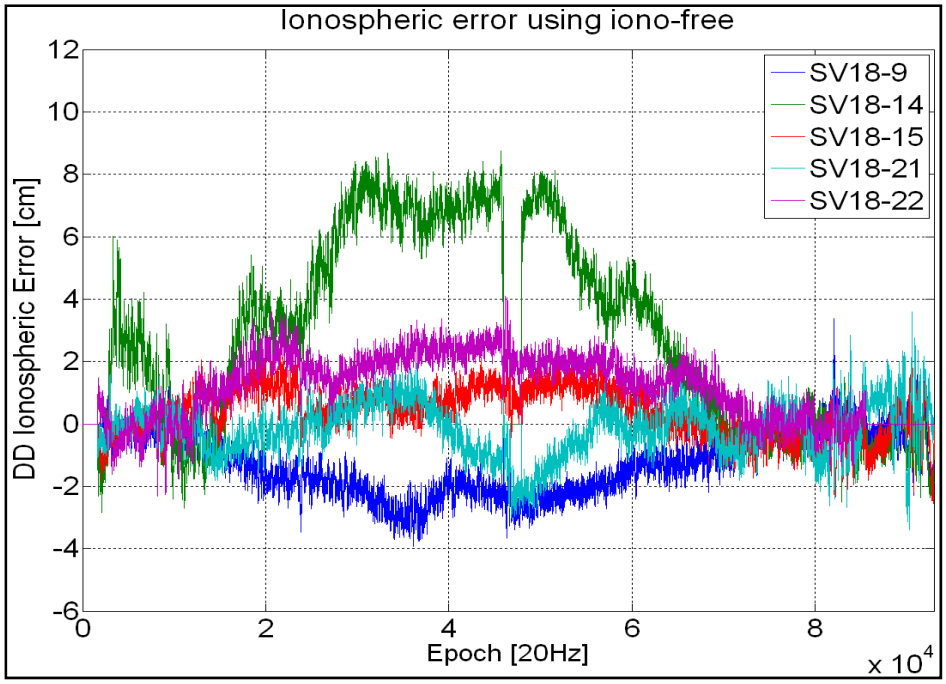

Figure 5.20 Double difference ionospheric errors using the ionosphere-free model for different SV combination.

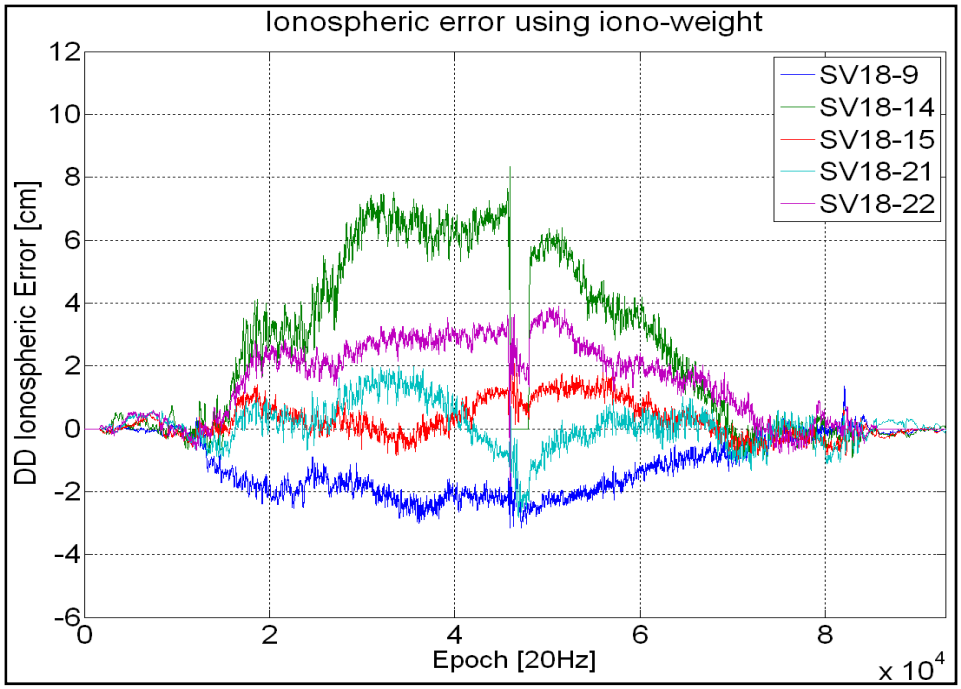

Figure 5.21 Double difference ionospheric errors using the ionosphere-weighted model for different SV combination.

5.3.3 Ambiguity resolution performance of the solution

The carrier ambiguities are easily resolved in the early stage of the process, when the baseline distance stays small. In fact, only less than 3 seconds is necessary to resolve the ambiguities. Then, the new satellite and ambiguities management algorithm allows the system to stay in fixed mode during the rest of the process, in a robust way.

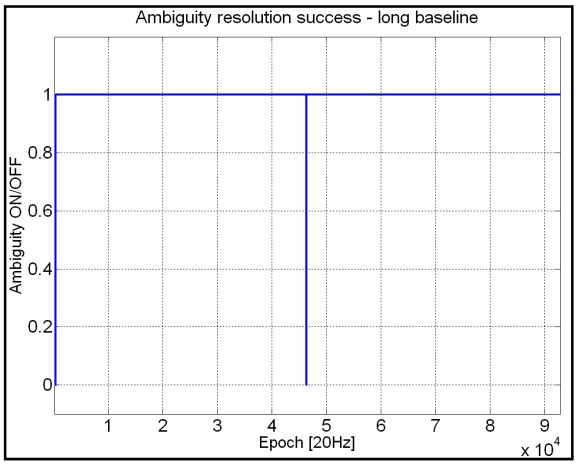

Figure 5.22 Ambiguity resolution success during the long baseline test.

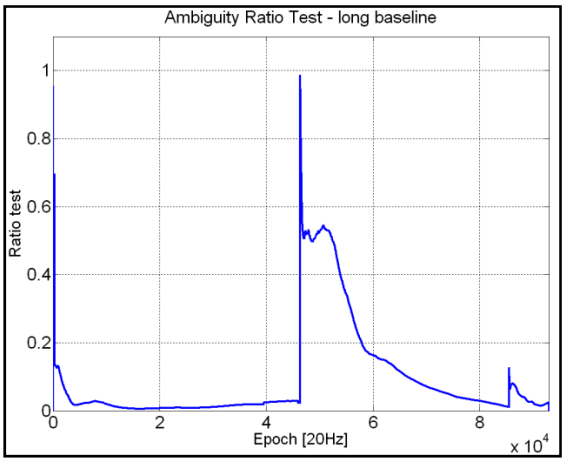

Figure 5.23 Evolution of the ratio test during the long baseline test.

Table 5.5
Ambiguity success rate and Time to First Fix (TFF) using Ionospheric modeling

	Time to first fix	% success	% error
Ambiguity Resolution	2 second	91.9%	0%

To evaluate the performance of the ambiguity resolution for long baseline, the ratio test described in section 3.3.4, is used in float mode for the overall test. The ratio test presents a high value when a new satellite arises in the solution in long baseline. The time to first fix in this long baseline case will be relatively long (approximately 10 min). This can be really a problem for real-time applications. In this case, there is no need for being alarmed by such a result, since the ambiguity validation has already been made at the short baseline period. Without any major failures, the ambiguities remain constant during the whole time. When a

new satellite arises in the solution in long baseline, its ambiguity is quickly resolved and does not have major impact on the solution precision.

This demonstrates the relative complexity of estimating the carrier ambiguities and the ionospheric errors at the same time in a long baseline scenario. Usually RTK users like surveyors use static situation and long observations to resolve phase ambiguities in real-time before recording and making observations. For high dynamics test, RTK is used in post-processing, and it uses the shortest baseline available to determine the ambiguity and keep it along the process.

5.3.4 Analysis of the long baseline fixed solution

The results presented here are obtained using the same RTK algorithms that used in the previous tests. The solution is compared to the post-processing software Waypoint. The ionosphere corrections are used with the weighted ionosphere technique and the ambiguity resolution presented in section 5.3.3.

Figure 5.24 and Table 5.6 show the solution precision of the RTK algorithm compared to the Waypoint solution. In latitude and longitude, the standard deviation is below the centimeter for the overall test with respect to Waypoint solutions which contains errors. The main errors are located in the height domain (altitude). This difference may occur because of a specific height corrections provided by the Novatel post-processing software, which is not include in the developed algorithm.

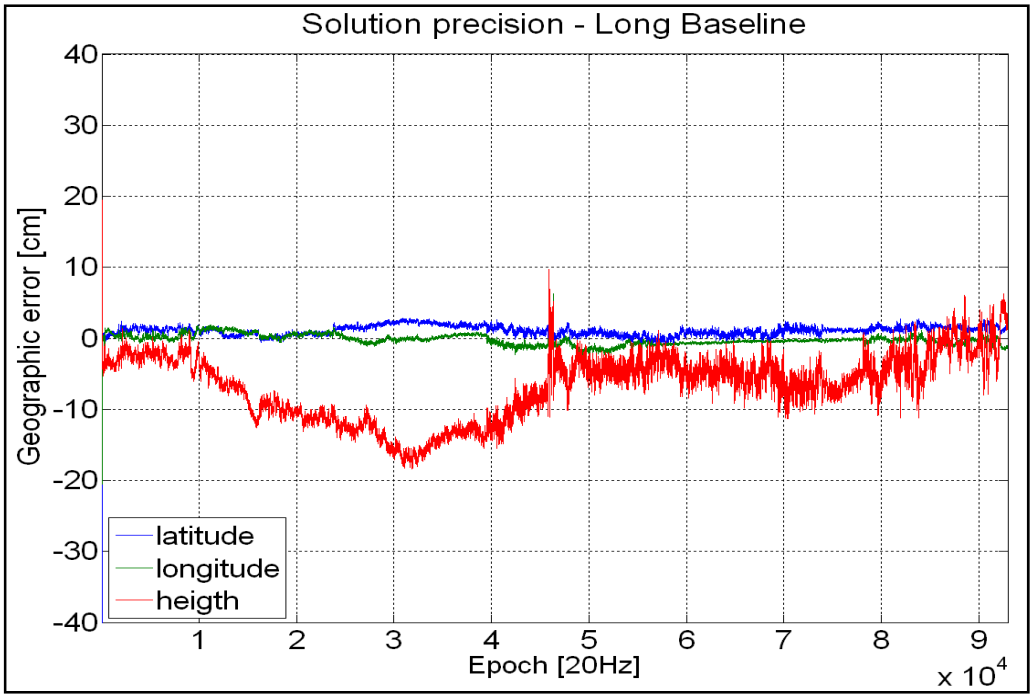

Figure 5.24 Difference between the geographic RTK solution compared to the Waypoint solution for the long baseline dynamic test.

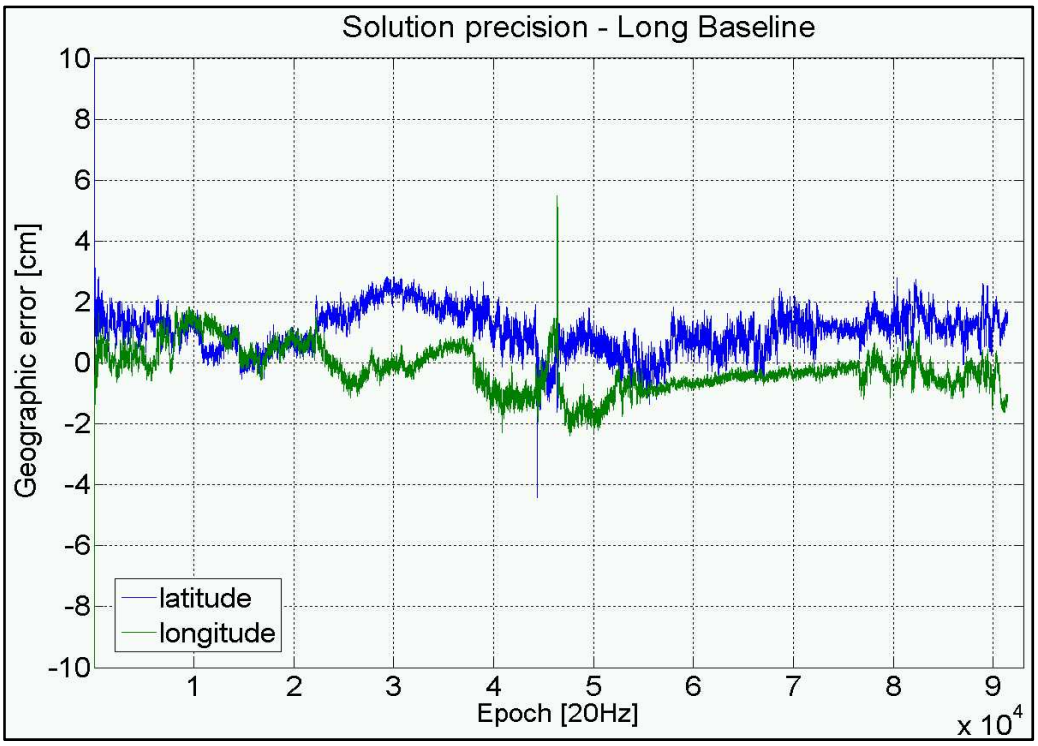

Figure 5.25 Zoom on the latitude and longitude axes of the difference between the RTK solution and the Waypoint solution for the long baseline dynamic test.

Table 5.6
Standard deviation of the RTK solution for the long baseline test
(maximum of 140 km), compared to the post-process Waypoint solution

	std LAT	**std LONG**	**std HEIGTH**
RTK Solution	0.67 cm	0.72 cm	4.54 cm

The 'true' position comes from the Novatel commercial post-processing software Waypoint. It has been processed using the differential correction, dual frequency and an ionospheric correction (using the iono-free and iono-weighted technique). The Waypoint post-process uses the Kinematic Ambiguity Resolution (KAR) technique for ambiguity resolution and reverse processing. This commercial post-process solution is the only one available to compare the developed RTK solution for this test. By using this reference for our solution precision, we removed most of the unknown errors presented in the solution (e.g. multipath, ephemeris errors). So the performance of the RTK software for long baseline test needs to be taken with care, before better reference comparison.

Figure 5.26 shows the evolution of the standard deviation errors for the RTK solution compared to the Waypoint post-processing software. Figure 5.27 shows the estimated standard deviation of the Waypoint solution. It is a good indicator of the quality and performances of the developed RTK solution. Indeed, as mentioned earlier, the only available reference for us is the Waypoint post-processing solution, so it is important to know its estimated position precision. With these results, one can conclude that the developed solution is as much precise as the Waypoint solution.

As it has been shown, the RTK algorithm performs adequately for long baseline situations, under specific constrains, as short baseline initialization. In the developed RTK algorithm, efforts have been made to have a robust and reliable solution for real-time environment. The main challenges of such long baseline situations are ambiguity resolution and non-common error modeling.

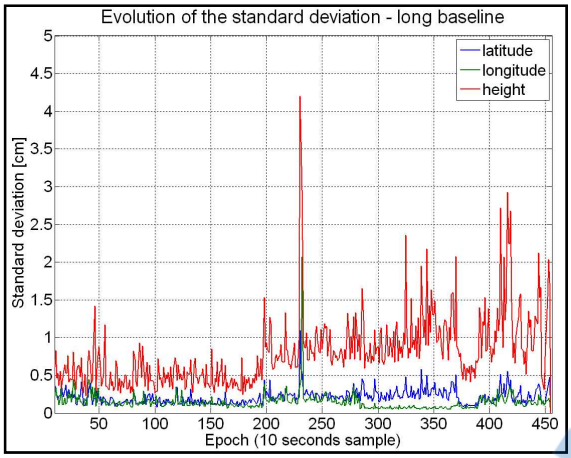

Figure 5.26 Evolution of the standard deviation 3D error for the long baseline solution, compared to Waypoint.

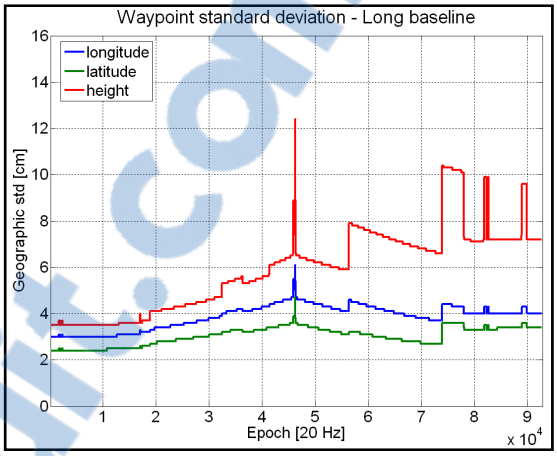

Figure 5.27 Waypoint estimated standard deviation of the 3D position errors.

Situations are more difficult than others, for example:

1- When the rover is in dynamic mode and looses phase tracking during just a few seconds in a long baseline mode. In that case, ambiguity recovery or completed reinitialization has to be performed in a quick manner and to keep robust tracking;

2- Static initialization in very long baselines (more than 200 km). Long period of convergence is necessary to achieve accurate centimeter position precision;

3- High ionospheric activities and strong TEC. In that case, the ionospheric weighted mode has to be strengthened, specifically in the variance estimation.

More details on future works and recommendation works will be discussed next.

CHAPITRE 6

CONCLUSION AND RECOMMENDATIONS

6.1 Conclusion

The RTK algorithm presented here is a state-of-the-art RTK positioning solution. It has intelligent satellite selection for dynamic real-time, quasi-optimum Kalman filtering, fast and reliable ambiguity resolution, ionospheric and non-common error mode handling for long baseline situations.

In a practical aspect, the real-time implementation of the algorithm for the Novatel and LACIME-GNSS receivers has been an interesting challenge. Intelligent and comprehensive satellite selection, dynamic management of the Kalman filter and the ambiguities, has been necessary for the robustness of the algorithm. The algorithm can be used in many situations, even in really shadowed environment, where the satellite visibility is unpredictable and changing. Meeting these constraints has been an important factor in the credibility of the RTK algorithm.

The thesis presents in detail the different aspects of the RTK algorithm. First, history and perspective for new satellite constellation has been presented. Then, the observations, the GPS measurements, have been presented in detail. All the errors related to the computation of the satellite-receiver distance has been detailed and analyzed. This was an important step before the Kalman filter theory. This estimation process is the core of the solution computation, and all the details of the RTK Kalman filter implementation have been presented. Ambiguity resolution and related robust technique have also been detailed.

This algorithm has been validated for different scenarios, from static short baseline to dynamic long baseline mode. The Waypoint post-process solution has been the reference all along this study and the results looks very similar to the proposed software. The accuracy and

robustness of the developed RTK algorithm has been highlighted, as well as its structure. It can be used for many situations, using Novatel and the LACIME-GNSS receivers. In static mode, the RTK algorithm offers centimeter to millimeter precision in fixed mode for both the Novatel and the GNSS configuration. Ambiguity resolution technique is enabled after few seconds. In dynamic mode, the RTK algorithm presents the same precision as Waypoint and offers a robust and dynamic real-time high precision positioning technique.

The long baseline scenario has been the most challenging theoretical aspects. The modelings of the different systematic errors, mainly ionospheric delays, as well as suitable observation model were the two main issues. The ionospheric delays are the most unpredictable and limited factors RTK users face in medium and long baseline scenario. It needs proper handling to achieve the desired RTK centimeter performance in fixed mode. An accurate ionosphere weighted model has been presented to correct this parameter. The solution presents centimeter precision in geographic axes and it need further results to be validated in a real-time situation.

The developed RTK shows very promising applications for the future. When the solution is at the centimeter level precision at any time, it brings new perspective to the industry for the users. For now, the cost and set-up technique of classic RTK has limited its use to surveyors or geophysicists. With the emergence of new constellations and signals in the next decade (Galileo, Compass, L5 etc.), more performance and lower costs can be expected. New algorithms and technique have to be developed to overcome the limitation of RTK. The present algorithm can be adapted in an easy way for new techniques and experimentation in the subject.

6.2 Recommendations

The following is a list of recommendations for subsequent research:

1- To record different controlled static long baseline test. It will be interesting to integrate these tests with the RTK algorithm to evaluate the non-common mode error correction. With exact position of different baseline length, more research can be made on real-time correction of non-common mode errors.

2- To develop a real-time adaptive and intelligent stochastic model for medium and long baseline positioning. An adaptive stochastic model adapts itself to the measurements stochastic estimation. It will allow faster convergence, better accuracy and faster ambiguity resolution.

3- To integrate external measurements. INS is being developed in the LACIME laboratory and will be used with RTK positioning in an ultra-tight couple configuration. INS system provides accurate positioning in short time duration without any additional signals. Integrated with RTK positioning, the global system can provide ultra robust real-time positioning in shadowed environment.

4- To develop a real-time analyzing interface. Up to now, a post-process Graphic User Interface (GUI) has been developed for post-processing RTK positioning and development. It will be really interesting to have the same functions for real-time positioning.

5- To develop an advanced multipath corrections, both in a hardware and software way. Multipath stays the remaining unknown errors in satellite system. In urban area and shadowed environment, it is an important parameter for accuracy and integrity.

6- To develop a better signal and system integrity. It will be interesting to test the RTK algorithm for integrity specifications and applications. Passing integrity tests could be a challenge for the RTK algorithm and could lead to new industrial purposes.

ANNEXE I

ORBIT/CLOCK SATELLITE DETERMINATION USING BROADCAST EPHEMERIS

The accuracy of the satellite position and satellite clock is one of the major interests to reach centimeter precision in standard positioning and in long-baseline RTK. Usually, the user could only use the broadcast ephemerides to obtain the satellite clock and position. The accuracy of the 2-hours daily broadcast ephemerides can reach 160cm precision for the satellite position and 1 microsecond for the satellite clock (Misra and Enge 2006).

The IGS proposes precise GPS ephemerides since the early 90's and are now widely used for post-processing and near real-time solution for geodetic purposes. The IGS products come in various flavors, from the Final, Rapid and Ultra-Rapid ephemerides, depending on the latency of their computation. In the case of the Final ephemerides, the precision can reach 5cm for the satellite position and 0.1ns for the satellite clock (IGSproducts 2008). The Ultra-Rapid ephemerides have near real-time latency, which makes them useful for real-time applications (Kouba and Héroux 2001). The IGS products are in the SP3 formats and consist of satellite position using different frequencies (daily to 5 min).

The positions of the satellite are computed using orbital parameters in the case of the broadcast ephemerides and using interpolation in the case of the IGS products.

Satellite position and clock using broadcast ephemerides

To determine the satellite position, a time of reception t_r has to be expressed in GPS time, in which all the satellite positions will be computed. This time of reception also represent the time of the observations and is used to compute the positioning solution.

Each satellite has a different time of emission, represented by the time of reception minus the time of travel. To have the time of emission, the pseudo-range is used:

$$t_e^p = t_r - \frac{P^p}{c} \tag{16}$$

Where:

t_e^p	is the time of emission of satellite p.
t_e	is the time of reception at the receiver.
P^p	is the pseudo-range observations of satellite p.
c	is the speed of the light.

The ephemerides have also their own time t_{oe}, which represents the broadcast time of the ephemerides and is the reference time to compute the satellite position. Put in another way, position of the satellite will always be referred to this ephemerides time. The closer the GPS time is to the ephemerides time, the more precise the solution will be.

The satellite clock offset can be computed using broadcast ephemerides using:

$$\Delta t = a_{f0} + a_{f1}(t_c - t_{oc}) + a_{f2}(t_c - t_{oc})^2 + \Delta t_r - T_{GD} \tag{17}$$

Where:

Δt	is the satellite clock offset.
a_{f0}, a_{f1}, a_{f2}	are the broadcast clock correction terms.
t_c	is the time of emission of one satellite.
t_{oe}	is the broadcast time of ephemerides.
Δt_r	is the relativistic correction effect.
T_{GD}	is the broadcast group delay time.

To obtain the relativistic correction term, the mean motion is first calculated:

$$n = \sqrt{\frac{\mu}{a_s^3}} + \Delta n \tag{18}$$

Where:

n	is the mean motion.
μ	is the earth's universal gravitational parameter.
$a_s, \Delta n$	are broadcast parameters.

The mean anomaly can be found using:

$$M = M_0 + n(t_c - t_{oe}) \tag{19}$$

Where:

M	is a mean anomaly of the satellite's orbit.
M_0	is a broadcast parameter for each satellite.

The eccentric anomaly E for each satellite's orbit can be bound using iterative method:

$$E = M + e_s \sin E \tag{20}$$

Where:

E	is the eccentric anomaly.
e_s	is the broadcast eccentricity of the satellite orbit.

Finally, the relativistic correction term is:

$$\Delta t_r = F e_s \sqrt{a_s} \sin E \tag{21}$$

The GPS time of transmission t is

$$t = t_c - \Delta t \tag{22}$$

The positions of the satellite are derived from the Kepler's law and the general motion of the satellites. The position are all calculated in an Earth-centered, earth-fixed (ECEF) system.

The distance from the satellite to the center of the earth is:

$$r = a_s(1 - e_s \cos E) \tag{23}$$

The true anomaly υ can be found using:

$$\begin{aligned} \upsilon_1 &= \cos^{-1}\left(\frac{\cos E - e_s}{1 - e_s^2 \cos E}\right) \\ \upsilon_2 &= \sin^{-1}\left(\frac{\sqrt{1 - e_s^2}\sin E}{1 - e_s \cos E}\right) \\ \upsilon &= \upsilon_1 sign(\upsilon_2) \end{aligned} \tag{24}$$

The argument ω can be found from the ephemerides data. The value of Φ is

$$\phi = \upsilon + \omega \tag{25}$$

$$\begin{aligned} \delta\phi &= C_{us}\sin 2\phi + C_{uc}\cos 2\phi \\ \delta r &= C_{rs}\sin 2\phi + C_{rc}\cos 2\phi \\ \delta i &= C_{is}\sin 2\phi + C_{ic}\cos 2\phi \end{aligned} \tag{26}$$

where the parameters C_{us}, C_{uc}, C_{rs}, C_{rc}, C_{is}, and C_{ir} come from the ephemerides data.

$$\begin{aligned} \phi &= \phi + \delta\phi \\ r &= r + \delta r \\ i &= i + \delta i + idot \cdot (t - t_{oe}) \end{aligned} \tag{27}$$

where idot comes from the ephemerides data.

The last term to be found is the angle from the ascending node and the Greenwich meridian:

$$\Omega_{er} = \Omega_e + \dot{\Omega}(t - t_{oe}) - \dot{\Omega}_{ie}\, t \tag{28}$$

Where:

$\dot{\Omega}_{ie}$ is the earth rotation rate.

$\dot{\Omega}, \Omega_e$ are fund in the broadcast ephemerides.

Finally, the satellite position is calculated using the following equation :

$$\begin{bmatrix} x \\ y \\ z \end{bmatrix} = \begin{bmatrix} r\cos\Omega_{er}\cos\phi - r\sin\Omega_{er}\cos i\sin\phi \\ r\sin\Omega_{er}\cos\phi + r\cos\Omega_{er}\cos i\sin\phi \\ r\sin i\sin\phi \end{bmatrix} \tag{29}$$

ANNEXE II

RESULTS OF ANOTHER GEDEX FLIGHT, FOR MEDIUM BASELINE HIGH DYNAMIC SCENARIOS

Trajectory and velocity of Flight 0

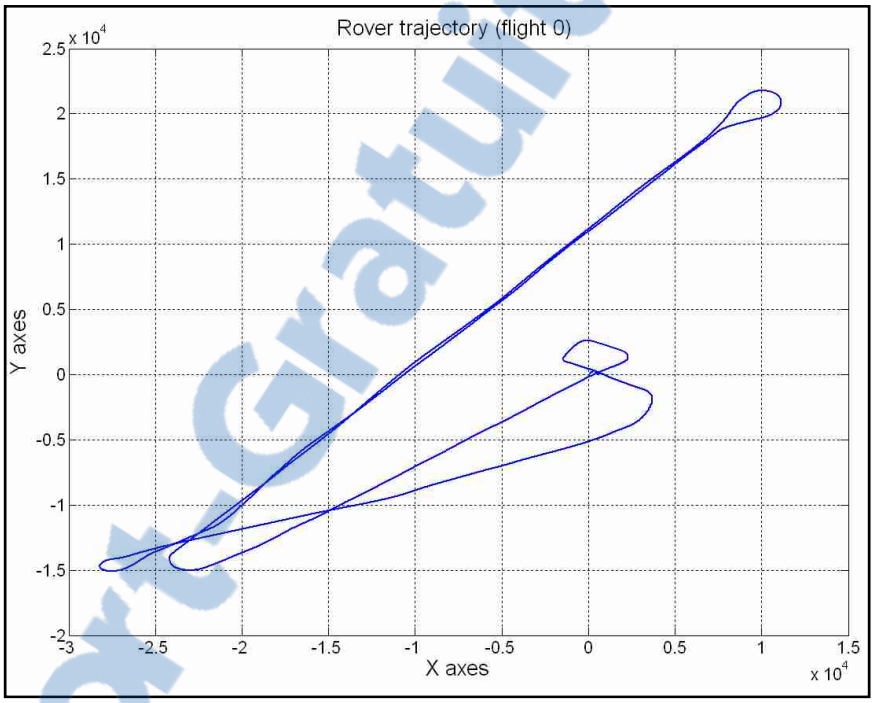

Figure AII.1 Trajectory of medium basline dynamic test Flight 0.

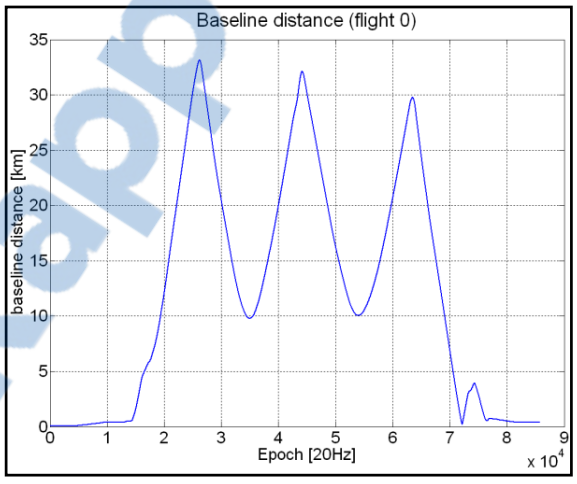

Figure AII.2 Baseline distance evolution.

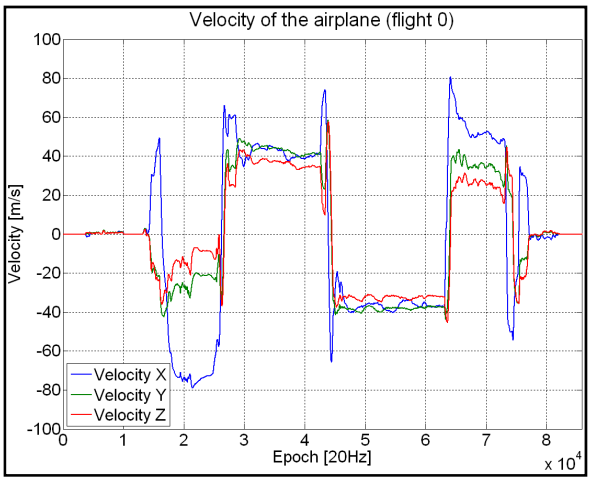

Figure AII.3 Rover velocity for Flight 0.

Geographic errors compared to Waypoint for Flight 0.

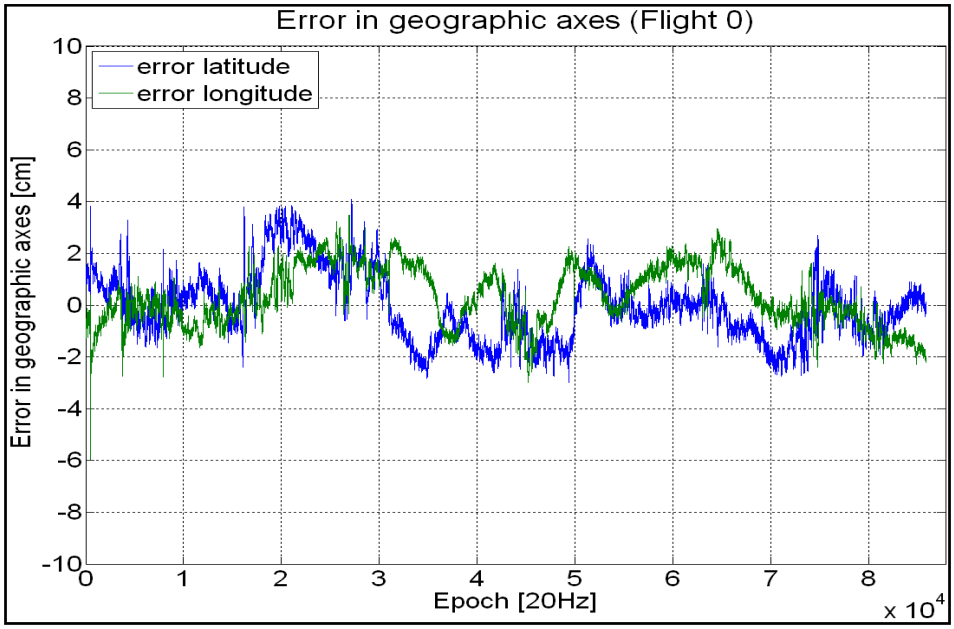

Figure AII.4 Latitude and Longitude errors for Flight 0.

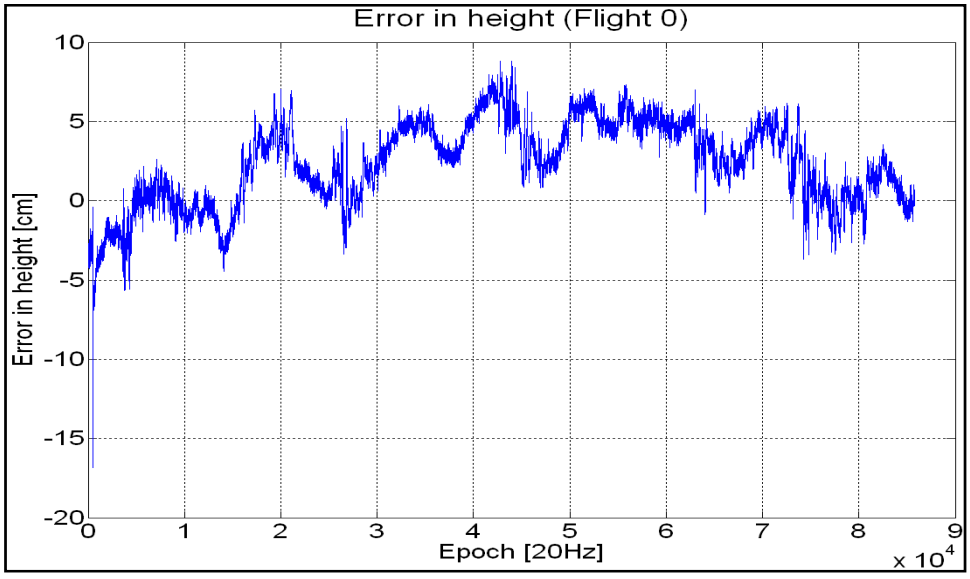

Figure AII.5 Height error compared to Waypoint for Flight 0.

Atmospheric corrections

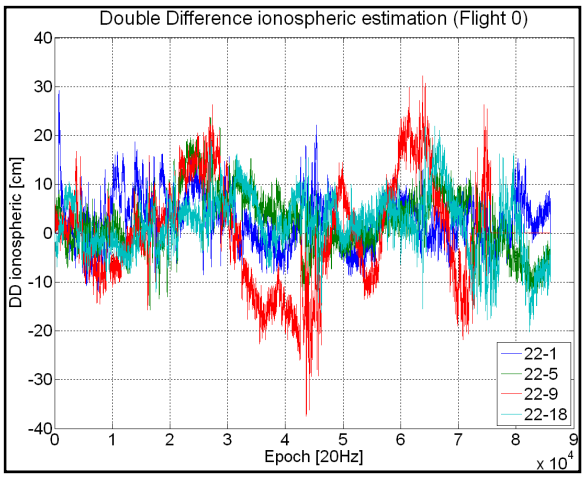

Figure AII.7 DD ionospheric errors estimation for flight 0.

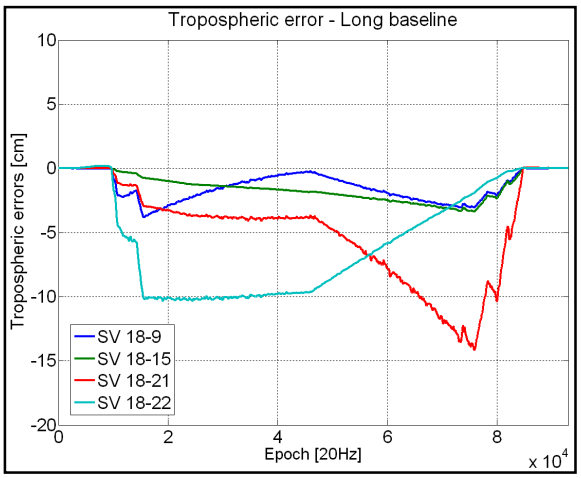

Figure AII.8 DD tropospheric errors esitmation for flight 0.

Satellite selection and the associated PDOP

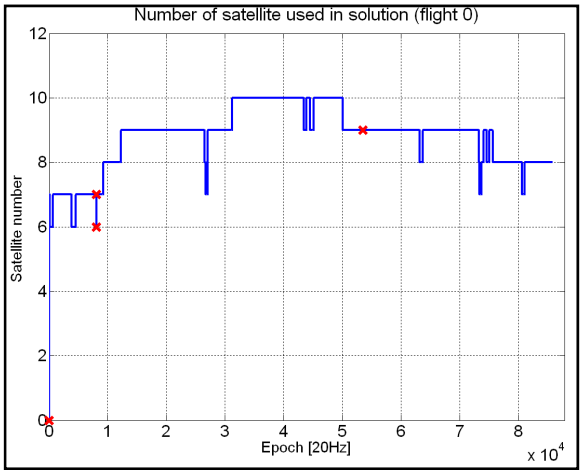

Figure AII.9 Number of satellite used.

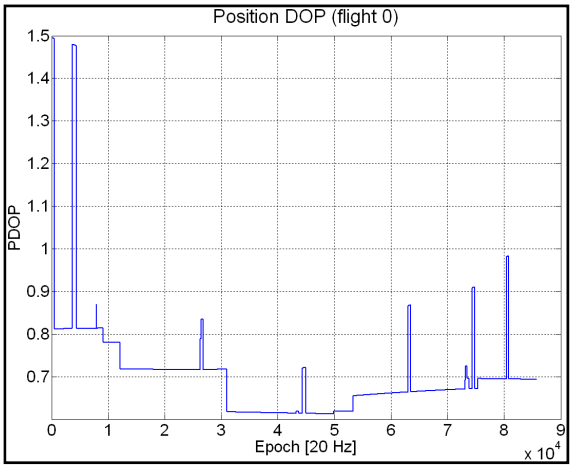

Figure AII.10 Position DOP for flight 0 scenario.

Statistics of the solution precision compared to Waypoint

Table AII.1
Standard deviation of the solution precision error compared to Waypoint for Flight 0

	Latitude	**Longitude**	**height**
Mean	-0.05	0.31	2.37
Std (100%)	1.33	1.13	2.64
Std (95%)	**1.17**	**1.09**	**2.45**

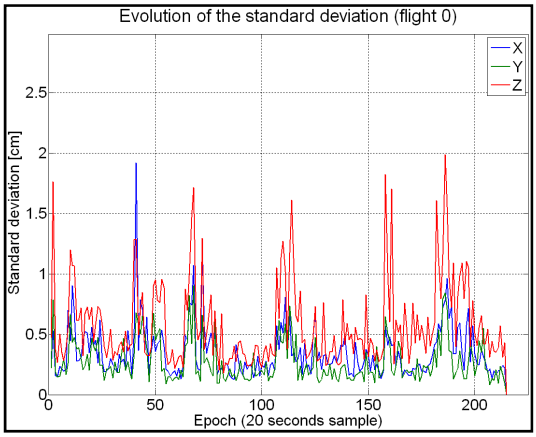

Figure AII.11 Estimated standard deviation compared to Waypoint.

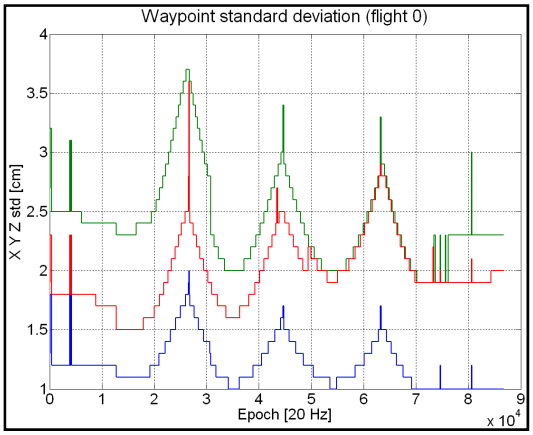

Figure AII.12 Waypoint estimated standard deviation.

ANNEXE III

OVERVIEW OF THE RTK SOFTWARE AND THE C FUNCTIONS FOR RTK POSITIONING USING NOVATEL AND GNSS RECEIVER.

Algorithm parameters of the algorithm

These parameters can be defined before using the RTK algorithm.

LT	Minimum Lock Time of satellite selection
mask	Elevation angle cut-off angle of satellite selection.
Ionoweight	Enable the ionospheric weight corrections for the all filter
L2_frequency	Use the L2 frequency (only if available)
tropo_enabled	Enabled tropospheric corrections
iono_enabled	Enabled iono-free corrections
amb_on	Enabled LAMBDA ambiguity resolution
sat_nb_min	Define the minimum number of satellite to be used in the solution
weight_R	Enabled robust management
k_variance	Variance of all the Kalman filter matrix
init_P_variance	Initial value of matrix P
init_Q_variance	Initial value of variance in matrix Q in regular process
init_QN_variance	Initial value of variance in matrix Q in initial process

Important variables of the algorithm

Data extracted from Novatel receiver or copied from the GNSS receiver:

roverrangecmp	Structure of rover measurements
baserangecmp	Structure of base measurements

basebestpos	Structure of base position
roverbestpos	Structure of rover position
roverrawephem	Structure of raw ephemeris for the rover
baserawephem	Structure of raw ephemeris for the rover

Main functions of the algorithm

This section presents the main function of the developed Kalman filter.

Main function of the Kalman filter.

void **Kalman_loop**

best_sats, position, basexyz, h_float, sat_nbr

Overall function to be called to perform all the RTK process.

Compute the observation matrix H

void **h_comput_cor**

best_sats, position, basexyz, h_float, sat_nbr

Compute the main Kalman filter matrices

void **compute_kalman_matrix**

DDL1L2, X, x_est, R, P_est, P, H, K, sat_nbr

This section describes the main function of the developed satellite selection management.

Main function for satellite management

void **Satellite_management**

best_sats, position, basexyz, h_float, sat_nbr

Select the satellite selection

void **select_sat_psr**

best_sats, position, basexyz, h_float, sat_nbr

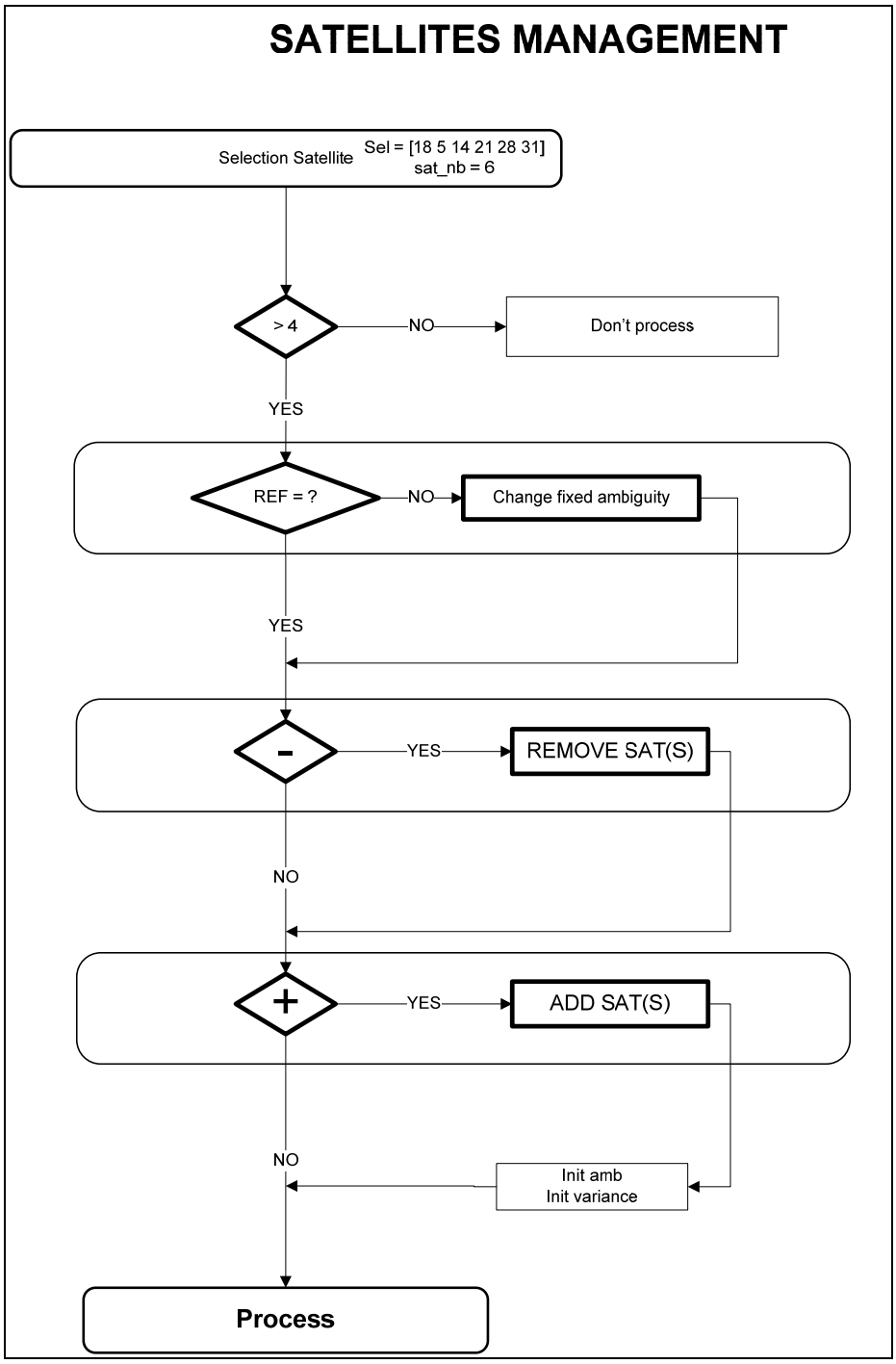

Figure AIII.1 Diagram of the satellite selection process.

REFERENCES

Allen, L. W. (1999). "United States' Nationwide Differential GPS." GPS Solutions 2.

Alves, P., G. Lachapelle, et al. (2002). Use of Self-Contained Ionospheric modeling to Enhance Long Baseline Multiple reference Station RTK Positioning. ION GPS, Portland, OR.

ARINC (2005). IS-GPS-705 (GPS L5).

ARINC Engineering Services (1993). NAVSTAR GPS Space Segment/Navigation User Interfaces Rev C. A. R. Corporation, S. 2250 E. Imperial Highway and C.-. El Segundo: 160.

Avila-Rodriguez, J.-A., G. W. Hein, et al. (2008). "The MBOC Modulation: the Final Touch to the Galileo Frequency and Signal Plan." Journal of Navigation 55.

Banville, S., R. Santerre, et al. (2008). Satellite and Receiver Phase Bias Calibration for Undifferenced Ambiguity Resolution. ION NTM.

Beran, T., R. B. Langley, et al. (2007). "Hig -Accuracy Point Positioning with Low-Cost GPS Receivers." Journal of Navigation 54.

Cannon, E., G. Lachapelle, et al. (1997). "DGPS Kinematic Carrier Phase Signal Simulation Analysis for Precise Velocity and Position Determination." Journal of the institute of navigation 44 no2.

Collins, J. P. and R. B. Langley (1997). Estimating the Residual Tropospheric Delay for Airborne Differential GPS Positioning. ION GPS, Alexandria, VA.

Delaporte, T., R. J. Landry, et al. (2008). A Robust RTK Software for High-Precision GPS Positioning. Annual European Navigation Conference – Global Navigation Satellite Systems, Toulouse.

FAA (1990). FAA FAA-E-2492/2 REV C CATEGORY I INSTRUMENT LANDING SYSTEM EQUIPMENT REQUIREMENTS.

FAA, U. S. D. (2008). Global Positioning System WASS performance standard, Federal Aviation of Administration: 60.

Gauthier, L., P.Michel, et al. (2001). "EGNOS: The First Step in Europe's Contribution to the Global Navigation Satellite System." ESA bulletin 105.

Gibbons, G. (2008). "Galileo's New Era, step by step, the program advances." Inside GNSS.

GlobalSecurity. (2007). from http://www.globalsecurity.org/space/systems/gps.htm.

Glonass. (2008). from http://en.wikipedia.org/wiki/GLONASS.

Grejner-Brzezinska, D. A., P. Wielgosz, et al. (2006). "The impact of Severe Ionospheric Conditions on the Accuracy of Kinematic Position Estimation: Performance Analysis of Various Ionosphere Modeling Techniques." Journal of Navigation 53(3).

Hwang, P. Y. (1991). "Kinematic GPS for Differential Positioning: Resolving Integer on the Fly." Journal of Navigation 38.

Hwang, P. Y., G. A. Mcgraw, et al. (1999). "Enhanced Differential GPS Carrier-Smoothed Code Processing Using Dual-Frequency Measurements." Journal of the institute of navigation 46.

IGSproducts. (2008). "http://igscb.jpl.nasa.gov/components/prods.html."

Jonge, P. d. and C. Tiberius (1996). The LAMBDA Method for Integer Ambiguity Estimation : Implementation Aspects. LGR-series, Delft Geodetic Computing Centre

Joosten, P. (2001). The LAMBDA-Method: Matlab Implementation Delft University of Technology.

Julien, O., P. Alves, et al. (2004). Improved Triple-Frequency GPS/Galileo Carrier Phase Ambiguity Resolution Using a Stochastic Ionosphere Modeling. ION NTM 2004, San Diego, CA.

Keefee, K., M. Pettovelo, et al. (2006). "Assessing Probability of Correct Ambiguity Resolution in the Presence of Time-Correlated Errors." Journal of Navigation.

Kim, D. and R. B. Langley (2000). A reliable Approach for Ambiguity Resolution in Real-Time Long Baseline Kinematic GPS Applications. ION GPS Salt Lake City.

Kim, D. and R. B. Langley (2001). Estimation of the Stochastic Model for Long-Baseline Kinematic GPS Applications. ION NTM, Long Beach, CA.

Kim, D. and R. B. Langley (2003). "On Ultrahigh-Precision GPS Positioning and Navigation." Journal of The Institute of Navigation 50.

Kim, D. and R. B. Langley (2005). Nullification of Differential Ionospheric Delay for Long-Baseline Real-Time Kinematic Applications. ION 61st annual meeting, Cambridge, MA.

Kouba, J. and P. Héroux (2001). "Precise Point Positioning Using IGS Orbit and Clock Products." GPS solutions 5.

Kunches, J. (2008). "GNSS and Space Weather, Making the Least Out of Solar Max." Inside GNSS 2(8).

Lau, L. and P. Cross (2005). Use of Signal-to-Noise Ratios for Real-Time GNSS Phase Multipath Mitigation. NAV, The Royal Institute of Navigation.

Laurichesse, D. and F. M. J. P. Berthias (2008). Real Time Zero-difference Ambiguities Fixing and Absolute RTK. ION NTM 2008.

Leick, A. (2003). GPS Satellite Surveying.

Leveson, I. (2006). "Benefits of the New GPS Civil Signal, The L2C Study." Inside GNSS July/August 2006.

Liu, G. C. and G. Lachapelle (2002). Ionosphere Weighted GPS Cycle Ambiguity Resolution. ION NTM 2002, San Diego, CA.

Liu, X. (2002). A Comparison of Stochastic Models for GPS Single Differntial Kinematic Positioning. ION GPS, Portland, OR.

Misra, P. and P. Enge (2006). Global Positioning System: Signals, Measurements, and Performance. Lincoln, Massachussetts, Ganga-Jamuna Press.

Neumann, J. B., A. Manz, et al. (1996). Test Results from a New 2 cm Real Time Kinematic GPS Positioning System. ION GPS, Kansas City.

Odjik, D. (2000). Weighting Ionospheric Corrections to Improve Fast GPS Positioning Over Medium Distances. ION GPS, Salt Lake City, UT.

Omnistar. (2008). from http://www.omnistar.com/.

Rao, K. D., MN.S.Swam, et al. (2004). "GPS Navigation with Increased Immunity to Modeling Errors." IEEE Transactions on Aerospace and Electronic Systems 40.

RTCM (2001). RTCM recommended Standards for Differential GNSS

RussianSpaceAgency. (2007). from http://www.glonass-ianc.rsa.ru/ .

Saastamoinen (1972). "Atmospheric Correction for Troposphere and Stratosphere in Radio Ranging of Satellites." The Use of Artificial Satellites for Geodesy, Geophysics Monograph Series Vol. 15.

Sahmoudi, M., R. J. Landry, et al. (2007). Satellite Augmentation Systems for Acceleration Determination in Airborne Gravimetry: a Comparative Study. ION 2007, Fort Worth, TX.

Simon, D. (2006). Optimal State Estimation, Kalman, H and nonlinear approaches.

Starfire. (2008). from http://www.navcomtech.com/StarFire/

Talbot, N. C. (1991). "High-Precision Real-Time GPS Positoning Concepts: Modeling and Results." Journal of Navigation 38.

Teunissen, P. J. G. (1993). Least-Squares Estimation of the Integer GPS Ambiguities. IAG General Meeting, Beijing, China.

Teunissen, P. J. G. (1997). "The geometry-free GPS ambiguity search space with a weigthed ionosphere." Journal of Geodesy 71.

Teunissen, P. J. G. (2002). Integer Least-Squares. V Hotine-Marussi Symposium on Mathematical Geodesy, Matera, Italy.

Teunissen, P. J. G. and S. Verhagen (2007). GNSS Carrier Phase Ambiguity Resolution: Challenges and Open Problems. the Scientific meetings of the IAG General Assembly, Perugia, Italy.

Uratani, C., K. Sone, et al. (2003). Dynamical Models for Carrier-Phase Kinematic GPS Positioning. ION GNSS, Portland, OR.

Verhagen, S. (2005). The GNSS integer ambiguities: estimation and validation, University of Delft, NL.

Wang, J. (2000). "Stochastic Modeling for Real-Time Kinematic GPS/GLONASS Positioning." Journal of Navigation 46(4).

Warren, D. L. M. and J. F. Raquet (2003). "Broadcast vs. Precise GPS Ephemerides: a Historical Perspective." GPS Soluitons.

Zarchan, P. and H. Musoff (2005). Fundamentals of Kalman filtering: a practical approach. Second edition.

Zhang, K., F. Wu, et al. (2007). The Latest Development of a State-wide GNSS Network-based RTK System in Australia. ION GNSS, Fot Worth, Tx.